THE UNIVERSITY OF MANITOBA

THERMALLY ACTIVATED DEFORMATION IN NIOBIUM-ZIRCONIUM SOLID SOLUTIONS

by

SHYAM NARAYAN TIWARI

A THESIS

SUBMITTED TO THE FACULTY OF GRADUATE STUDIES

IN PARTIAL FULFILMENT OF THE REQUIREMENTS FOR THE DEGREE OF

DOCTOR OF PHILOSOPHY

DEPARTMENT OF MECHANICAL ENGINEERING

WINNIPEG, MANITOBA

May, 1973

ABSTRACT

The deformation behaviour of zone refined polycrystalline niobium solid solutions containing upto 4.7 at%Zr has been studied between the temperatures $77^{o}K$ and $490^{o}K$. The strain rate change and stress relaxation techniques were used to determine the activation parameters of deformation, the dislocation velocity stress exponent m* and the thermal and athermal components of the flow stress as a function of strain, temperature and concentration.

At room temperature the flow stress increased linearly with concentration but the individual thermal and athermal components did not obey this simple relationship. Solution softening instead of solution hardening was observed in all the alloys at $77^{o}K$ and the softening temperature range decreased with increasing Zr content. It has been shown that the softening effect was due to a decrease in the thermal component of flow stress on alloying. At $77^{o}K$, the addition of upto $\sim$2.4 at%Zr caused softening but beyond this concentration the alloys began to show hardening once more. The variations of m* with temperature and concentration were essentially analogous to those of the thermal stress σ^{*}.

The solution softening in Nb - Zr was accompanied by a decrease in the magnitude of activation parameters for deformation as compared with those of pure niobium. It was concluded that the alloy softening was a lattice softening phenomenon and scavenging probably had only a minor effect. The deformation of pure Nb obeyed

the Dorn-Rajnak theory of double kink nucleation over the entire temperature range studied but in the case of alloys it was obeyed only in the Nb - 0.87 at%Zr alloy in the solution softening region. Beyond the softening region, deformation was controlled by solute hardening.

The flow stress and its thermal and athermal components were studied as a function of strain. The rate of work hardening increased slowly with solute concentration and was mainly a reflection of the increase in the athermal component of the flow stress.

Transmission electron microscopy of the deformed specimens showed that the dislocation arrangement was dependent on the thermal stress, σ^*. It was found that as σ^* increased the screw dislocation density increased and the amount of tangling decreased. At higher strains dislocation cells were formed and their diameter decreased with increase in σ^*.

ACKNOWLEDGMENT

The author gratefully acknowledges the advice and help given by his research director, Professor K. Tangri and Dr. D. J. Lloyd. The author is thankful to the National Research Council of Canada for financial support.

TABLE OF CONTENTS

List of Figures

TABLE OF MICROGRAPHS

LIST OF TABLES

THERMALLY ACTIVATED DEFORMATION IN NIOBIUM-ZIRCONIUM SOLID SOLUTIONS

BACKGROUND OF THE PROBLEM

1.1 Introduction

In the past, extensive investigations have been made on the deformation behaviour of body centred cubic metals, especially to resolve the rate controlling dislocation mechanism responsible for the large temperature dependence of flow stress in these metals. There are experimental supports for both the interaction between moving dislocations and residual interstial impurities in solution, and intrinsic lattice friction as the rate controlling factor. The deformation behaviour of body-centred cubic (bcc) solid solutions, however, has received relatively little attention.

There have been several attempts to correlate the solid solution strengthening (sss) in b.c.c. metals with the existing theories on this subject but no single theory seems to be applicable to all the b.c.c. metals; different theories are applicable to different metals. It was only recently realized that the addition of solute can alter either or both components of the flow stress if the flow stress is considered as consisting of thermal and athermal components. Thus, it is necessary to study each component individually, especially in the case of solution softening which is now a well established phenomenon in dilute alloys of b.c.c. metals. In the literature, various effects have been suggested to be responsible for solution softening,

the most important being the scavenging of interstials and the decrease in the lattice friction stress, both being effected by the solute atoms present in the lattice.

It was due to the abovementioned differing views on deformation and solution softening that the present study was conceived and niobium was selected as the base metal. Niobium is a refractory metal with low neutron capture cross section and thus it is a potential structural material for nuclear reactors. The creep resistance of niobium is greatly improved by alloying it with zirconium which too has a low neutron capture cross section. Since there is a negligible modulus difference but a large atom size difference between niobium and zirconium, the number of variables is reduced in studying the solid solution effect of zirconium on niobium. Also, the dilute solid solutions of niobium and zirconium show alloy softening at subambient temperatures and thus provide an opportunity for the study of the hardening and softening effects of alloying in the same system. Superconductivity is still another property of niobium-zirconium alloys which makes this system attractive for the study of its deformation behaviour.

In most of the earlier studies on niobium solid solutions, the effects of solute on the thermal and athermal components of the flow stress have not been studied individually. Previous investigators have usually correlated solid solution effects in niobium with the size mismatch between niobium and the solute atom. However, this may not

be valid if the individual components of the flow stress are considered.

Some of the studies of deformation behaviour of niobium solid solutions have used the "rate theory" to analyse and explain the observed results in terms of a rate controlling mechanism. Alternatively, the Johnston and Gilman's "power law" relationship between dislocation velocity and the effective stress has been found to hold in pure niobium, but the effect of solute on this relationship has not been looked into in detail.

In order to aid the understanding of the deformation behaviour and its dependence on solute, it is necessary to study the work hardening and dislocation substructure of the material. And, such studies have been carried out on single crystals of niobium and its alloys, however, polycrystalline alloys have not been studied.

Definition of the Problem

Now, it would seem necessary that the first step in resolving the points mentioned above, should be to find the flow stress and its thermal and athermal components as a function of concentration, temperature and strain. Secondly, the activation parameters of deformation are necessary to define the rate controlling mechanism in different temperature ranges. Finally, the transmission electron microscopy of the dislocation substructure as a function of strain, temperature and composition in deformed specimen is necessary to gain an insight into the deformation behaviour of the material.

Thus, this thesis deals with the study of solution strengthening/softening, deformation behaviour of the polycrystalline niobium-zirconium specimens of controlled grain size and electron microscopy i.e. study of the dislocation structure in deformed specimens.

1.2 Important Theoretical Relationships Used in this Study

As it has been stated in the previous section, this study deals with the effects of solute on 1) the thermal and athermal components of the flow stress, 2) the activation parameters of plastic deformation, 3) the work hardening behaviour and 4) the dislocation substructure in Nb-Zr alloys. Since there are excellent reviews available on the general topics just mentioned, only those theoretical relationships that have been employed to calculate the different parameters and to interpret the results of this investigation are given here along with their references.

(i) Solid Solution Hardening:

Solid solution hardening has been studied in single crystals of several body-centered cubic (b.c.c.) metals and either c(atomic concentration of solute) or $\sqrt{c}$ dependence of flow stress was found. The following macroscopic characteristics have been used to characterize the strength of interaction between a solute atom and a dislocation: a) the size misfit between the solute and solvent atoms and b) the effect of solute on the shear modulus as a measure of the local change in binding on introduction of the solute atoms. It has been pointed out that the modulus mismatch may be less effective in the body-centered cubic than in the face-centered cubic alloys, but it can not be neglected.

According to the Mott-Nabarro theory the isolated solute

atoms give rise to small local internal stress fields, the magnitude of which was assumed to depend on only the size mismatch between the solute and the solvent atoms. According to their original calculation, the shear stress

$$\tau = G\varepsilon_a^2 c$$

where τ = shear stress

ε_a = size mismatch = $\frac{1}{a} \cdot \frac{da}{dc}$

a = lattice parameter of solvent

c = atomic concentration of solute

G = shear modulus

Due to a later modification of the calculation by Mott, the shear stress is given by the equation

$$\tau = 2.5\ G\varepsilon_a^{4/3} c.$$

However, this equation was shown by Cottrell to predict about ten times too large solution hardening than it was observed.

The Fleischer's theory takes into account both the size interaction and the modulus interaction. According to this theory, both the edge dislocation and the screw dislocation interact with the different modulus of the solute atom as elastically hard or soft spot in the matrix and thus the dislocations do more or less work than usual in elastically shearing the foreign atom. The rate of change of shear modulus, $\varepsilon_G = \frac{1}{G} \cdot \frac{dG}{dc}$ was suggested as a measure of the atomic modulus mismatch. The shear stress

$$\tau = \frac{G}{760} \left|\alpha\varepsilon_a - \varepsilon_G'\right|^{3/2} c^{1/2}$$

where $\varepsilon_G' = {}_G/(1 + |\varepsilon_G|/2)$

$\varepsilon_G = \frac{1}{G} \cdot \frac{dG}{dc}$

α = 3 for screws and ± 16 for edges.

τ, G, ε_a and c have the meaning given before.

References

1. Mott, N.F. and Nabarro, F.R.N., Report on Conf. on Strength of Solids, Phys. Soc. London, p. 1, 1948.

2. Mott, N.F., Imperfections in Nearly Perfect Crystals, ed. Shockley W., John Wiley, p. 173, 1952.

3. Cottrell, A.H., Dislocations and Plastic Flow in Crystals, Oxford Univ. Press, 1953.

4. Fleischer, R.L., The Strengthening of Metals, ed. Peckner, D., Reinhold Publishing Corp., p. 93, 1964.

(ii) Work Hardening

The strain hardening effect can be evaluated by using the slope of the true stress-true strain curve. The rate of work hardening $\frac{d\sigma}{d\varepsilon}$ decreases continually with strain during the uniform elongation of the material and hence to evaluate the effect of temperature, alloying etc. on $\frac{d\sigma}{d\varepsilon}$ the comparison should be made at the same strain. Alternatively, the power expression of work hardening has been used. If the power expression is obeyed then a straight line is obtained in the log-log plot of true stress and true strain however, change in slope of the straight line have been observed in materials after a certain amount of deformation. The formulae used in studying the work hardening behaviour are given below.

1. Rate of work hardening = $\frac{d\sigma}{d\varepsilon}$
2. Power expression of work hardening
   $\sigma = K\varepsilon^n$
3. or $\sigma = \sigma_y + K\varepsilon^n$ also
4. n = slope of the curve in log-log plot of true stress and true plastic strain.
5. and K = value of ordinate at $\varepsilon=1$ in the above plot
6. when necking occurs $\frac{d\sigma}{d\varepsilon} = \sigma$
   and since $n = \frac{\varepsilon}{\sigma}\frac{d\sigma}{d\varepsilon}$
   $\varepsilon_{necking} = n$

σ = true stress

ε = true plastic strain

K = strength coefficient

n = strain hardening exponent

σ_y = yield stress

References

1. McGregor Tegart, W.J., Element of Mechanical Metallurgy, Macmillan Company, New York, p. 13, 1967.

2. Morrison, W.B., Trans. A.S.M., 59, p. 824, 1966.

(iii) Rate Theory of Plastic Deformation

The plastic deformation of metals has been extensively discussed as a thermally activated motion of dislocations. Calculations are usually made with the rate equation in the simple exponential form based on the assumption that there is a single equivalent activation energy instead of differing activation energies at different points in a system. The formulae that are employed in determining the parameters of deformation are given below.

1. $u = P\gamma_o \exp\{-(\frac{H-V^*\sigma^*}{KT})\}$

2. $\dot{\varepsilon} = \phi b\zeta u = \phi NAbu/P = \dot{\varepsilon}_o \exp\{-\frac{\Delta H}{KT}\}$

3. $\sigma = \sigma_u + \sigma^*$

4. $\Delta H = KT \ln (NA'b\phi\gamma_o/\dot{\varepsilon})$

5. $\gamma = NA'b\phi\gamma_o$

6. $V^* = KT \left(\frac{\partial \ln\dot{\varepsilon}}{\partial \sigma^*}\right)_T$

7. $\Delta H = -KT^2 \left(\frac{\partial \ln\dot{\varepsilon}}{\partial \sigma^*}\right)_T \left(\frac{\partial \sigma^*}{\partial T}\right)_{\dot{\varepsilon}}$

8. $H = \Delta H + V^*\sigma^*$

9. $\Delta H = A - B \ln (\sigma^*/\sigma_p)$

10. $(\partial \sigma^*)_T = (K/B)(\partial \ln\dot{\varepsilon})_T \sigma^* T$

11. $T_m = (B/K) \ln (\gamma/\dot{\varepsilon})$

u = mean velocity of a dislocation

P = distance moved after a successful activation

γ_o = Frequency factor

H = total energy

ΔH = activation energy

V^* = activation volume

σ = flow stress

σ^* = thermal stress

σ_μ = athermal stress

K = Boltzman constant

T = Absolute temperature

$\dot{\varepsilon}$ = Macroscopic strain rate

ϕ = orientation factor

b = Burgers vector

ρ = mobile dislocation density

N = Effective number of activation sites per unit volume at which dislocation segments are halted

A' = Area of glide plane swept by a dislocation line after a successful activation

A & B are constants

σ_p = Peierls stress at $0^{o}K$

T_m = the temperature of the maximum $\Delta\sigma$

References

1. Christian, J.W. and Masters, B.C., Proc. Roy. Soc., Ser. A, 281, p. 240, 1964.

(iv) Dislocation Dynamics

An alternative approach to the dislocation motion is dislocation dynamics. Johnston and Gilman have originally and extensively studied this approach and found an empirical power law relationship between the velocity of dislocation and the applied stress.

$$v = B(\sigma^*)^{m^*}$$

where v = velocity of dislocation

B = mobility or the velocity produced by unit σ^*

σ^* = thermal stress and

m^* = dislocation velocity stress exponent.

Li has developed an analysis of the stress-relaxation technique to determine m^*, and the components, thermal and athermal of the flow stress at increasing plastic strains. In this method a log-log plot of the relaxation rate ($d\sigma/dt$) and the time (t) is linear and the value of m^* is given by the slope of the linear region via the equation,

$$m^* = \frac{\text{slope}}{\text{slope} + 1}$$

The athermal component at any plastic strain is found by using the relation

$$\frac{\sigma_1 - \sigma_\mu}{\sigma_2 - \sigma_\mu} = \left(\frac{t_1 + a}{t_2 + a}\right)^{-\frac{1}{m^*-1}}$$

where σ_1 and σ_2 are the flow stresses after times t_1 and t_2 in a stress relaxation curve,

a is the deviation from linearity in the log ($d\sigma/dt$) - log(t) plot,

σ_μ is the athermal component of the flow stress

m^* is the dislocation velocity stress exponent.

Assuming $\sigma = \sigma_\mu + \sigma^*$ and knowing σ and σ_μ at any strain σ^* can be found.

The other useful relationships are given below

1. $m^* = \frac{V^*\sigma^*}{KT}$

2. $\left(\frac{\partial m^*T}{\partial T}\right)_{\sigma^*} = 0$ at 0^oK

3. $\left(\frac{\partial \Delta H}{\partial \ln\sigma^*}\right)_{\varepsilon} = -m^*KT$

4. $\left(\frac{\partial \ln\sigma^*}{\partial T}\right) = \frac{-\Delta H}{m^*KT^2}$

5. $(m^*T)_o \simeq \frac{\Delta H_o}{2.5K}$

m^* = dislocation velocity stress exponent

V^* = activation volume

σ^* = thermal stress

K = Boltzmannconstant

T = absolute temperature

ΔH = activation energy

$(m^*T)_o$ = limiting value of (m^*T) as $T \to 0^oK$.

References

1. Johnston, W.G. and Gilman, J.J., J. App. Phys., 30, p. 129, 1959.

2. Li, J.C.M., Can. J. Phys., 45, p. 493, 1967.

1.3 Summary of Experimental Results of Earlier Studies on Nb and Its Solid Solutions.

Only a few of the earlier attempts to identify the solution hardening mechanism in niobium have also been concerned with the deformation behaviour and electron microscopy of the deformed sub-structure. Here we shall summarize only the general effects of solute on various parameters of Nb as follows while any discussion pertinent to polycrystalline Nb-Zr alloys will be dealt with at the appropriate places.

1.3.1 Lattice Parameter

Neighbouring elements in the periodic system that have a favourable size factor to niobium to form a wide range of solid solutions have been shown by Knapton[1] in a diagrammatic form, fig. 1. The information available on the rate of change of lattice parameter of niobium with solute content is given in table I. It is seen that the change in the lattice parameter of niobium can be positive, negative or zero depending upon the specy of the solute. Knapton[1] has determined the lattice spacings of niobium-zirconium alloys and his results are shown in fig. 2. Zirconium increases the lattice parameter monotonically in the entire range of solid solution with niobium and is one of the most effective elements in changing the lattice parameter.

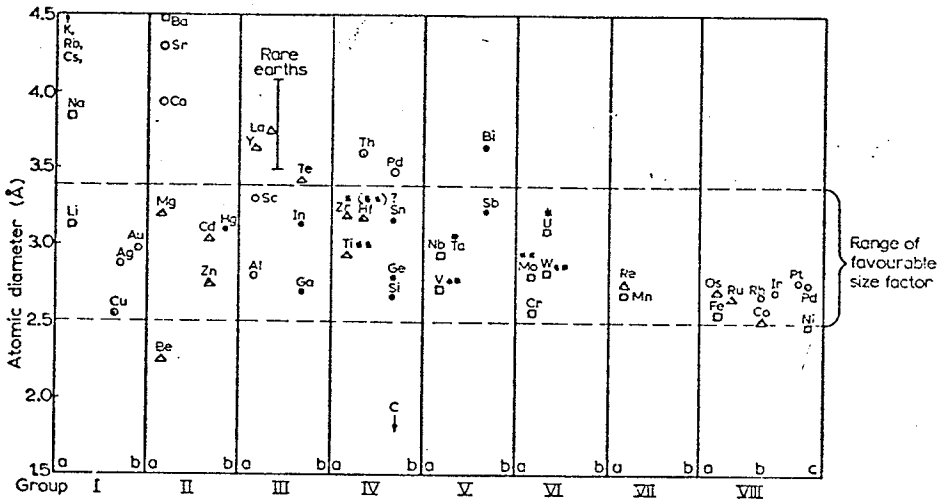

Fig. 1. Favourable size factors for solid solution formation in niobium and tantalum. ⊡, BCC; ⊙, FCC; △, HCP; ●, others; *, CSS with Nb; **, CSS with Nb and Ta.

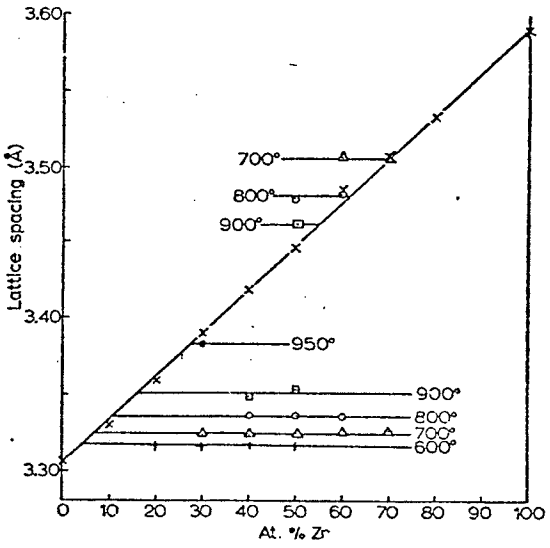

Fig. 2. Lattice spacings of body-centred-cubic niobium–zirconium alloys. ×, annealed in β; • 950°C; ⊡ 900°C; ⊙, 800°C; △, 700°C; + 500°C.

TABLE I

Solute in Nb	Solid Solubility Limit at Room Temperature in at%	1/a . da/dc per at%	1/G . dG/dc per at%
Hf	-	$(4.8 \pm 0.5)10^{-4}$	0.455
Mo	Completely Soluble	$-(4.6 \pm 0.5)10^{-4}$	2.1 ± 0.2
Pd	$\sim$23	$-(6.4)10^{-4}$	3.0 ± 0.7
Re	$\sim$45	$-(8.5 \pm 0.4)10^{-4}$	3.23
Ta	Completely Soluble	$(0.0 \pm 0.5)10^{-4}$	1.15 ± 0.15
V	Completely Soluble	$-(7.4 \pm 0.5)10^{-4}$	1.05 ± 0.15
W	Completely Soluble	$-(5.0 \pm 0.4)10^{-4}$	1.7 ± 0.2
Zr	$\sim$14	$(8.4)10^{-4}$	-

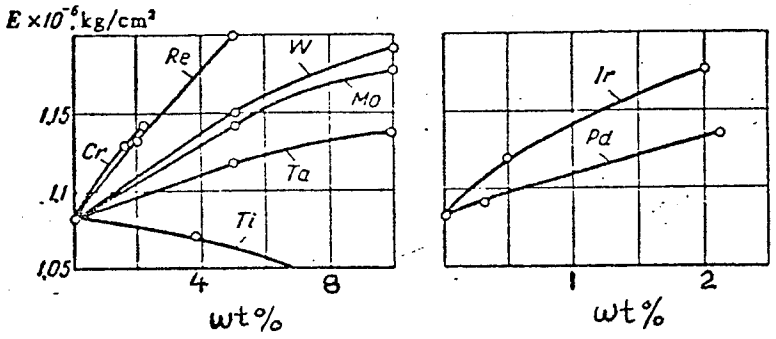

Figure 3: E the elasticity modulus Vs concentration for the Nb base alloys.

1.3.2 Elastic Constants

For the examination of solid solution hardening theories, it is necessary to know the change in lattice parameter and the elastic constants of the solvent with addition of solute. Results from earlier studies on such changes in niobium are given in table I, along with their sources. Tarasov[5] et.al. determined the effect of alloying elements on the modulus of elasticity of niobium. Their results are shown in fig. 3 and are self explanatory. Nedyukha & Chernyy[6] showed that the elastic and shear moduli of niobium are considerably raised by the addition of chromium upto 5 wt% and then with further addition the rate of change is slower. They found that iron, aluminum, tantalum and vanadium also raised the moduli very considerably but additions of more than 5% of titanium reduced the moduli below those of pure niobium. Harris[7] has shown that the modulus of elasticity increased very sharply upto 1 at% Zr (from 10×10^3 to 11.5×10^3 Kg/mm^2) and then remains almost constant, while the addition of upto 1 at% Ta decreased it and beyond 1 at% increased it again. Vanadium increased the modulus linearly and monotonically.

In applying the solution hardening theories at temperatures other than the ambient, or comparing the results of a deformation study at different temperatures, it is necessary to know the change in elastic constants with change in test temperature but such information is scarce in the literature. Results of such a study by Tarasov et.al.[5] are given for some niobium base alloys in table II. Harris[7] has studied this behaviour in niobium base alloys of Ta, V, W and Zr. His results are shown in figs. 4 & 5.

TABLE II

Influence of temperature on the elasticity modulus of alloys on niobium base

Composition, wt. %	Elasticity modulus, $E \times 10^{-6}$ kg/cm² at temperatures (0°C)						
	20	300	500	700	900	1100	1300
Nb	1.083	1.081	1.082	1.085	1.091	1.097	1.108
Nb+5.0 Mo	1.144	1.135	1.136	1.149	1.172	1.186	1.213
Nb+10.0 Mo	1.180	1.175	1.191	1.210	1.232	1.233	1.233
Nb+5.0 Ta	1.118	1.117	1.118	1.124	1.145	1.152	1.152
Nb+10.0 Ta	1.139	1.137	1.138	1.145	1.155	1.156	1.156
Nb+5.0 W	1.151	1.145	1.143	1.153	1.168	1.175	1.175
Nb+10.0 W	1.192	1.185	1.196	1.201	1 212	1.225	1.225
Nb+2.0Re	1.135	1.128	1,126	1,127	1,129	1.134	1.136
Nb+5,0Re	1.210	1.211	1,210	1,213	1.215	1.223	1.225
Nb+1.55 Cr	1.128	1,130	1.135	1.135	1.136	1.130	1.134
Nb+2.3 Cr	1.142	1.140	1,140	1.142	1.141	1,138	1.138
Nb+3.83 Ti	1.072	1.073	1,074	1.075	1.076	1.076	1.076
Nb+7.6 Ti	1.044	1.043	1.044	1.042	1.042	1.037	1.032
Nb+0.5 Ir	1.119	1.117	1.101	1.111	1.118	1.116	1.112
Nb+2.0 Ir	1.174	1.165	1.165	1,172	1,175	1.180	1.180
Nb+0.3 Pd	1.094	1.095	1.102	1.114	1,116	1.113	1.110
Nb+2.17 Pd	1.136	1.139	1,142	1.144	1,143	1.137	1.130
Nb+0,4 La	1.096	1.095	1,096	1.103	1.110	1.120	1.123
Nb+0,55 La	1.072	1.071	1.074	1.082	1.084	1,090	1.096
Nb+0,17B	1.114	1.112	1.118	1.135	1.151	1.159	1.162
Nb+0.23B	1.190	1.180	1,172	1.184	1.198	1.210	1.214
Nb+0,32 Si	1.101	1.101	1.104	1.120	1.129	1,148	1.154
Nb+0.5 Si	1.121	1.121	1,124	1.144	1.162	1.174	1.176

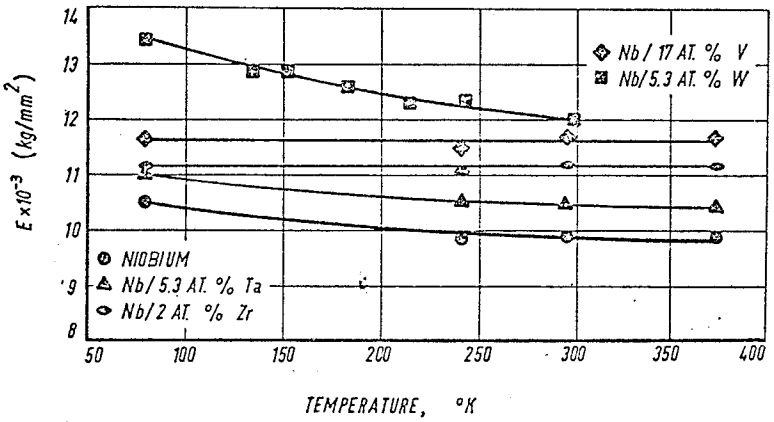

Fig. 4a Temperature-dependence of Young's modulus for some binary niobium alloys.

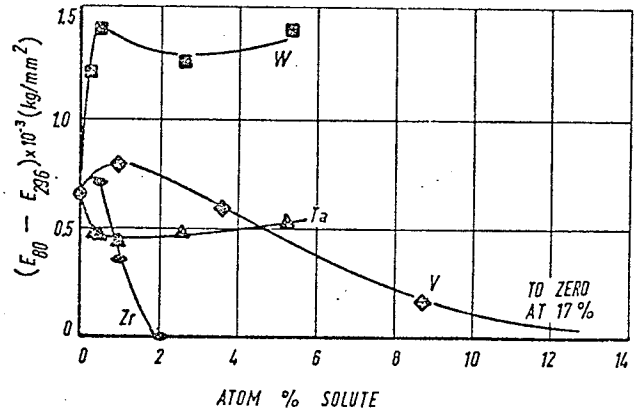

Fig. 4b Effect of solute concentration on the temperature-dependence of E between 80 and 296°K.

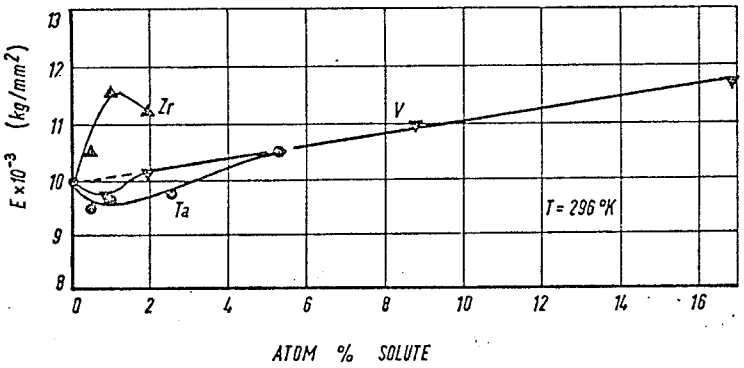

Fig. 5a Effect of vanadium, zirconium, and tantalum on Young's modulus of niobium at 296°K.

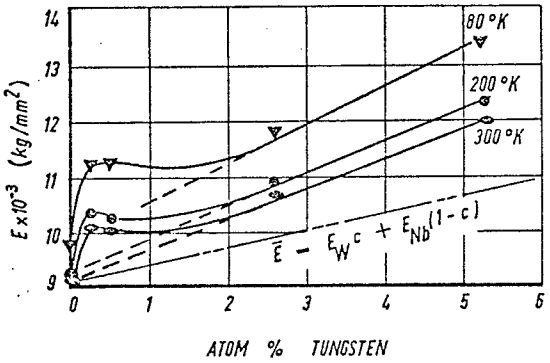

Fig. 5b Effect of tungsten on Young's modulus of niobium at 80, 200 and 300°K. The curve designated $\bar{E}$ represents the ideal linear variation of modulus with composition at 300°K.

1.3.3 Solid Solution Strengthening/softening and hardness.

Attempts have been made in the past to evaluate the solution strengthening in niobium in terms of the current solution hardening theories. The earlier results are summarized in table III. Begley and Bechtold[8] conducted tensile tests at room temperature and 1100°C on several niobium base polycrystalline solid solutions but no correlation was found between the solution strengthening and a simple physical parameter such as atomic size mismatch of the alloy additions etc. However, Harris[9] has shown that in his various polycrystalline niobium solid solutions, atomic size mismatch, rather than modulus mismatch, was the dominant factor in hardening of the alloys, except in the Nb-W system where modulus mismatch seemed to be more important. On the other hand, Kostorz[10] has shown that the athermal(plateau)solution strengthening in niobium single crystals by Ta, V, W or Zr was proportional to the square root of the solute concentration, and thus followed the Fleischer's theory[11] of solution hardening whereas Jax[12] found that the plateau hardening at 915°K in Nb-W and Nb-Mo increased linearly with concentration. Kan[13] also found linear dependence of athermal strengthening in Nb-Mo. Palmer and Flewitt[14] showed that athermal strengthening in Nb-25 wt% Zr was in close agreement with the predictions of Mott & Nabarro theory[15] based on size mismatch, and thus obeyed the linear concentration dependence. Koss[16], working on Nb-W crystals, came to the conclusion that no current theory was completely consistent with the observed

TABLE III

Alloying Element	Crystal	Interstitials wt ppm	Strength vs Concentration σ	Strength vs Concentration σ_μ	Mechanism	Solution softening, σ_o^* upto at%	Solution softening, σ_o^* below °K	Reference & Year
1. Cr	Poly	720	-	-	No correlation			Begley & Bechtold[8] (1961)
Hf	"	"	-	-	"			"
Mo	"	"	-	-	"			"
Ti	"	"	-	-	"			"
V	"	"	-	-	"			"
W	"	"	-	-	"			"
Zr	"	"	-	-	"			"
2. Ta	Poly	250	C	C	Size mismatch	Not seen		Harris[9] (1966)
V	"	"	"	"	"	8.8*	300	"
W	"	"	"	"	"	5.3*	"	"
Zr	"	"	"	"	"	2.0*	"	"
3. Ta	Single	1500 atom ppm		$C^{1/2}$	size & modulus mismatch			Kostorz[10] (1968)
V	"			"	"			"
W	"			"	some S.R.O. also+			"
4. Ta	single	80	C	C		Not seen		Peters & Hendricson[18] (1970)
Mo	"	80	"	"		5	~250	"
5. Zr	Poly	500		C	Size mismatch			Palmer & Flewitt[14] (1970)
6. Pd	single	100		$C^{2/3}$ or C				Jax[12] (1971)
Mo	"	60		C				"
W	"	60		C				"
7. W	single	20			No correlation			Koss[16] (1971)
8. Mo	single	100		C		2	175	Kan[13] (1971)

NOTE:

* These are the highest concentrations studied.

+ Some short range ordering (S.R.O.) also present.

athermal strengthening of the alloys. Thus, it is seen that there is no general agreement between different authors regarding the solution hardening mechanism in niobium. However, it should be borne in mind that these investigations were carried out in a span of last decade during which the purity of niobium has increased continuously and this could be one of the possible reasons for conflicting observations. Secondly, there were some studies in which flow stress instead of the individual components - thermal and athermal - was evaluated as a function of solute concentration and as mentioned earlier, any addition of solute could have different effects on these components of the flow stress.

Apart from the solution strengthening, alloy softening has also been observed in niobium. Harris[9] has shown that in his polycrystalline niobium solid solutions, 5 at% Ta addition did not alter the shape of the effective stress-temperature curve but additions of 9 at% V or 2 at% Zr or 5 at% W increasingly reduced the temperature-dependence in the range $77^{o}K$ - $300^{o}K$. However, at all temperatures the flow stresses in the alloys were higher than that of the pure niobium and thus he showed that the thermal component of flow stress was reduced by alloying and at the same time athermal component was increased. Solution softening at $77^{o}K$ by the addition of Mo upto $\sim$2 at% in Nb has been reported by Foxall & Statham[17], Peters & Hendricson[18] and Kan[13]. Alloy softening has been observed by several investigators in other b.c.c. metals also e.g. Fe-Cr[19], Fe-Ni[20], Ta-Mo[21].

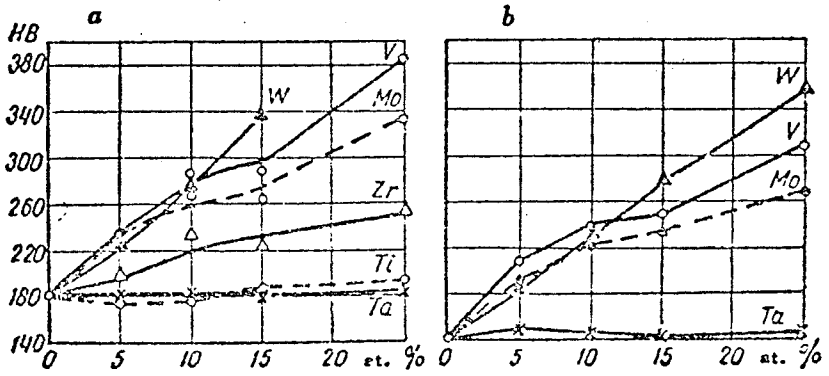

FIG. 6 Effect of alloying elements on the hardness of niobium: *a* - without heat treatment; *b* - after annealing.

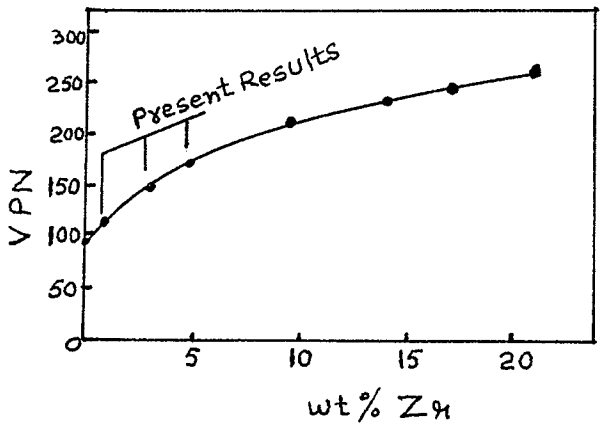

Figure 7: Effect of Zr solute on the hardness of niobium.

Information on the hardness values of niobium alloys as a function of solute content is very limited. Georgiyeva and Gulyaev[22] studied the hardness variations of niobium alloys at ambient and higher temperatures, fig. 6. They concluded that the hardening of binary alloys was related to the degree of lattice distortion and an increase in lattice parameter had less effect on hardening than an equivalent decrease e.g. although Zr increased the lattice parameter of niobium more than either Mo, V or W decreased it, yet Zr was a less effective hardener as compared to Mo, V or W. Further, they pointed out that if the alloying elements are those which cause a big change in the melting point (e.g. W), the above relation will not be observed and the comparison must be made at homologus temperatures. An incidental result[23] also showed that the hardness values of niobium increased rapidly with initial Zr additions but that they tapered off later, fig. 7.

1.3.4 Temperature Dependence of Yielding and Plastic Flow

Mitchell et.al.[24] have studied the deformation in niobium crystals as a function of purity, temperature, strain and strain rate and showed that the initial flow stress decreased with increasing purity but it increased rapidly with decreasing temperature or increasing strain rate. The initial flow stress became almost constant beyond 300^{o}K. They found that there was a tendency for the initial yield points to occur in low zone-pass crystals (i.e.

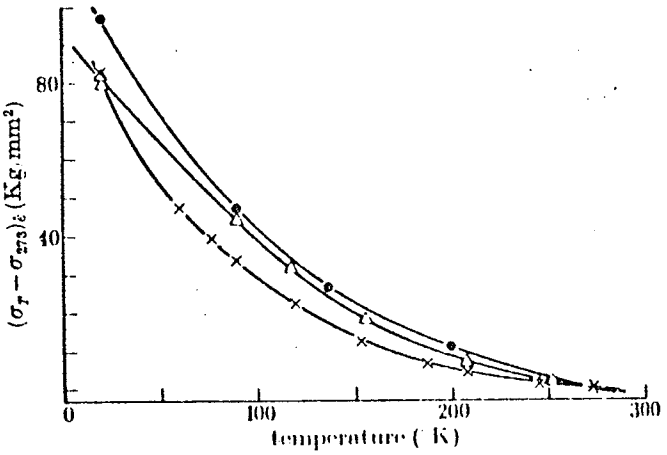

FIGURE 8 Flow stress plotted against temperature for niobium. ×, Polycrystalline (115 V.p.n.); ●, polycrystalline (150 V.p.n.); ○, single crystals (65 V.p.n.).

low purity Nb). The yield stress decreased sharply with increasing number of zone passes. At 77°K, the yield stress for the one zone-pass crystals was only slightly higher than that for the six-pass material, indicating that the impurity contribution to it was not very temperature dependent.

Christian and Masters[25] found that in polycrystalline niobium, yield drops occurred on initial testing at room temperature and rather ill-defined yield was seen if the testing was carried out near 100°K. On subsequent unloading and loading at subatmospheric temperatures no further yield drops were observed. They further showed that in niobium of different purities the change in flow stress with temperature, fig. 8 was nearly identical and thus concluded that the temperature dependence was not very sensitive to impurity when the metals are moderately pure.

Bowen et.al.[29] also noticed the similar behaviour of deformation in single crystals of niobium as observed in earlier investigations. They found that in niobium crystals, yielding at room temperature was fairly sharp but rather rounded curves were obtained at 158°K.

Harris[9] has shown that in polycrystalline niobium and its solid solutions, a yield drop and then work hardening occurred at temperatures above 243°K. However, there was a significant change in behaviour at 173°K, where there were large yield drops followed by very low or even negative rates of strain hardening. The temperature dependence of the yield stress and flow stress in pure

niobium increased very rapidly at temperatures below 250°K and this behaviour did not alter essentially on alloying. Foxall and Statham[17] conducted tests on niobium-molybdenum and niobium-rhenium crystals and found that as the yield stress was increased, either by an increase in alloy content or by a decrease in temperature, the size of the yield drop and the strain associated with the yield region increased. The temperature sensitivity of the flow stress for the alloys remained almost the same as for niobium except for solid solutions containing upto 5 at% Mo in which alloy softening took place at lower temperatures. However, Peters and Hendricson[18] working on niobium-tantalum and niobium-molybdenum crystals, saw solution softening in only 5 at% Mo alloy at 77°K.

1.3.5 Work Hardening and Electron Microscopy of Substructure

Gregory et.al.[26] studied work hardening in polycrystalline niobium subjected to different heat treatments. They found that the slope of the curve in log true stress-log true strain plot, changed to a much higher value at ~2% strain, fig. 9 and concluded that work hardening in fully recrystallized fine grain material resulted from simultaneous decrease in activation volume and in the number of mobile dislocations with increasing strain. Electron microscopy showed that the dislocation density during the first 2-3% strain was roughly 10^{10} per sq. cm. and it increased only by a factor of 1.5 to 2 during the next 7 or 8 percent strain. Fourdeux and Wrønski[34] found by electron microscopic examination of foils, loaded at room

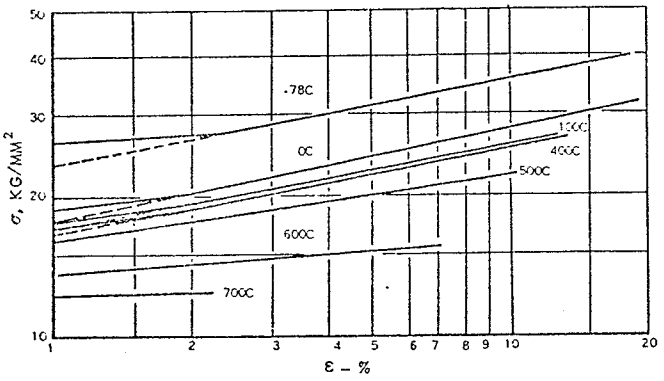

Fig. 9a Log true stress vs log true strain for recovered polycrystalline niobium at various temperatures, strain rate = 0.01 min^{-1}.

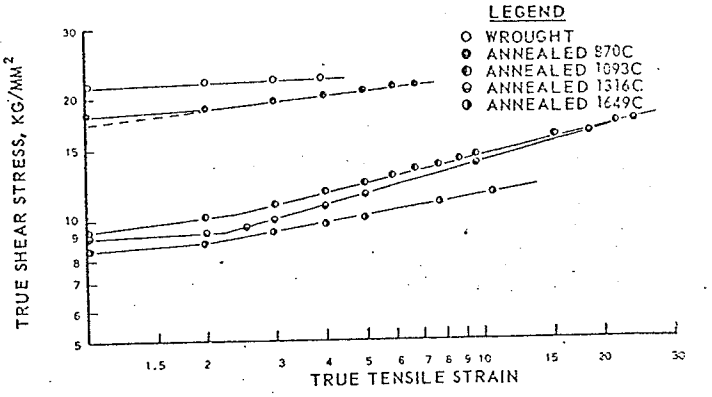

Fig. 9b Log true shear stress vs log true tensile strain for round niobium tensile specimens with various structures tested in tension at 24°C, strain rate = 0.01 min^{-1}. Specimens cold swaged 90 pct, annealed for 1 hr at indicated temperature.

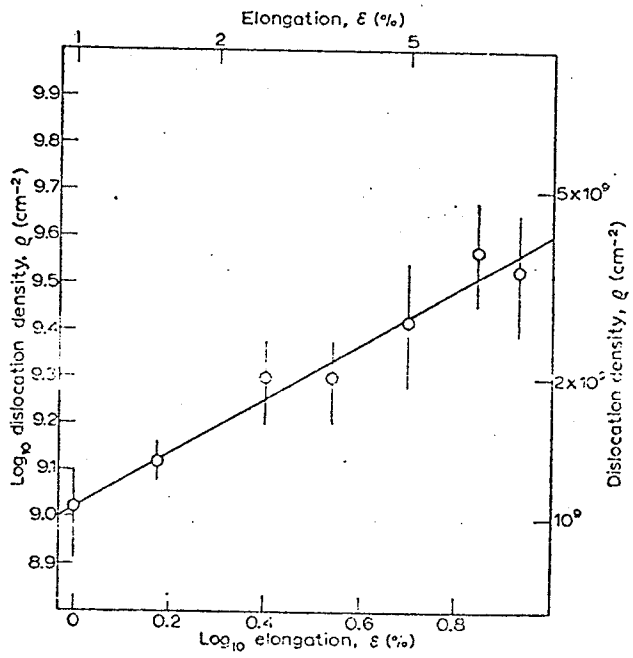

Fig. 10. The variation of the dislocation density with strain in "flash-annealed" niobium.

temperature to <3 kg/mm^2 that edge dislocations were mobile before the apparent proportional limit of the flash annealed niobium, ~ 3.5 kg/mm^2, was reached. As a result of a series of experiments on polycrystalline "flash annealed" niobium Wronski and Fourdeux[27] showed that the dislocation density and structure did not depend on purity and that dipoles, tangles and eventually cells were formed for all purities of the materials studied. The dislocation structures of deformed specimens were very similar to those of less pure niobium or iron. They commented that a new and surprising feature of the results was the observation that the strain rate, which apparently did not influence the dislocation density, had a pronounced effect on the dislocation arrangement. The variation of the dislocation density with strain in flash-annealed niobium is shown in fig. 10.

In a recent investigation Statham et.al.[33] showed that alloying increased the hardening rate of niobium single crystals in stage I but decreased it in stage II. In stage I edge dislocation dipoles were formed and after small deformations of the Nb-Mo crystals, the dipoles are shorter and less concentrated into bundles than in pure niobium. Alloying increased considerably the screw dislocation density of annealed niobium. Screw dislocation structures predominated on decreasing the temperature or increasing the solute content. Harris[9] working on polycrystalline niobium also found that the hardening rate increased with solute content. He showed that after 10% strain at 296^{o}K the reciprocal of cell diameter was linearly

proportional to the respective flow stress of the alloys.

1.3.6 Dislocation Dynamics

Although investigations have been carried out on niobium to study the dynamic nature of dislocation motion, its alloys have received little attention. In the earliest of such studies on niobium crystals Guberman[35] used the etch pit technique and found that the "power law" relationship between the average dislocation velocity and stress was obeyed in the range of velocities between $\sim 2 \times 10^{-7}$ cm. to 3×10^{-2} cm/sec. This relationship was obeyed regardless of temperature (between $77^{o}K$ and $300^{o}K$) or purity and was also the case in neutron irradiated Nb. He obtained different values of m^{*} from the strain rate change or stress relaxation and etch pit techniques. m^{*} did not vary as the inverse of the absolute temperature which should be observed in cases where the rate controlling mechanism of plastic deformation is the overcoming of Peierls stress by the nucleation of double kinks. Evans and Schwenk[36] have determined the values of m^{*} for niobium crystals as a function of temperature and strain from strain-rate sensitivity measurements of σ^{*} and showed that from $158^{o}K$ to $273^{o}K$, m^{*} was independent of strain while it increased at $77^{o}K$ and $113^{o}K$. The value of m^{*} at 5% strain increased from 5.5 at $273^{o}K$ to 27 at $77^{o}K$. They considered that above $158^{o}K$ the mobile dislocation density did not vary significantly with strain, while it did at $77^{o}K$ and $113^{o}K$

and was dependent upon the magnitude of the effective stress required by the imposed strain rate. They suggested that the discrepancy reported by Guberman regarding the temperature dependence of m^* could be accounted for by the utilization of effective stress rather than the applied stress in etch-pit calculations. Using the stress relaxation technique, Gupta and Li[37] have studied m^*, internal stress and work hardening in several b.c.c. metals and alloys. The value of m^* for one zone pass niobium single crystal and commercially pure polycrystal was initially 14 ± 1 at 298^oK and 193^oK, and it decreased with strain to 6 ± 1, the value obtained for three zone pass polycrystalline niobium. They suggested that plastic deformation had some kind of strain-induced purifying effect in niobium as in the three zone pass material m^* was independent of strain. They also found that m^* did not show any strain rate dependence, at least within the limited range of strain rates employed 1.33×10^{-4}/sec. to 33.3×10^{-4}/sec. At strains higher than 4% the internal stress developed at 195^oK was slightly larger than that at 298^oK. The temperature dependence of the flow stress in b.c.c. metals, they concluded, was due to the change of effective stress with temperature.

The dislocation velocity stress exponent, m^* in Nb and Nb-Mo single crystals have been evaluated by Kan[13] at 113^oK, 178^oK and 295^oK as a function of concentration and strain. At 295^oK m^* for pure Nb increased from 3 to $\sim$17 for Nb-5.3 at% Mo. m^* for Nb-2 at% Mo decreased markedly with plastic strain and reached the plateau value beyond 8% strain. The results of earlier studies on dislocation dynamics in Nb and its alloys are summarised in Table IV.

TABLE IV

System	Crystal	Zone Passes	Technique	Strain dependence $m^*f(\varepsilon)$	m^* $f(\dot{\varepsilon})$	m^* $f(^oK)$	m^* f(conc.)	Reference & Year
Nb	single	one & two	etch pit	Dependent	-	very small	-	Guberman[35] (1968)
Nb	single	high purity	strain rate cycling	Independent above 158^oK but depen. below 158^oK	-	Highly depend.	-	Evans & Schwenk[36] (1970)
Nb	single & poly	zero, one & two	stress relaxation	Independent	Indep.	-	-	Gupta & Li[37] (1970)
Nb-Mo	single	high purity	stress relaxation	Independent	—	Highly depend.	Increases with Mo content	Kan[13] (1971)
Nb-O	single	high purity	stress relaxation	—	—	Highly depend.	Increases with O_2 content	Ravi & Gibala[38] (1972)

1.4 Experimental Procedure

1.4.1 Materials and Alloy Preparation

The niobium and zirconium used in the present study were initially 99.8% and 99.9% pure respectively.

Electron Beam Zone Refining of Nb:

The 0.5" diameter Nb rod was cold swaged to ∿0.25" dia and cut into 11" long rods. These rods were zone refined in an MRC unit by giving a first pass of 9"/hour and a second pass of 4.5"/hour in the same direction. The zone refining parameters were as follows - current ~75 mA, volts ~3.5 K.V. and pressure lower than 10^{-6} mm of mercury. The rod was cut at ~0.75" away from the start and ~0.75" before the finishing point. The zone refined metal so obtained, was used for preparing the alloys, while the remnants were argon arc melted and swaged again to ~0.25" size for zone refining. This time three passes - first at the rate of 9"/hour and the second and third at 4.5"/hour (all in the same direction) were given. The zone refined portion was cut as before and was used for unalloyed Nb specimens.

Melting and Alloying:

Amounts of zone refined Nb and pure Zr were accurately weighed, so as to get pure Nb, and ~1 at% Zr, ~3 at% Zr and ~5 at% Zr alloys of Nb. The weighed stock was melted in an argon arc furnace with a partial pressure of argon. Each alloy was turned over and

remelted 5-6 times to ensure its homogeniety. On again weighing the alloys, no loss of Zr was found.

Fabrication of the Alloys:

Pure Nb - The ∿0.5" dia. cast ingot was cold swaged to∼0.4" dia. size to give it a uniform cross section and was annealed at 1000°C for 3 hours in vacuum. This ingot was then given ∿30 - 40% cold reduction and an intermediate anneal at 980°C/3 hrs. In this way, with several cold reductions and intermediate anneals the ingot was reduced to 0.04" and 0.02" thick strips. The 0.04" thick strip was for tensile test specimens while the 0.02" thick strip was used for electron microscopy specimens.

1, 3 and 5 at% Zr Alloys

As before, the alloy ingots were first cold swaged to 0.4" dia. size and annealed at 1250°C for 48 hours in argon. After∼15-20% reduction by cold rolling, these were annealed at 1250°C/24 hours. With subsequent cold rolling and intermediate annealing, the alloys were finally cold rolled to 0.04" and 0.02" thick strips and cut into tensile specimens, fig. 11. In order to obtain a recrystallised structure having uniform grains of size∼25-30 μ (diameter), the following annealing treatments were used.

1. Pure Nb was annealed at 1100°C for 3 hrs. and
2. 1, 3 and 5 at% Zr alloys were annealed at 1300°C for 4.5 hrs.

Along with microstructure, the hardness values were used as a check for the correct and suitable annealing treatments. For the optical metallography of Nb and Nb-Zr alloys the solution (1 part Hf (52%) + 1 part H_2SO_4 + 1 part H_2O + few drops of H_2O_2), at room temperature was found very satisfactory.

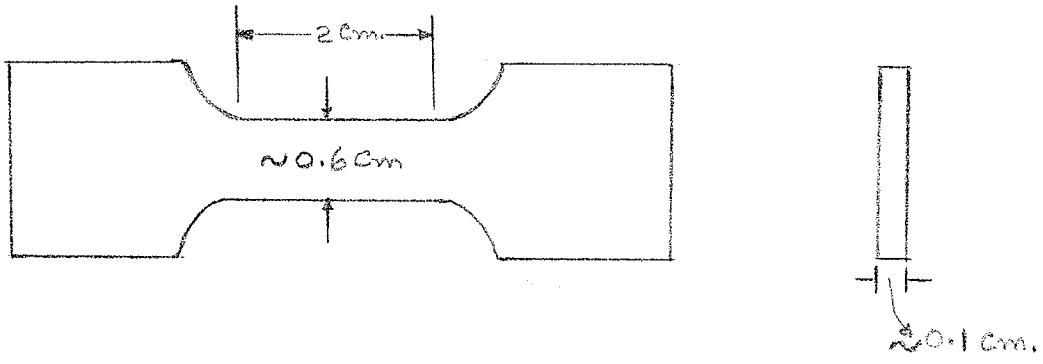

Figure 11: Tensile test specimen used in this investigation.

1.4.2 Testing Procedure

Tensile tests on specimens were performed on an Instron machine at a strain rate of 4.25×10^{-4}/sec. First, the specimen was strained upto a certain level, a strain rate change (increased by a factor of 10) was made and then the stress relaxation test was performed for 4-5 minutes. The specimen was then, unloaded and reloaded. After a further increment of strain, the above tests were repeated. Thus, these tests were made at 8-9 strains (upto $\sim$ 20% plastic strain) and 6 temperatures from 77 to 490^{o}K, using suitable temperature baths. The schematic representation of experimental procedure is given in fig. 12.

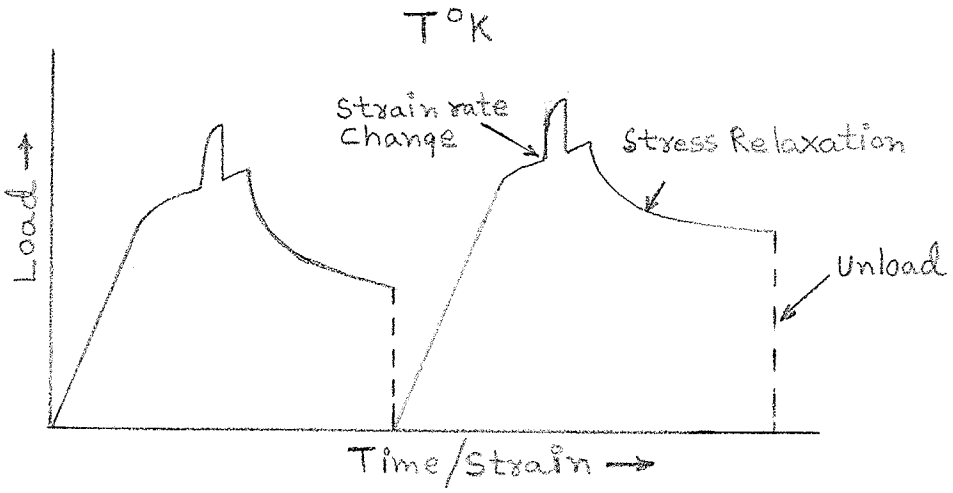

Figure 12: Schematic representation of experimental procedure.

All the specimens for 77^{o}K test were predeformed to about 2% plastic strain at 290^{o}K to avoid twinning.

The chemical analysis of Nb and Nb-Zr alloys used in this investigation are given in table V.

TABLE V

Chemical Analyses of Nb-Zr Alloys

Elements \ Alloys	Nb	Nb-0.87at%Zr	Nb-3at%Zr	Nb-4.7at%Zr
O_2 in µg/gm	60	90		
H_2 in µg/gm	5	2		
C in µg/gm	120	100		
N in µg/gm	8	6		
Ta in µg/gm	160	185		
Zr in wt%	-	0.87	3.0	4.7

From these tests, it was possible to find the values of σ^*, σ_μ, m^*, n, V^*, ΔH, at various strains and temperature for the 0, 1, 3 and 5 at% Zr alloys. Li's analysis[39] was employed to determine the values of σ^*, σ_μ and m^* values.

The 0.02" thick specimens were strained to ~3% and ~14% at 77°K, 215°K and 290°K and then thinned chemically to ~ 0.005" thickness in a (70% HNO_3 + 30% Hf) solution. The specimens for transmission electron microscopy were prepared by electrolytic polishing with no stirring in a fresh (87% H_2SO_4 + 13% Hf) electrolyte at room temperature. The specimen edges were lacquered and electropolished at ~21V and ~0.1 A/cm^2. These foils were examined in an EM300 Philips electron microscope at 100 K.V.

RESULTS

2.0 Deformation Characteristics of Nb-Zr Alloys.

2.1 Nature of the Stress Strain Curves

The true stress vs plastic strain curves for pure Nb and Nb-Zr alloys, deformed at temperatures $77^{o}K$, $215^{o}K$, $290^{o}K$ and $490^{o}K$, are shown in figs. 13-16. It is observed that alloying, in general, has raised the level of flow curves above that for niobium.. However, at $77^{o}K$ the curves for the Nb-Zr alloys are below that for pure Nb. At $215^{o}K$, this behaviour of alloy softening is seen in only Nb-0.87 at% Zr upto $\sim$2% plastic deformation and is not present in higher alloys.

The effect of temperature on the stress-strain curves of Nb and Nb-Zr alloys is shown in figs. 17-20. It is seen that the shape of the curves remains essentially the same for all compositions and temperatures, but the slope (work hardening rate) increases with decrease in test temperature. At $77^{o}K$ the initial rate of work hardening is much higher than that at higher temperatures.

2.2 The Flow Stress

The occurrence of yield point in niobium and its alloys depended upon the temperature of the test and the alloy content. Therefore, in the present study the stress at 0.2% offset strain was taken as the yield stress and stresses at higher strains were

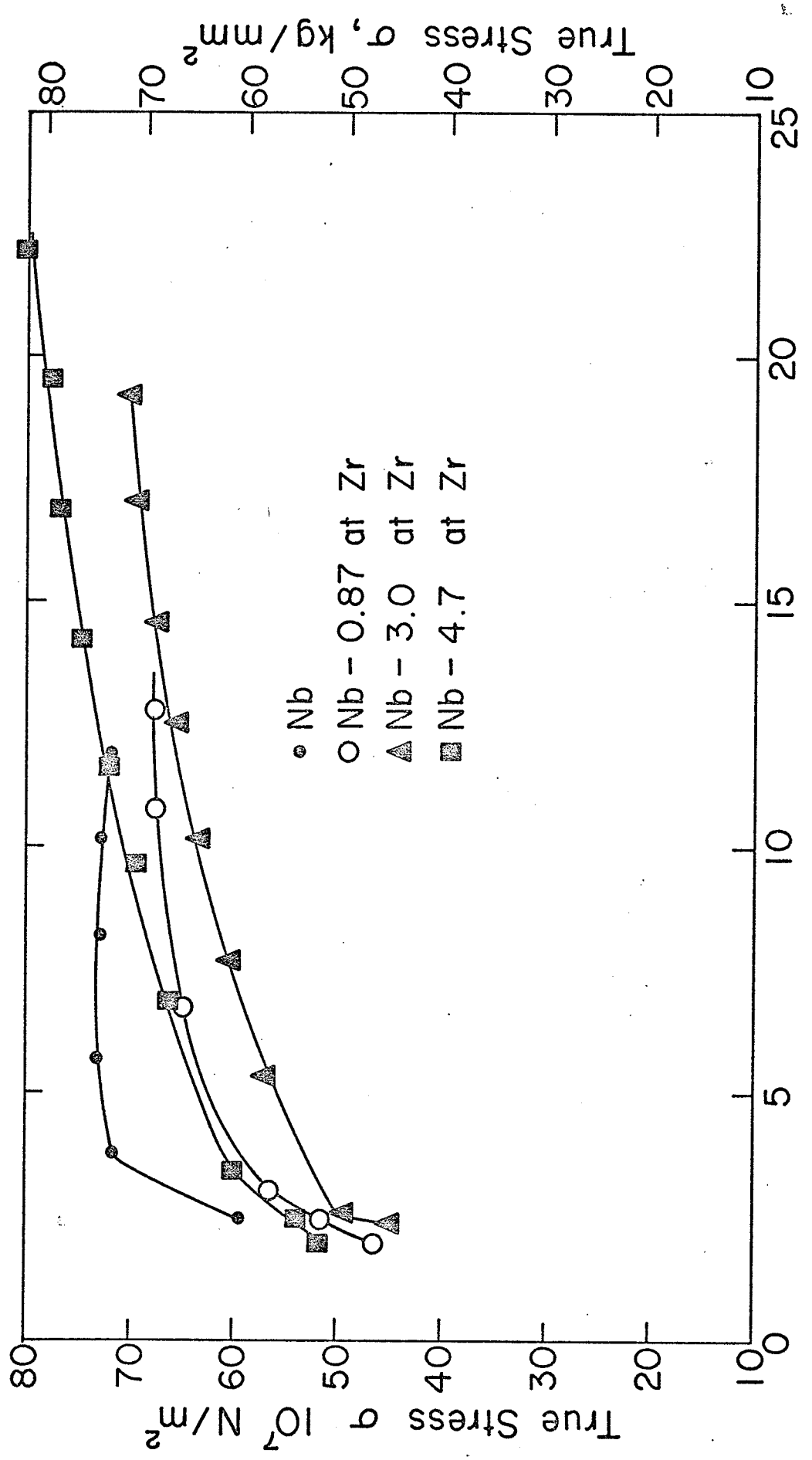

Figure 13: True stress Vs plastic strain for Nb and Nb - Zr alloys at 77^{o}K.

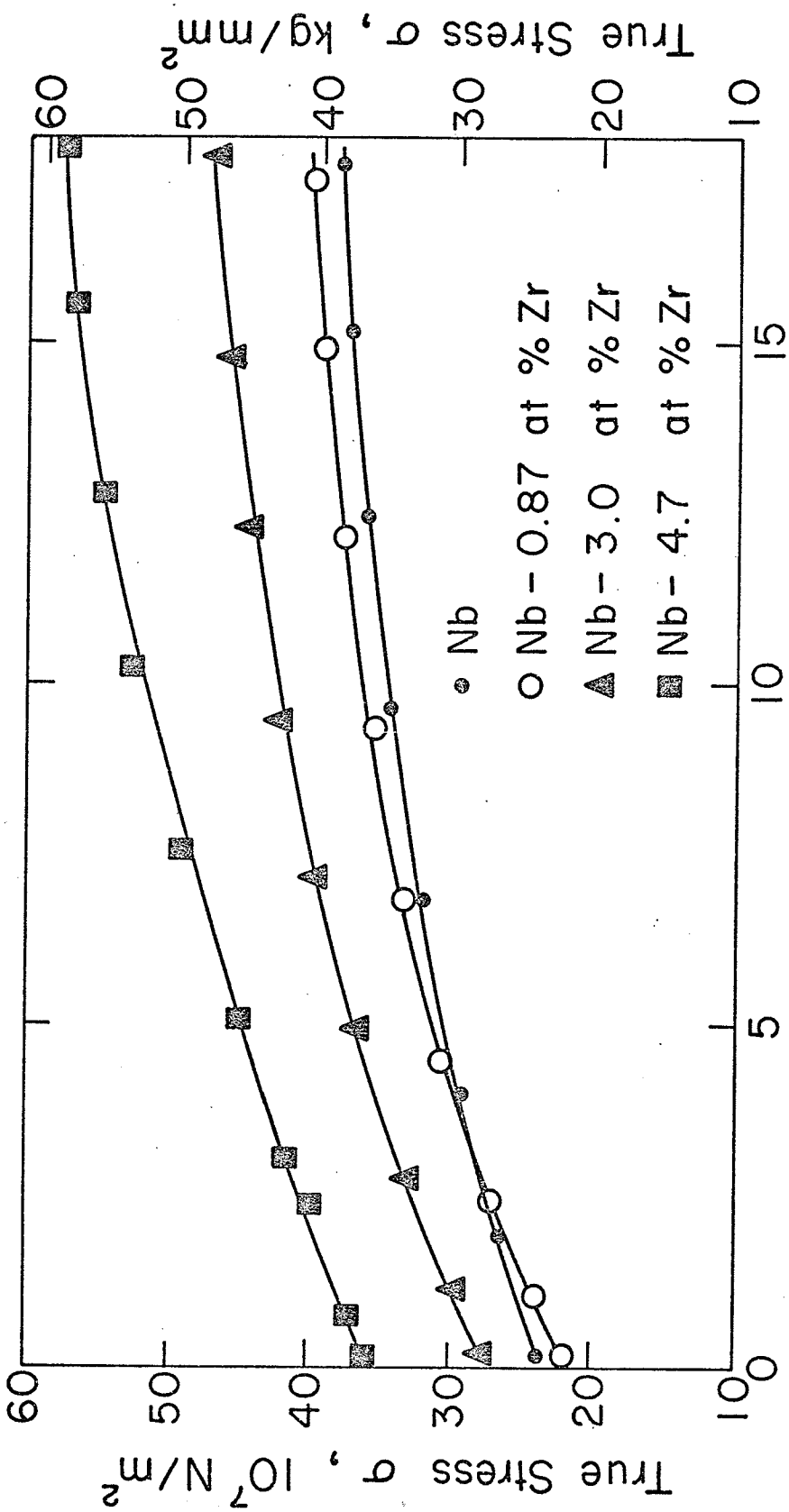

Figure 14: True stress Vs plastic strain for Nb and Nb - Zr alloys at 215°K.

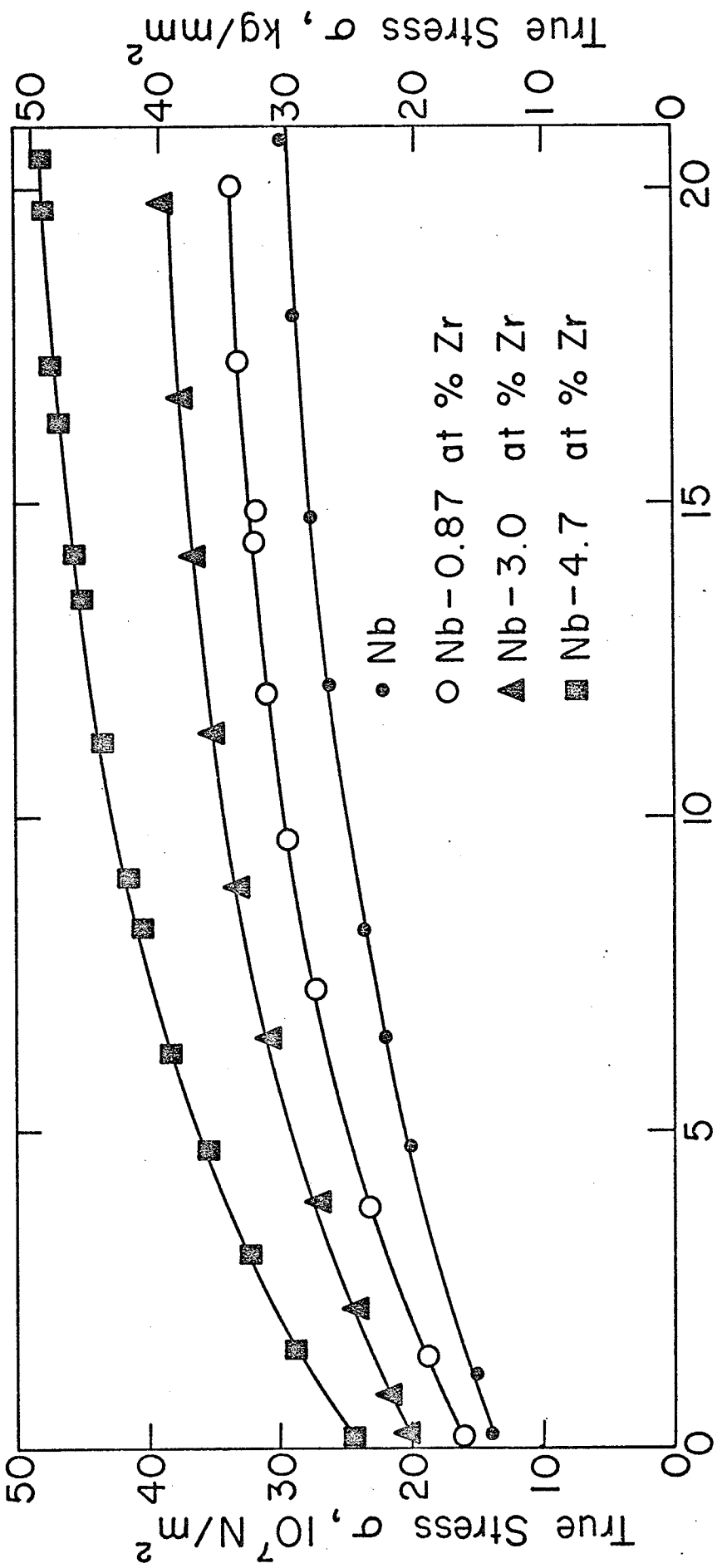

Figure 15: True stress Vs plastic strain for Nb and Nb - Zr alloys at 290°K.

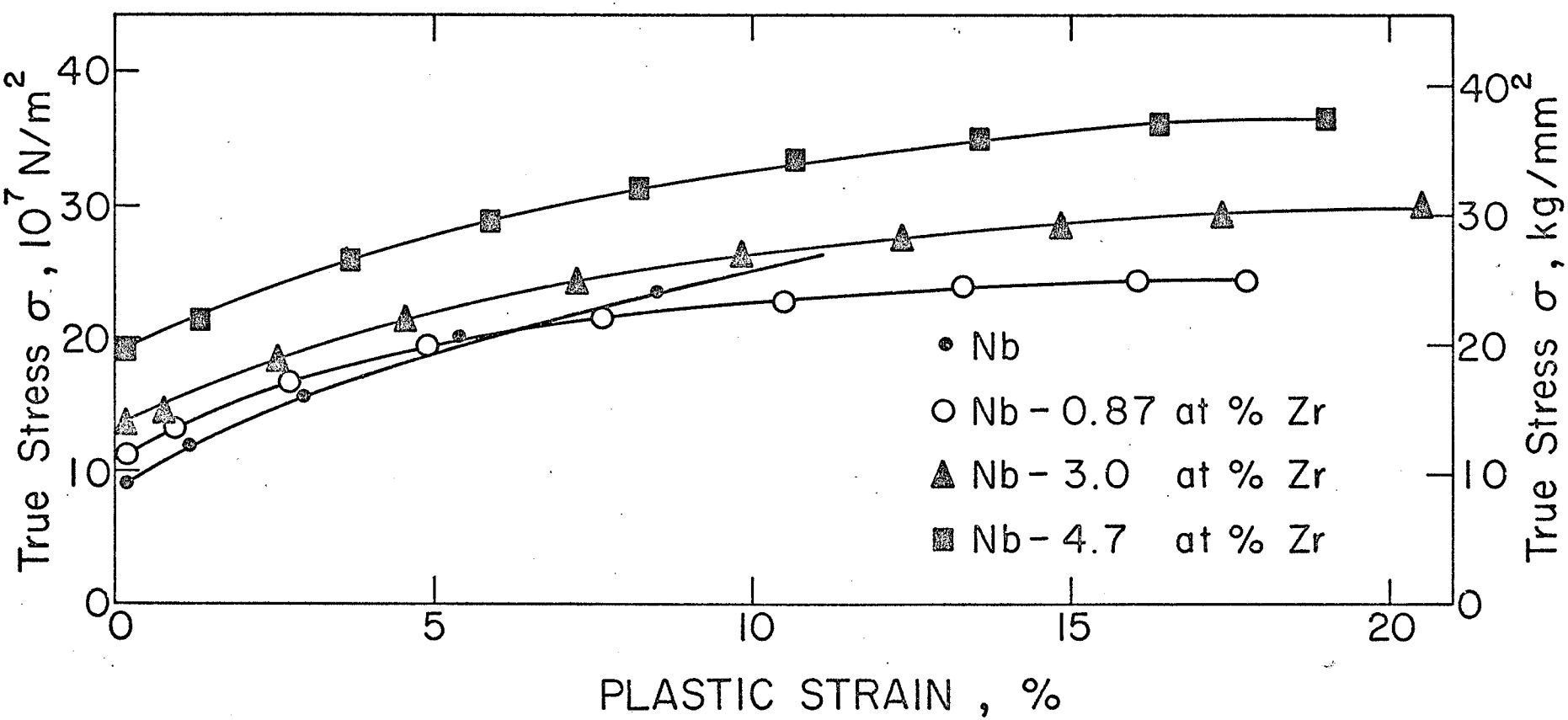

Figure 16: True stress Vs plastic strain for Nb and Nb - Zr alloys at 490^{o}K.

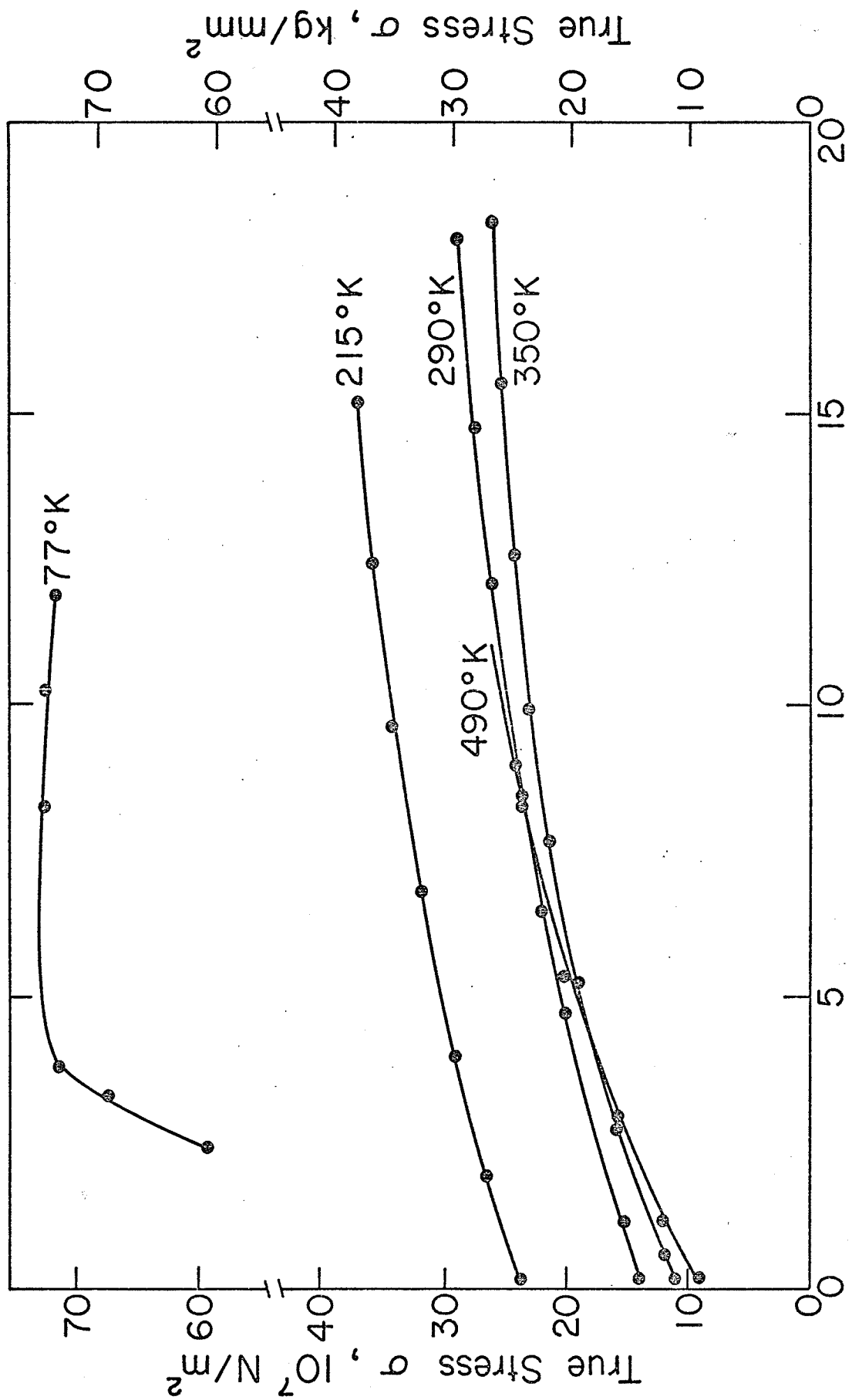

Figure 17: True stress Vs plastic strain for Nb at various temperatures.

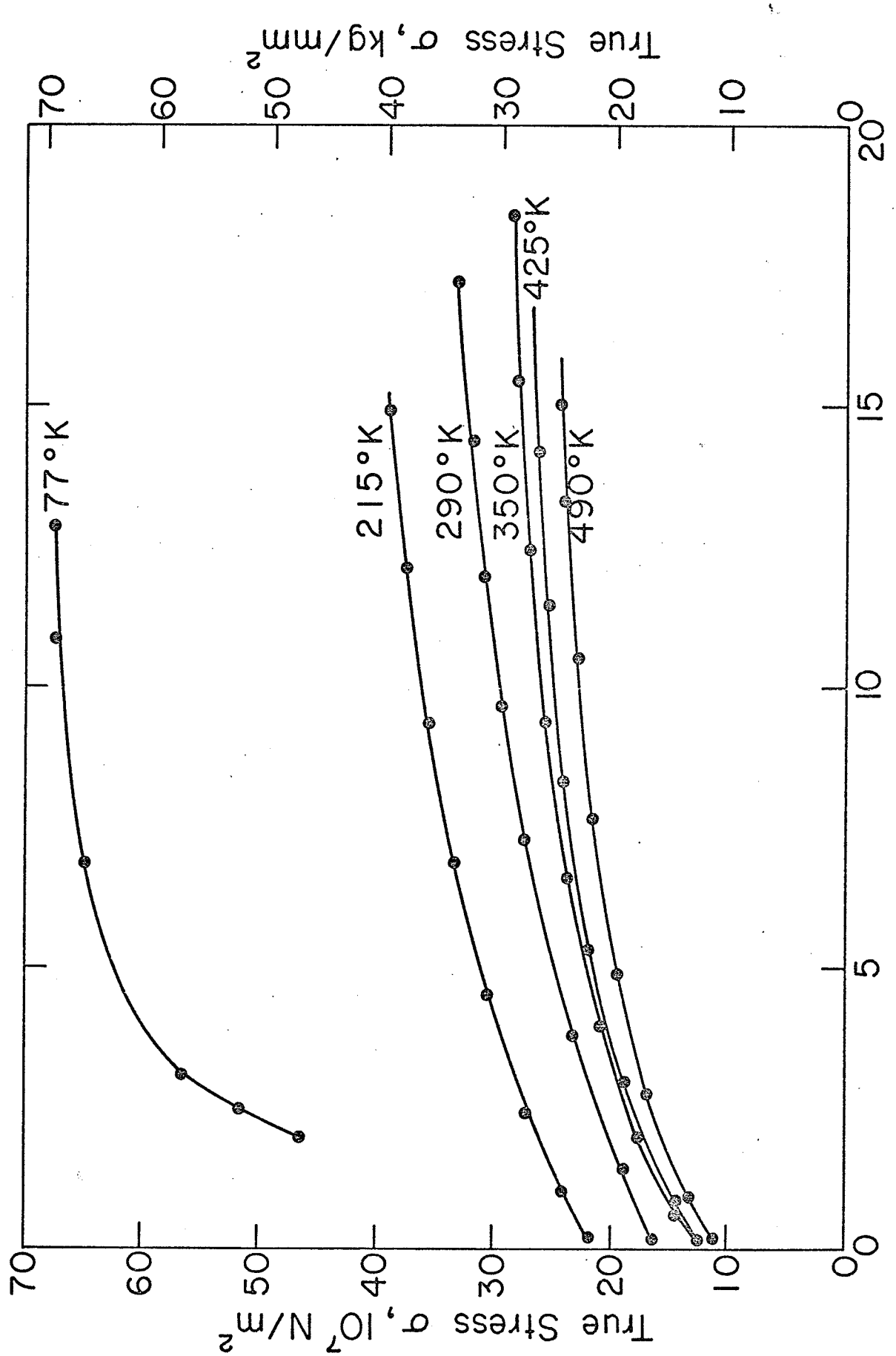

Figure 18: True stress Vs plastic strain for Nb - 0.87 at%Zr at various temperatures.

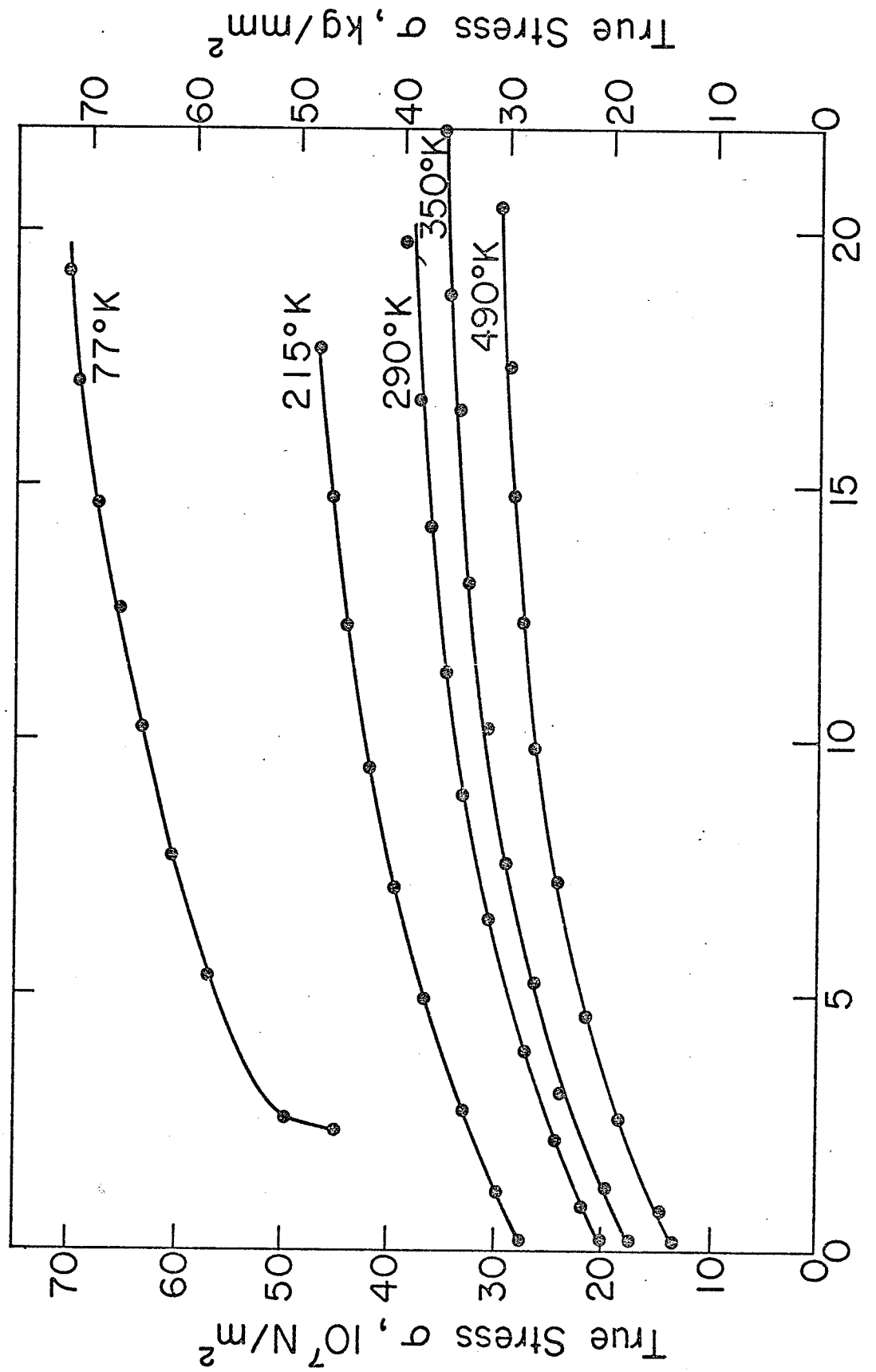

Figure 19: True stress Vs plastic strain for Nb - 3.0 at%Zr at various temperatures.

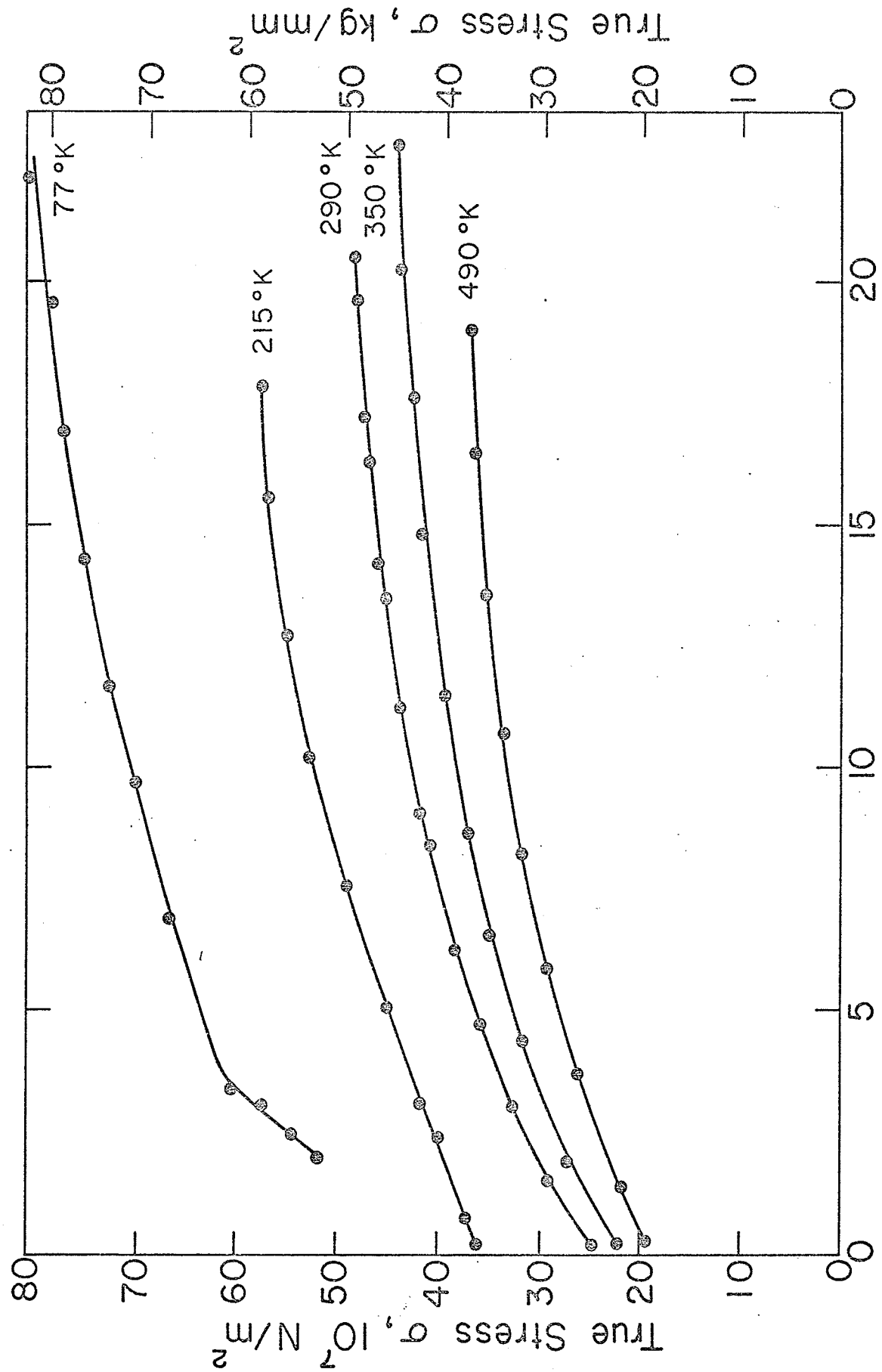

Figure 20: True stress Vs plastic strain for Nb - 4.7 at%Zr at various temperatures.

called flow stresses at those plastic strains.

2.2.1 The Concentration Dependence of Yield:

The flow stress at room temperature is plotted as a function of concentration for various plastic strains in Fig. 21. A linear relationship is observed between stress at any strain and the Zr content. This behaviour is seen in the temperature range of 290°K to 490°K but at 215°K and 77°K, solution hardening is preceded by alloy softening which is more pronounced at 77°K, fig. 22. Alloy softening has been observed extensively at subatmospheric temperatures in several b.c.c. metals (Fe, Ta)[20,21].

2.2.2 Concentration and Strain Dependence of σ^* and σ_μ

The two components, thermal and athermal, of the flow stress at room temperature are shown as a function of plastic strain and concentration in fig. 23 and fig. 24 respectively. It is readily observed from fig. 23 that the effective stress decreases slightly with strain upto ~5% and then remains essentially constant. Fig. 24 shows that the athermal stress σ_μ, unlike the thermal stress, increases with plastic strain.

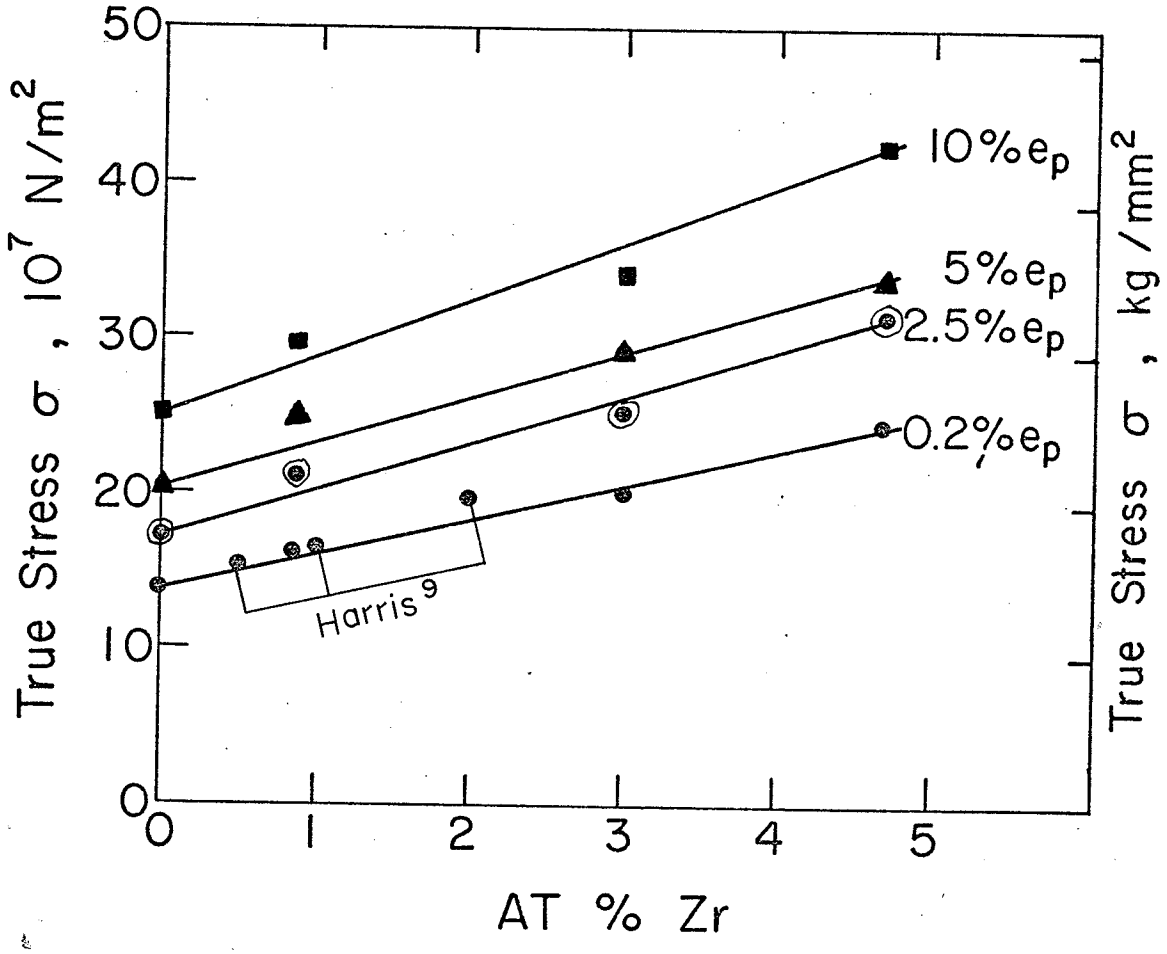

Figure 21: True stress Vs concentration for various plastic strains, e_p at 290°K.

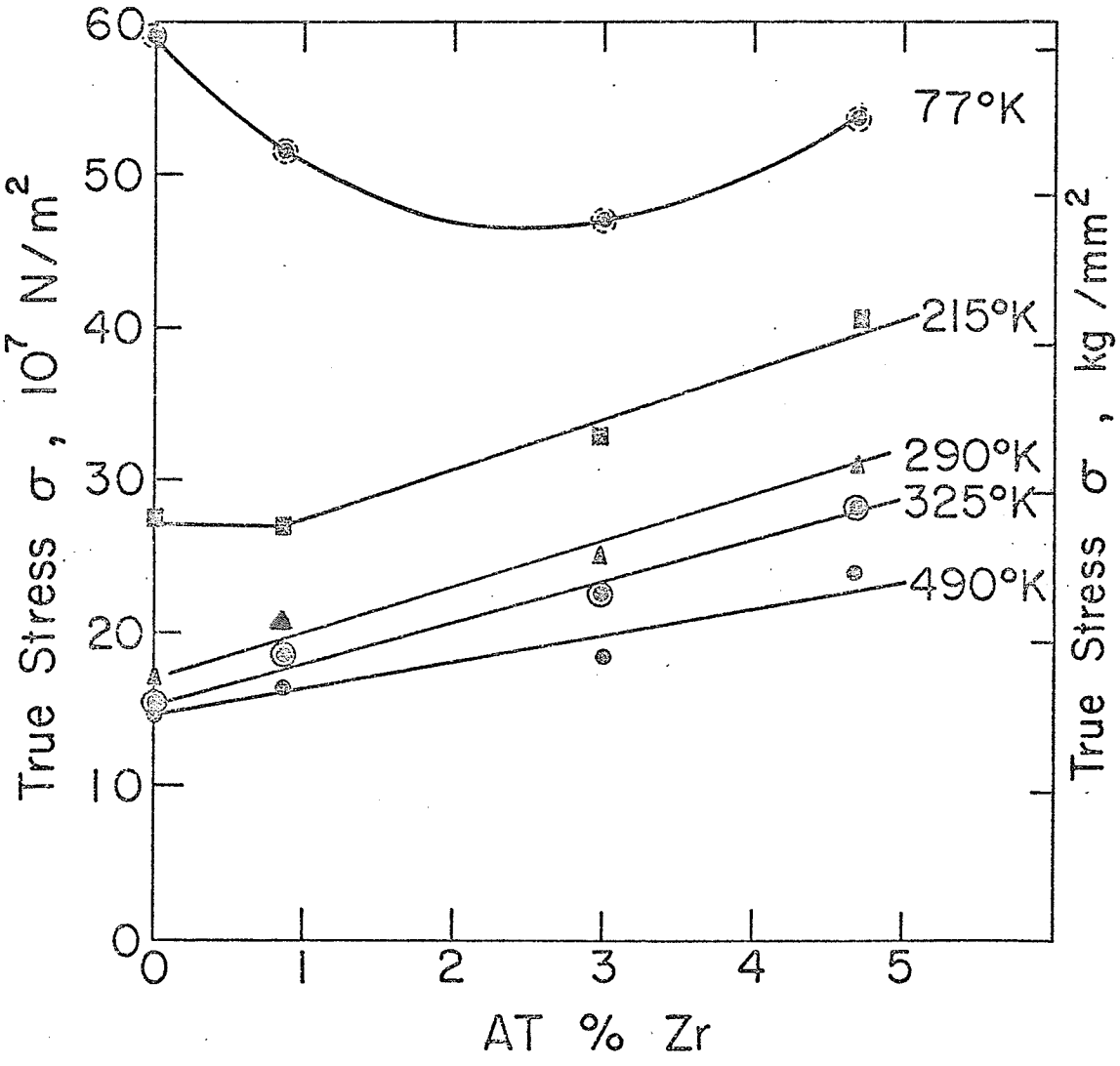

Figure 22: True stress Vs concentration at 2.5% plastic strain at various temperatures.

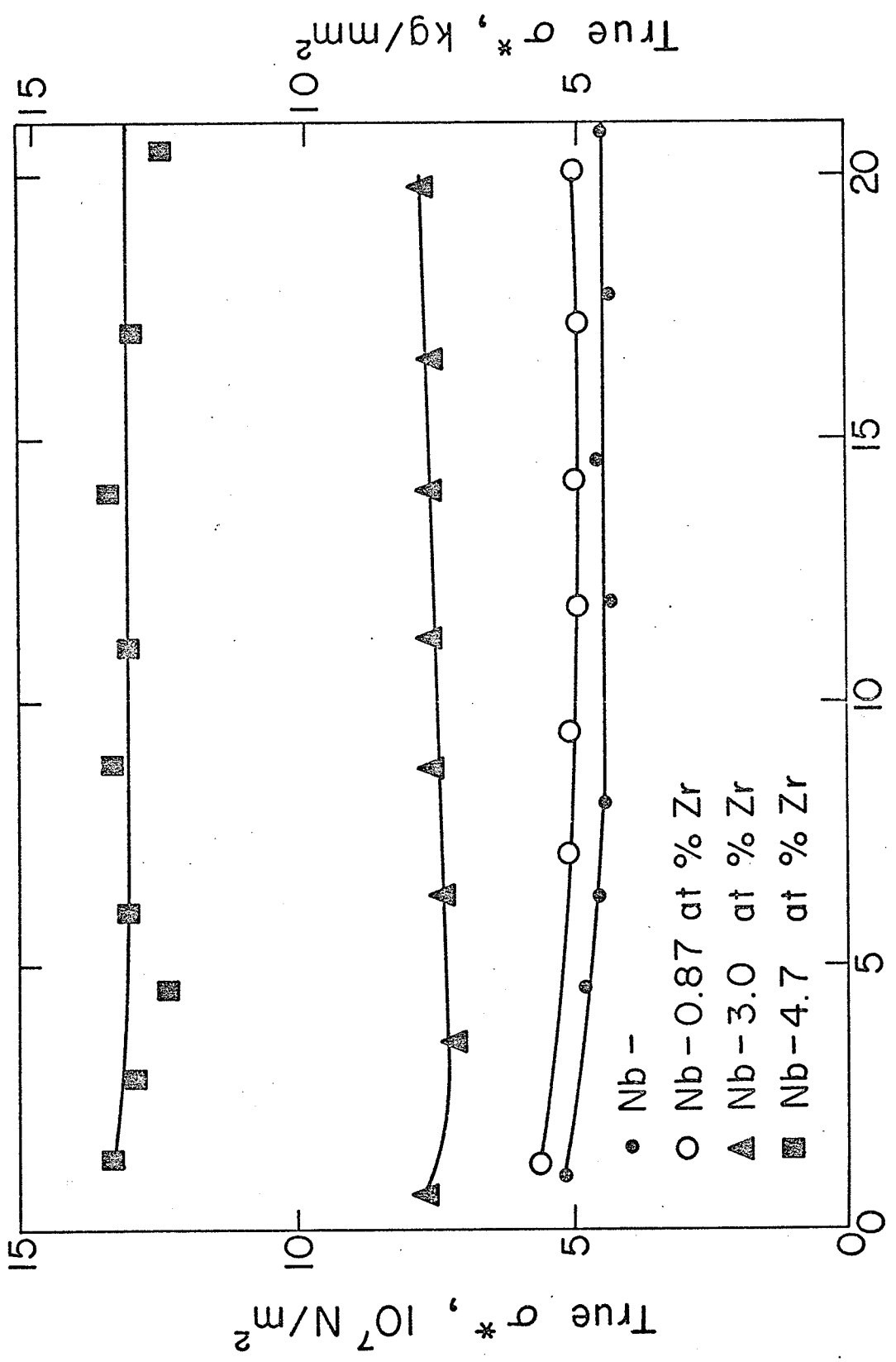

Figure 23: Thermal stress σ* Vs plastic strain for Nb and Nb - Zr alloys at 290°K.

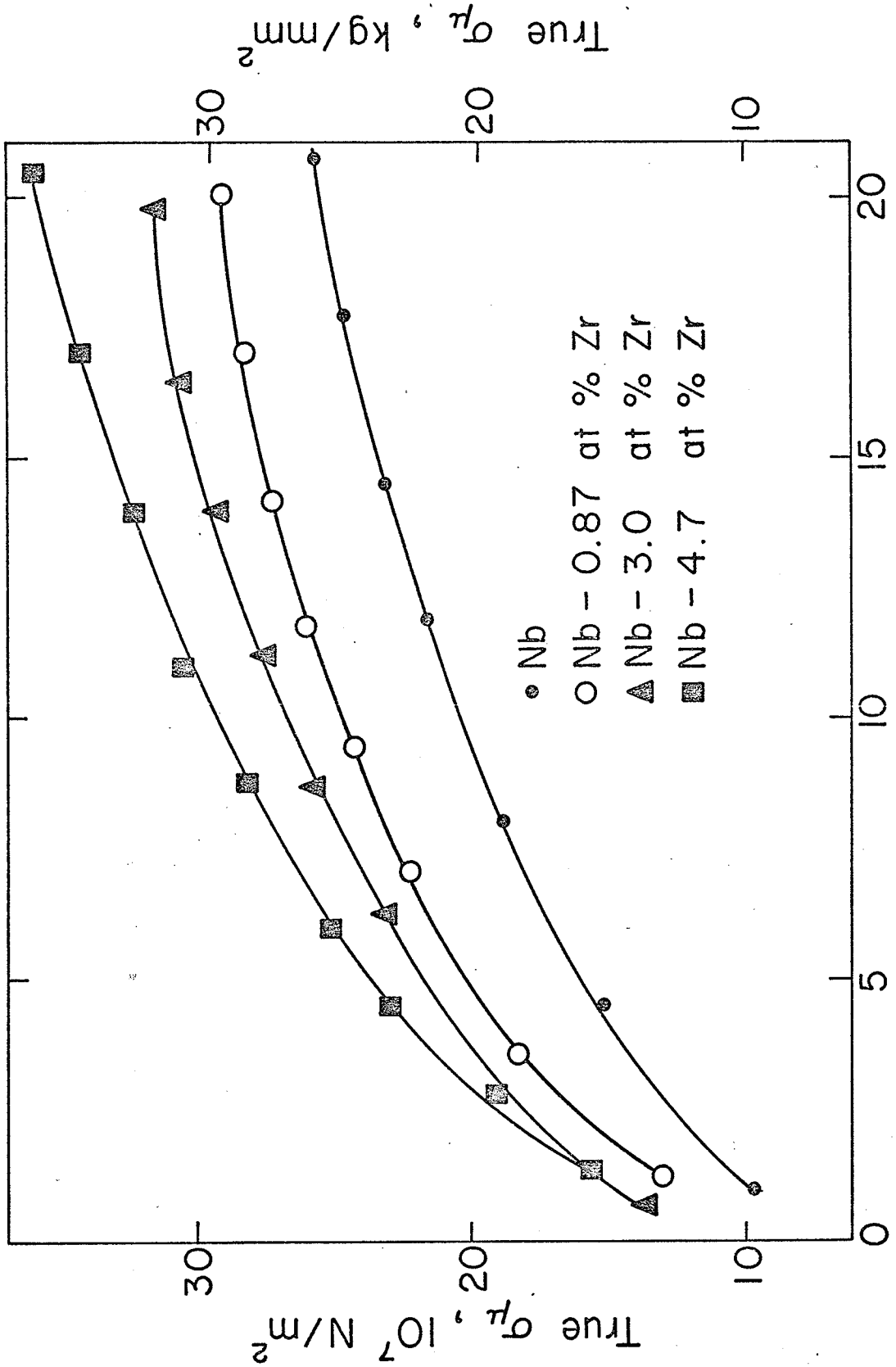

Figure 24: Athermal stress $\sigma\mu$ Vs plastic strain for Nb and Nb - Zr alloys at 290^{o}K.

2.2.3 The Temperature Dependence of Flow Stress

The effect of temperature on flow stress at 2.5% plastic strain is shown in fig. 25. Although σ^* depended upon strain upto ~5%, fig. 23, the 2.5% strain was selected because the 77°K specimens were predeformed to about 2% strain at 290°K and thus 2.5% was about the strain at which the flow stress was available at all the test temperatures. It is observed that the stress level was raised with the addition of solute but this was not so below the softening temperatures, Ts. At 77°K, the flow stress decreased with increasing Zr content upto 3 at% Zr while for Zr contents greater than this the flow stress increased again for increasing solute content. It is seen that the flow stress temperature curve contains three portions:

a) A steep (approximately linear) portion extending from 77°K upto ~200°K in which region the flow stress was markedly dependent upon temperature. This dependence decreases with increase in Zr content.

b) A transition region where the change in flow stress was much slower than that in the linear region. This region extends from ~200°K to 350°K in pure Nb whereas in the alloys the higher temperature limit seems to increase with concentration. In any case, this portion of the curve for 3 and 4.7 at% Zr alloys is very gradual and a correct determination of the higher temperature limit is difficult.

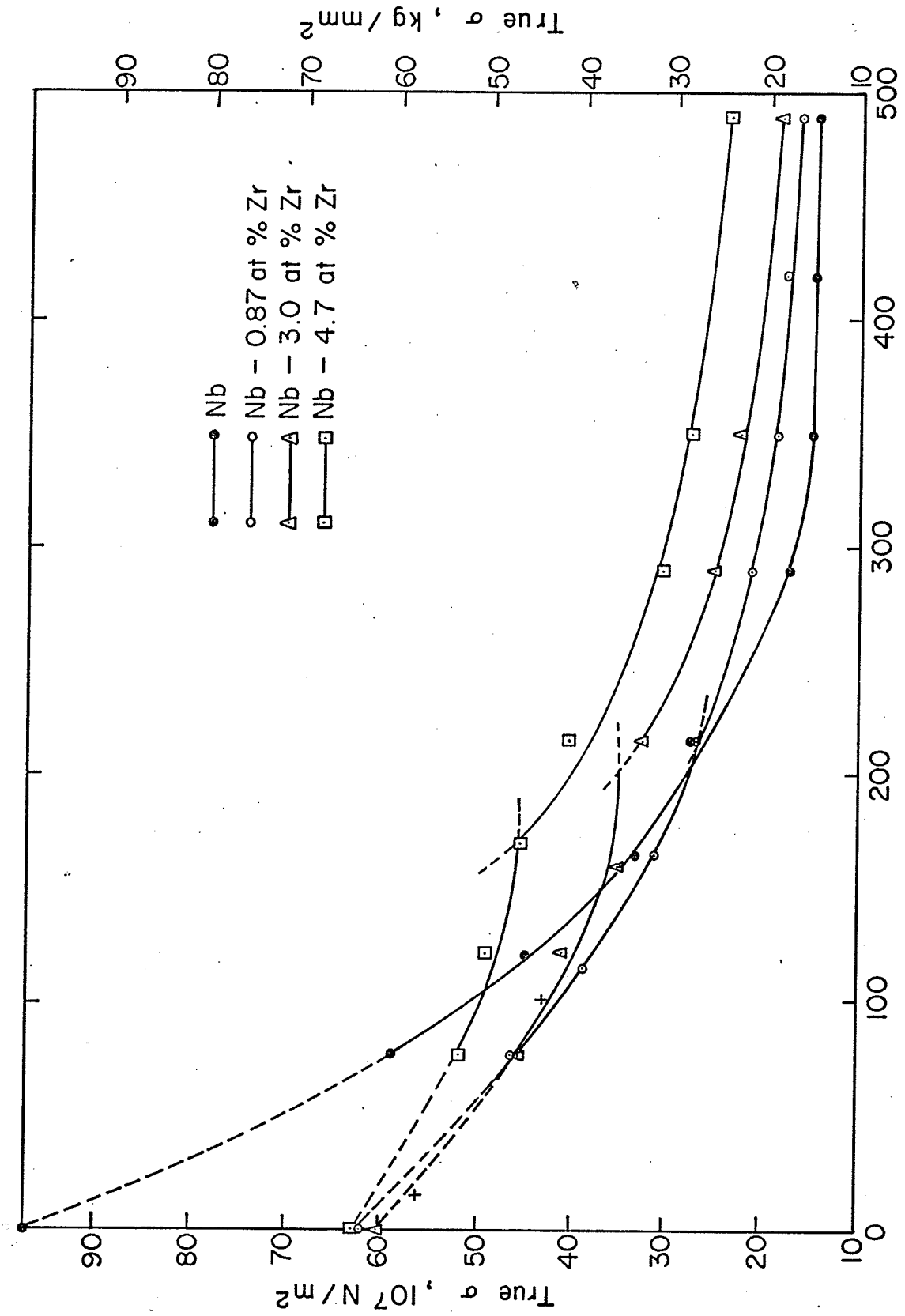

Figure 25: Flow stress σ at 2.5% plastic strain Vs temperature for Nb and Nb - Zr alloys.

c) An approximately horizontal portion where the change in stress is equal to the change in shear modulus with temperature. However, in the case of alloys the slope increases slowly with Zr content which reflects the fact that true athermal behaviour is not achieved until temperatures considerably higher than $350^{o}K$ are reached. Therefore, while in pure Nb the thermal component σ^{*} had become zero at $\sim 350^{o}K$, in the alloys it was still finite and decreasing with increase in temperature.

2.2.4 The Strain and Temperature Dependence of σ^{*} and σ_{μ}

The strain and temperature dependence of σ^{*} for the alloys is shown in figs. 26-29. Although in certain cases σ^{*} decreases slightly upto $\sim 5\%$ strain, it is essentially independent of strain at all the temperatures. It is seen that in all the alloys, the level of σ^{*} rises considerably with decrease in temperature.

In figs. 30-33 the athermal stress σ_{μ} for the alloys is shown as a function of plastic strain at various temperatures. It is seen that for all the alloys, σ_{μ} increases with strain at all temperatures. Another noticeable feature of these curves is that the separation between any two curves for a fixed composition is sensitive to the amount of plastic strain and this separation increases with strain. The curves in figs. 30-33 also show that at all strains, σ_{μ} is temperature dependent and it increases as the temperature decreases. It should also be noticed that the difference in σ_{μ} for all the strains at any two temperatures decreases with an increase in the Zr content.

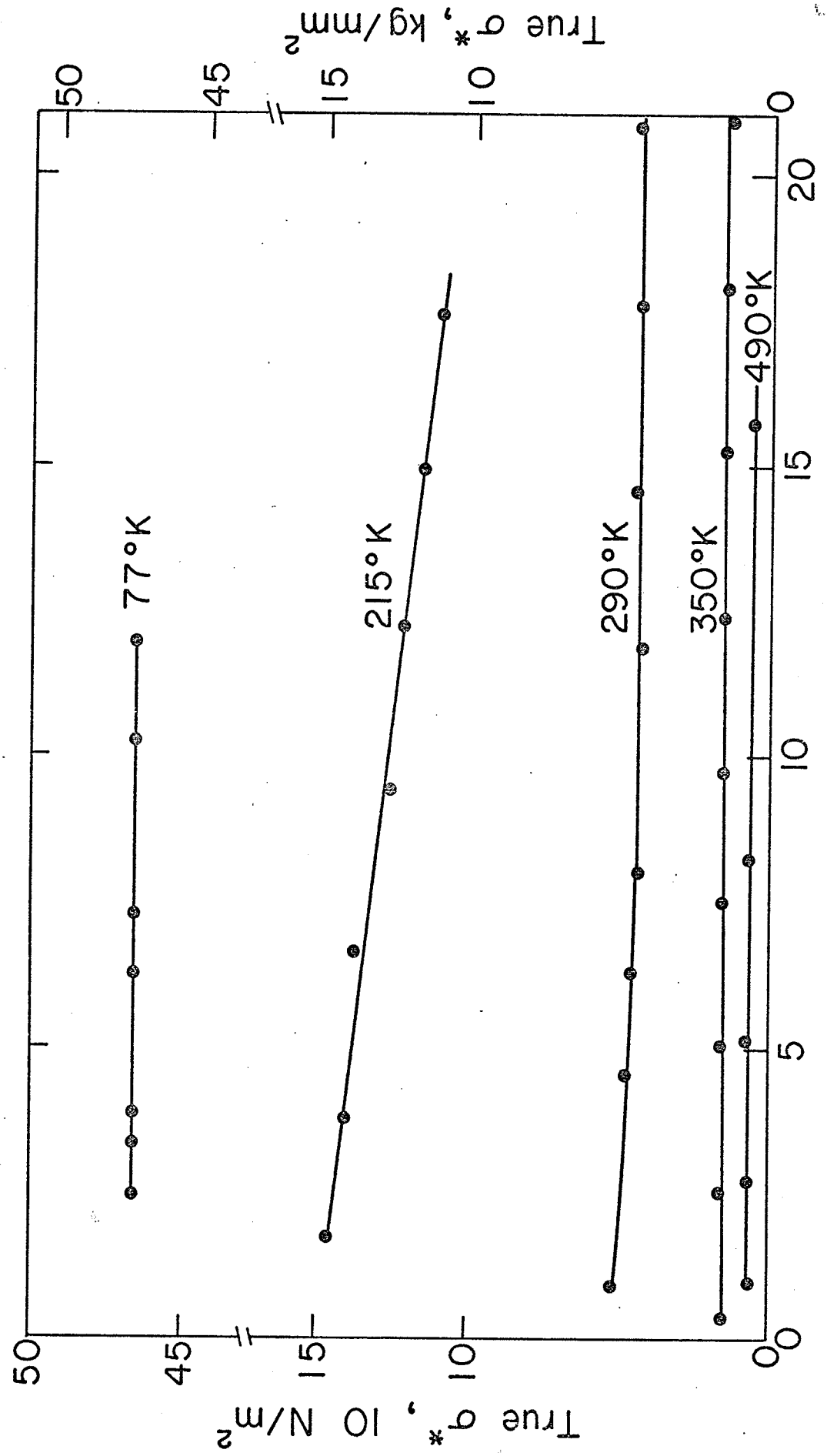

Figure 26: Thermal stress σ* Vs plastic strain for Nb at various temperatures.

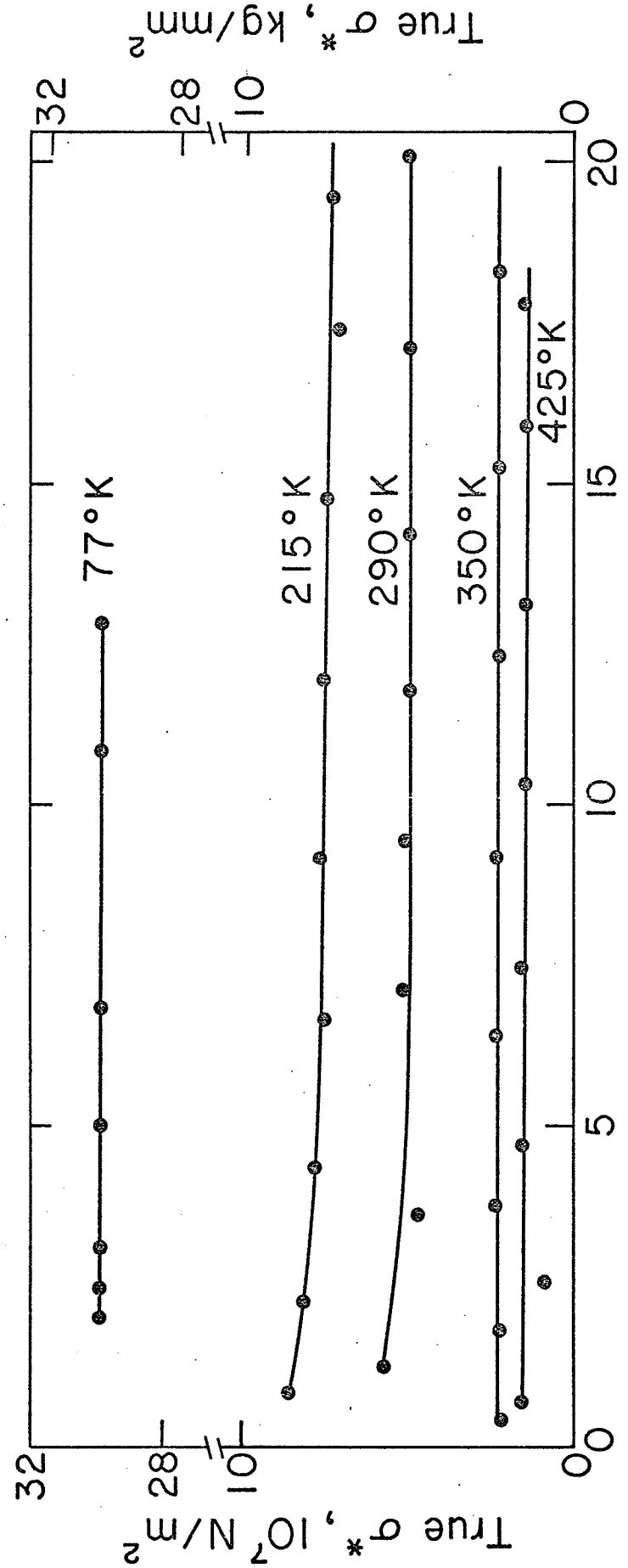

Figure 27: Thermal stress σ* Vs plastic strain for Nb - 0.87 at%Zr at various temperatures.

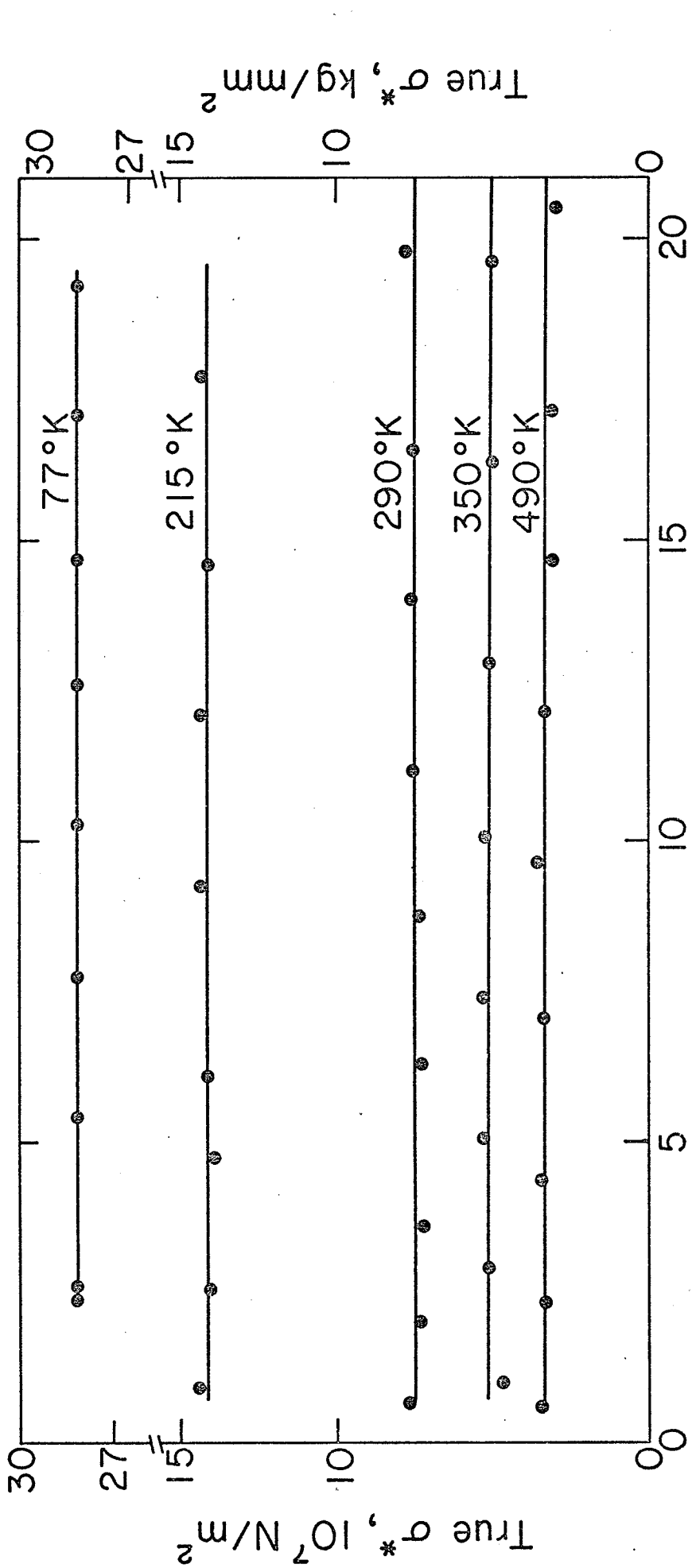

Figure 28: Thermal stress σ* Vs plastic strain for Nb - 3.0 at%Zr at various temperatures.

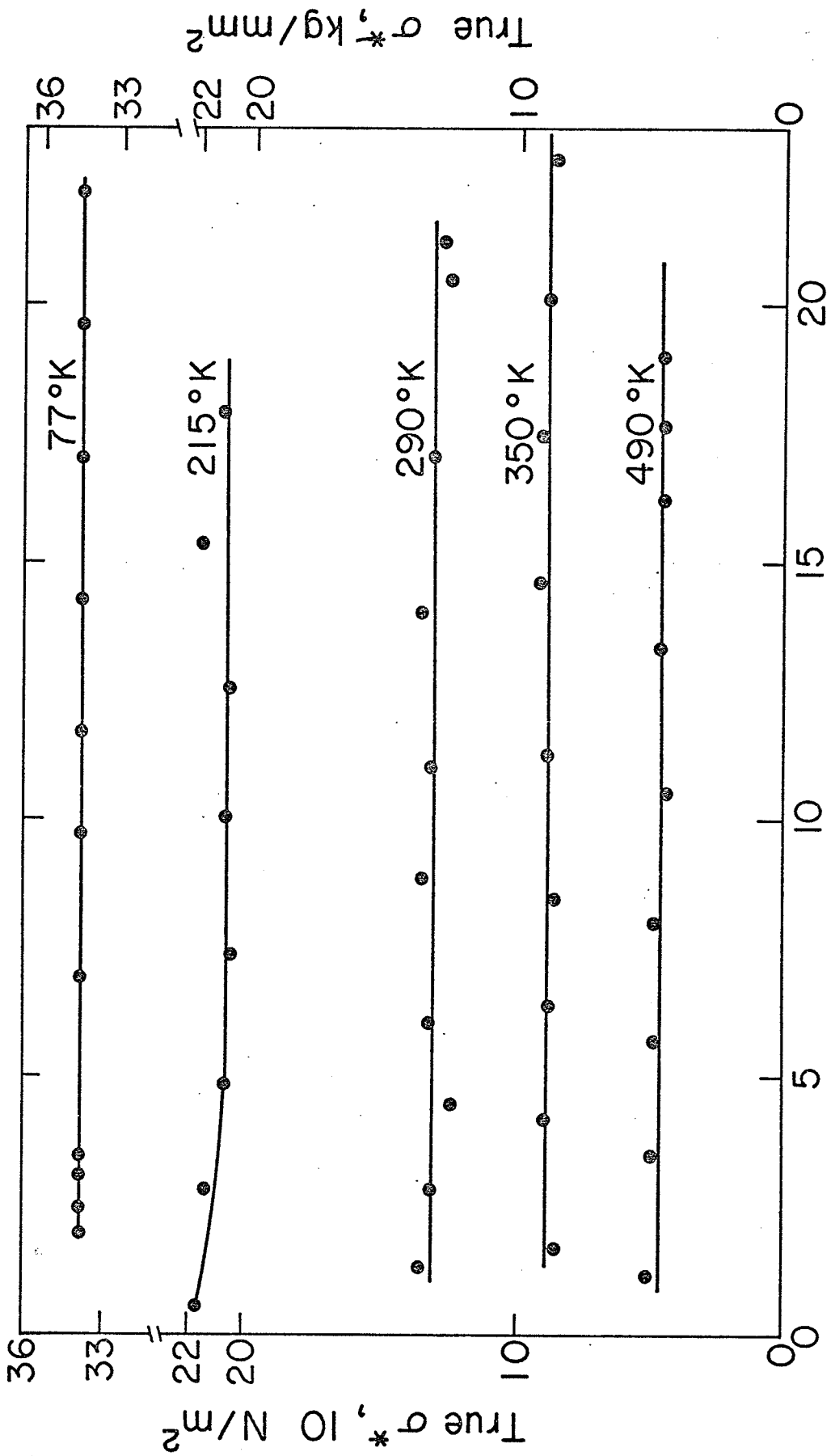

Figure 29: Thermal stress σ* Vs plastic strain for Nb - 4.7 at%Zr at various temperatures.

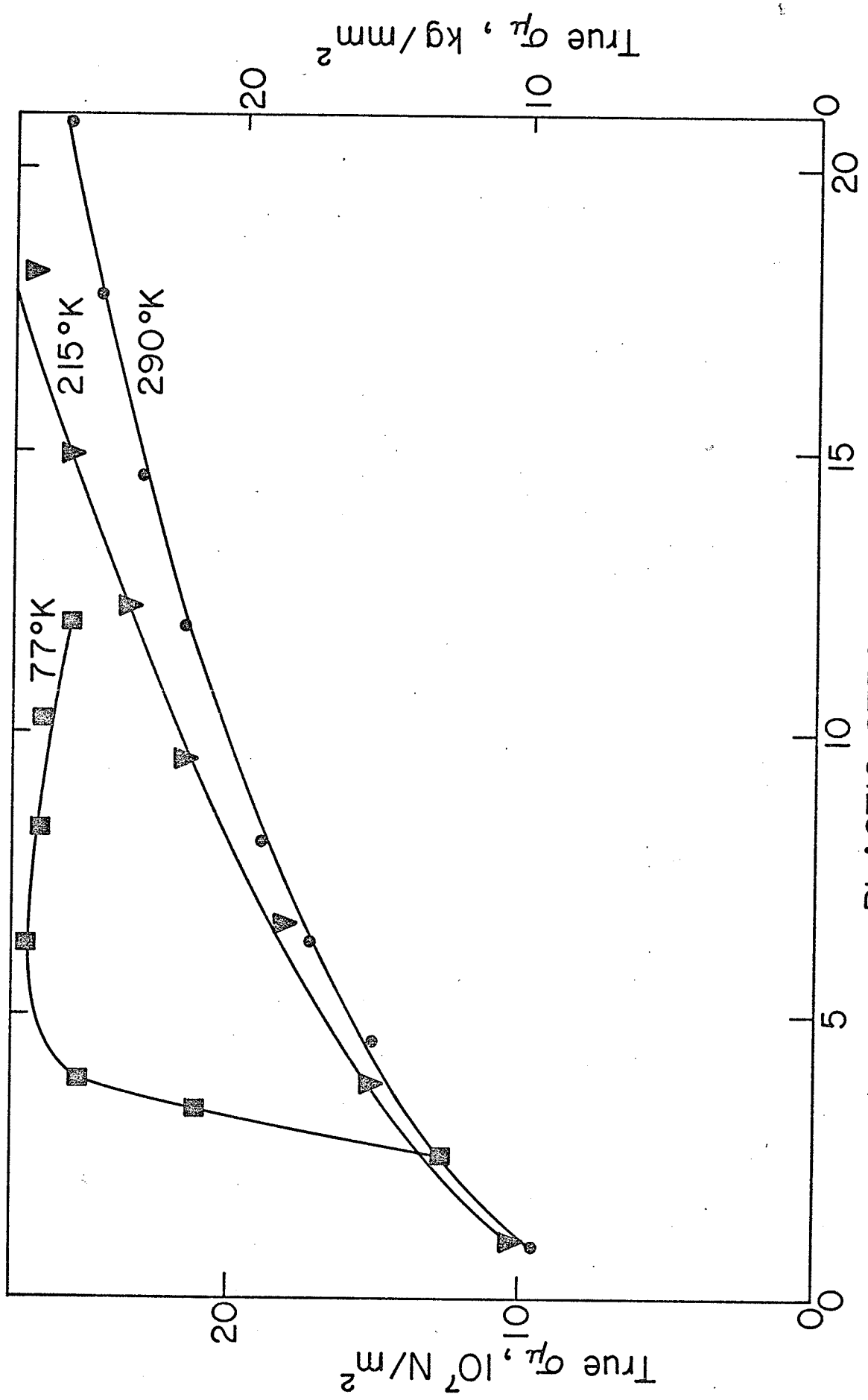

Figure 30: Athermal stress $\sigma\mu$ Vs plastic strain for Nb at various temperatures.

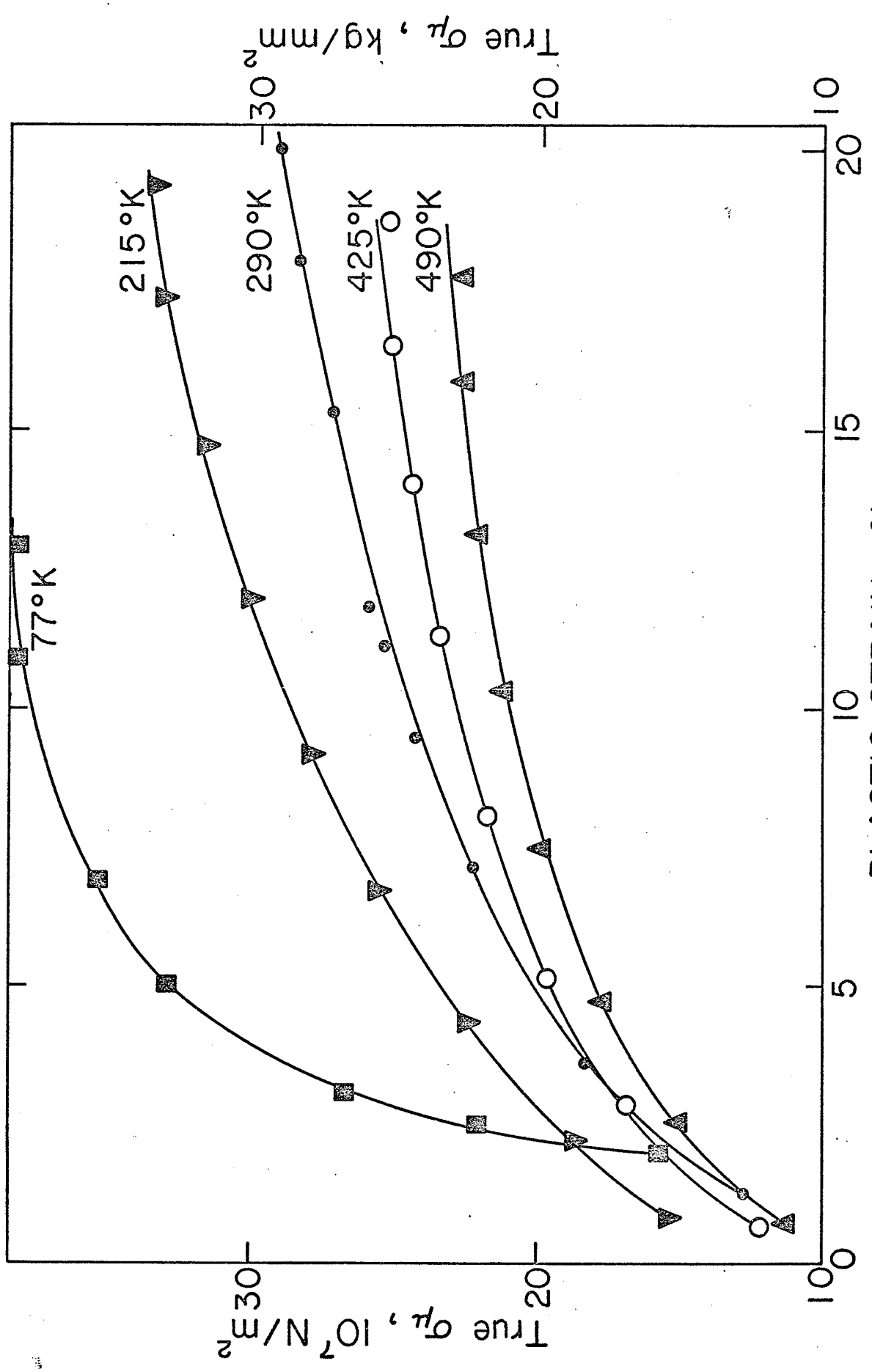

Figure 31: Athermal stress $\sigma\mu$ Vs plastic strain for Nb-0.87 at%Zr at various temperatures.

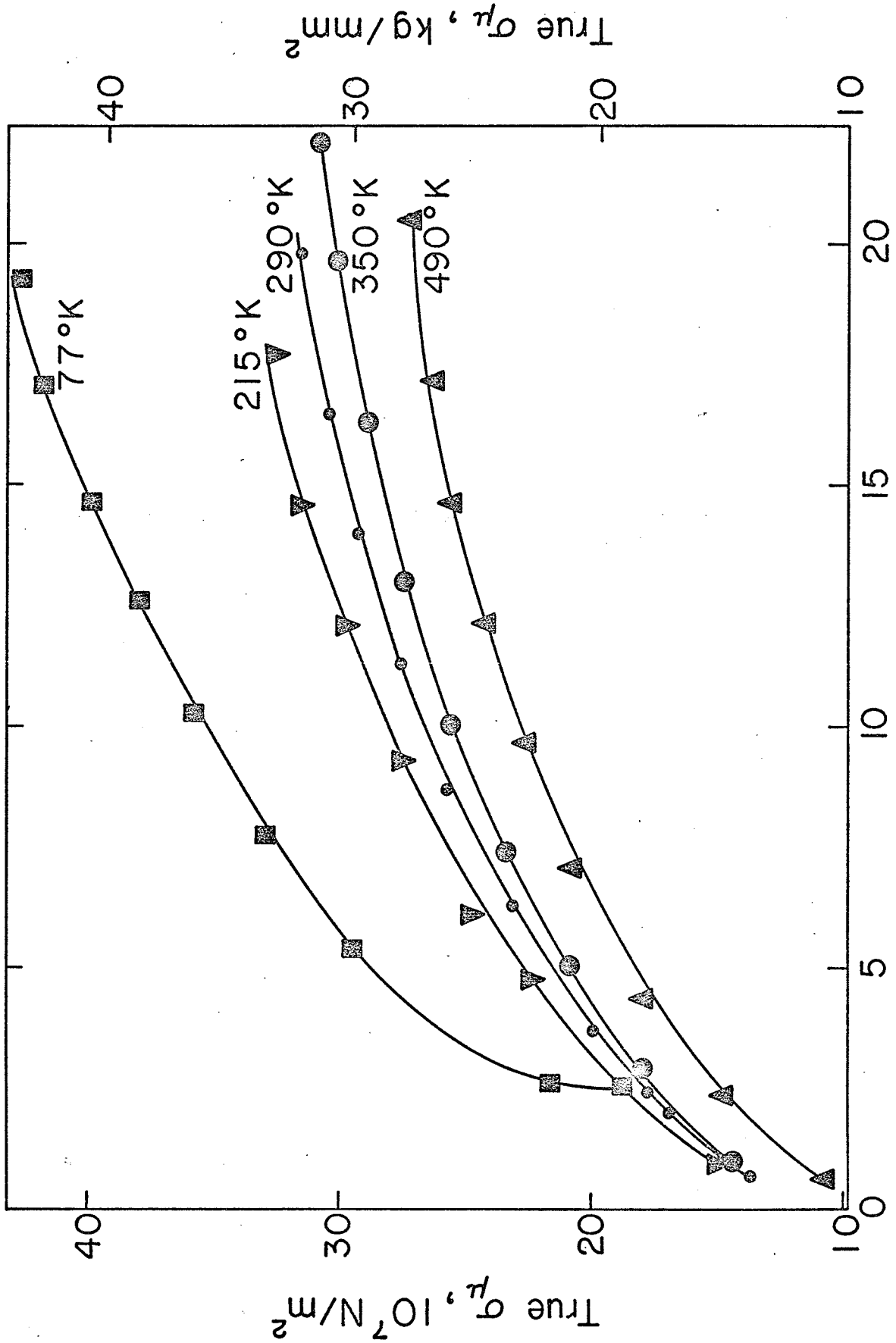

Figure 32: Athermal stress $\sigma\mu$ Vs plastic strain for Nb - 3.0 at%Zr at various temperatures.

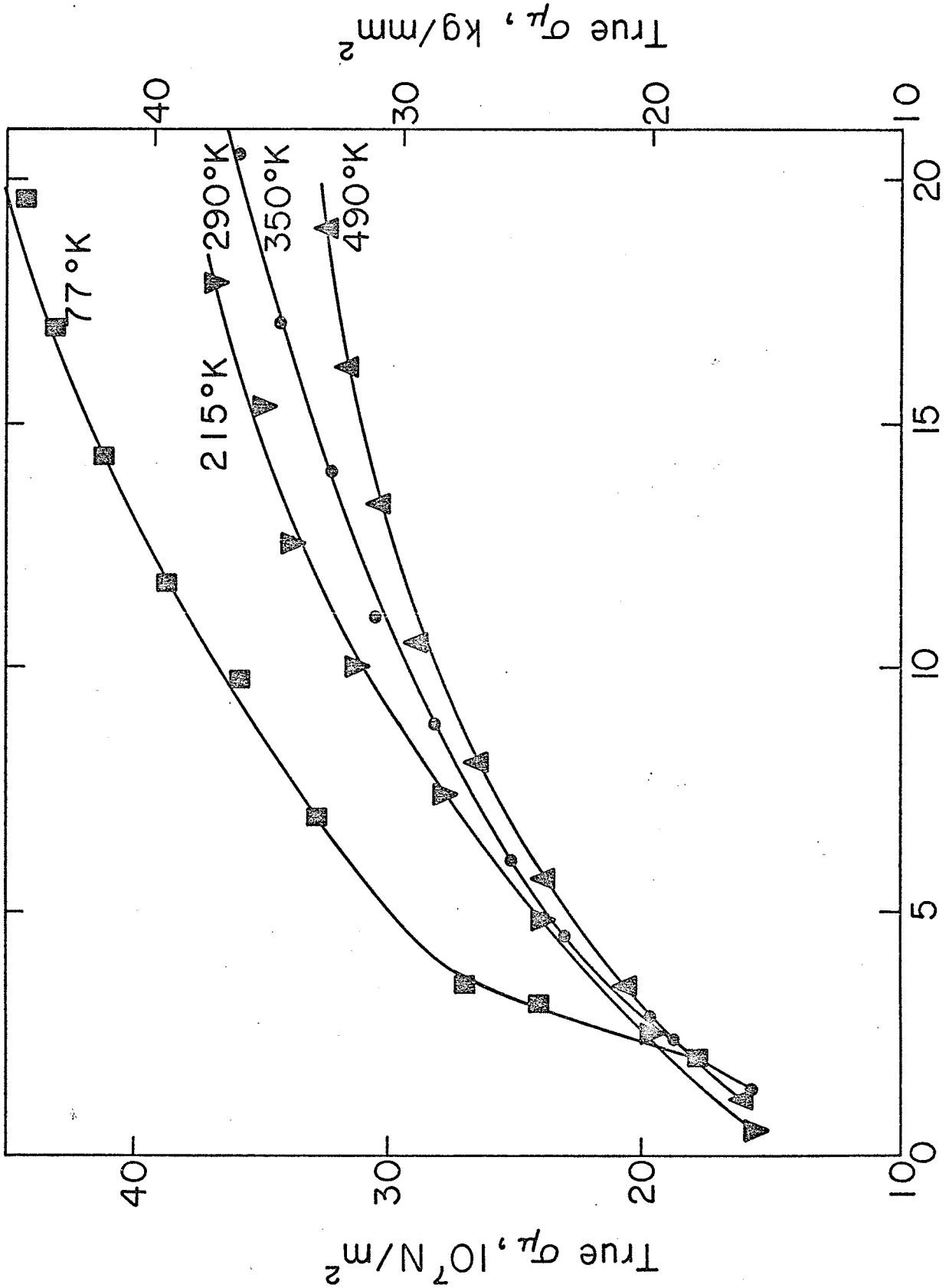

Figure 33: Athermal stress $\sigma\mu$ Vs plastic strain for Nb - 4.7 at%Zr at various temperatures.

2.3 Work Hardening

Two methods were employed in this study to evaluate the work hardening behaviour in Nb and Nb-Zr:

(1) the slope $\frac{d\sigma}{d\varepsilon_p}$ was determined as a function of strain, temperature and concentration, and

(2) the effects of the above variables were studied on the parameters n and K in the 'Power law' expression of work hardening, $\sigma = K\varepsilon^n$.

The results can be presented in the following manner.

2.3.1 Strain Dependence of Work Hardening

The rate of work hardening $\frac{d\sigma}{d\varepsilon_p}$ of Nb and Nb-Zr at room temperature are plotted against plastic strain in fig. 34. It was found that $\frac{d\sigma}{d\varepsilon_p}_{2.5\%}$ decreased to a value about four times smaller at 15% ε_p for all the compositions, and hence the initial difference in rates narrowed with increasing strain. This behaviour was maintained at other temperatures also. Since σ^* was nearly independent of strain, $\frac{d\sigma}{d\varepsilon_p}$ was almost equal to $\frac{d\sigma_\mu}{d\varepsilon_p}$ and therefore the other plots were drawn using σ_μ values instead of σ. The other reason for using σ_μ was because of the alloy softening which decreased σ^* at sub-atmospheric temperatures and hence σ decreased, but σ_μ was supposed to be unaffected.

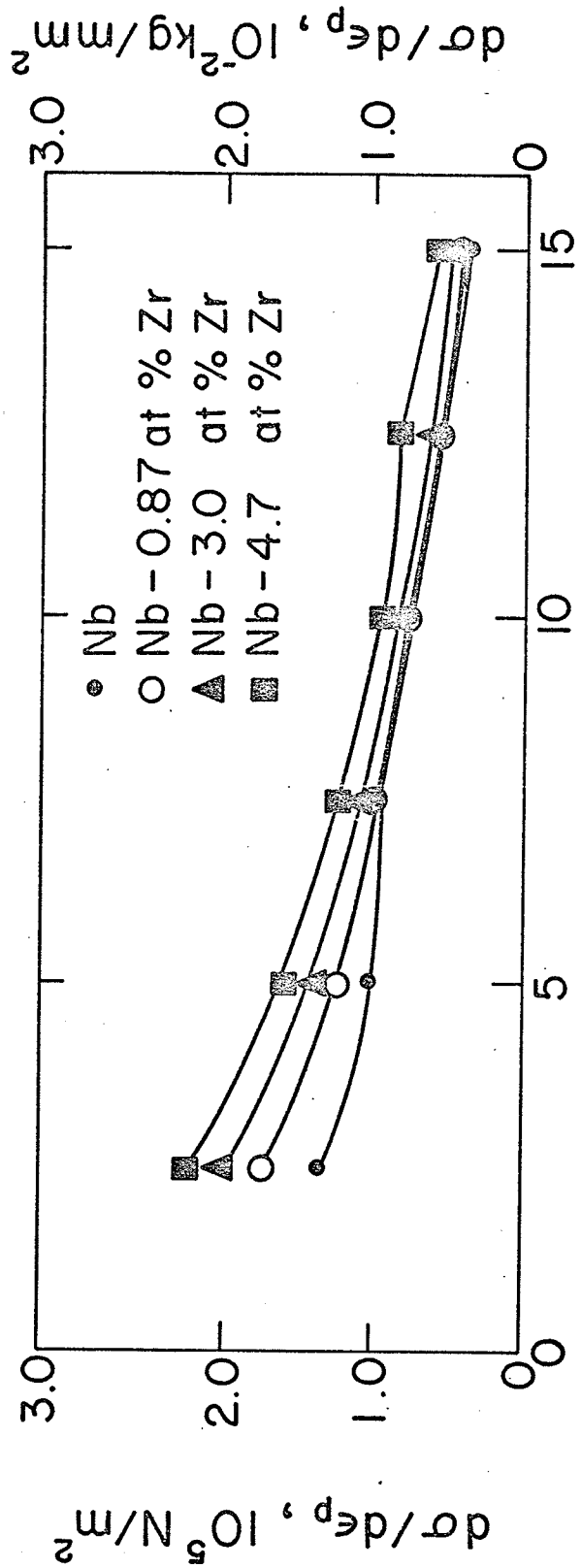

Figure 34: Work hardening rate $\frac{d\sigma}{d\varepsilon_p}$ Vs true plastic strain for Nb and Nb - Zr alloys at 290^{0}K.

Log σ - log ε_p relationship, figs. 35-38 showed that the slope increased significantly beyond ~1-2% ϵ_p and remained constant to about the necking strain. It should be noted here that the initial 1-2% ϵ_p were associated with the inhomogeneous yielding of the specimens (i.e. a yield point).

2.3.2 Temperature dependence of work hardening

Increase in temperature decreased $\frac{d\sigma_\mu}{d\varepsilon_p}$, fig. 39. The temperature dependence of $\frac{d\sigma_\mu}{d\varepsilon_p}$ seemed to decrease slightly with increase in Zr content, fig. 40.

The effect of temperature was almost non-existent on the value of n, figs. 35-38, however K increased systematically with decrease in temperature. The average value of n was 0.23.

2.3.3 Concentration dependence of work hardening

At all the temperatures investigated, except at 77^oK, the concentration dependence of $\frac{d\sigma_\mu}{d\varepsilon_p}$ seemed to be weak, figs. 39-42. At 77^oK, $\frac{d\sigma_\mu}{d\varepsilon_p}$ increases significantly with the initial addition of Zr but later on, it remains independent of concentration, fig. 40. No effects of solute content and temperature could be detected on the value of n, however additions of Zr increased K, figs. 35-38.

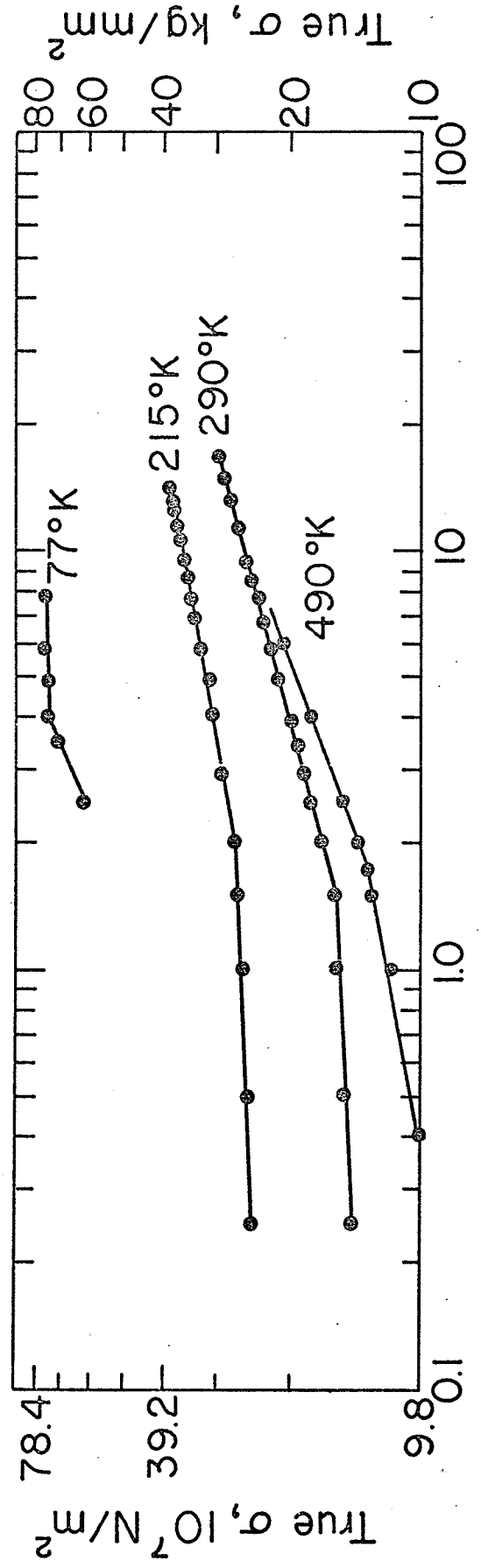

Figure 35: Log (stress) - log (strain) plot for Nb at various temperatures.

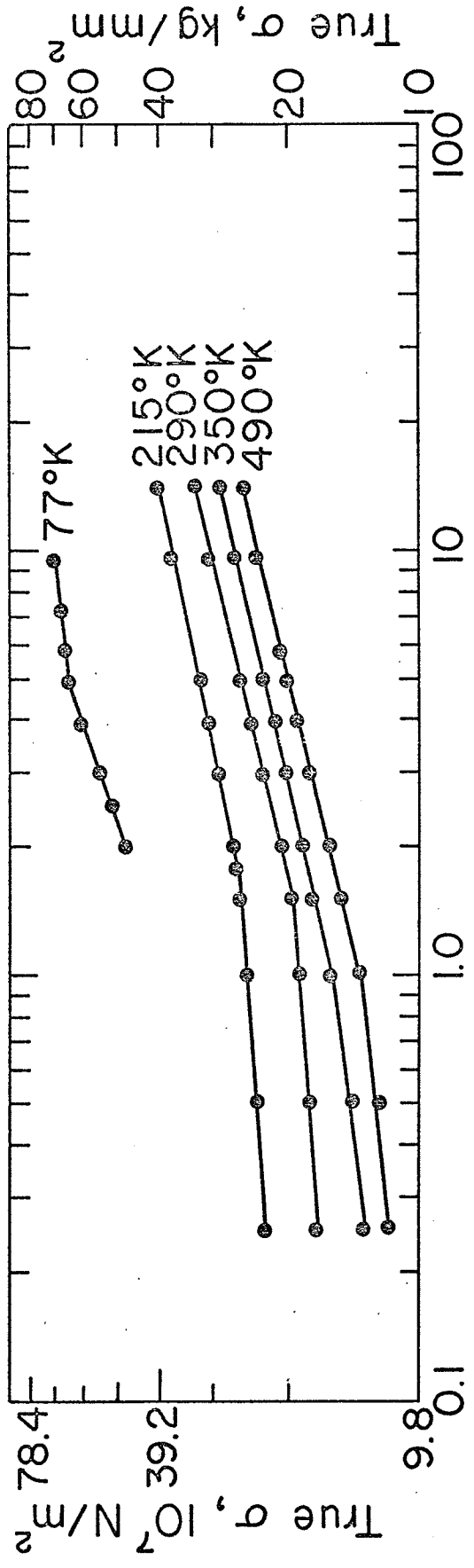

Figure 36: Log (stress) - log (strain) plot for Nb - 0.87 at%Zr at various temperatures.

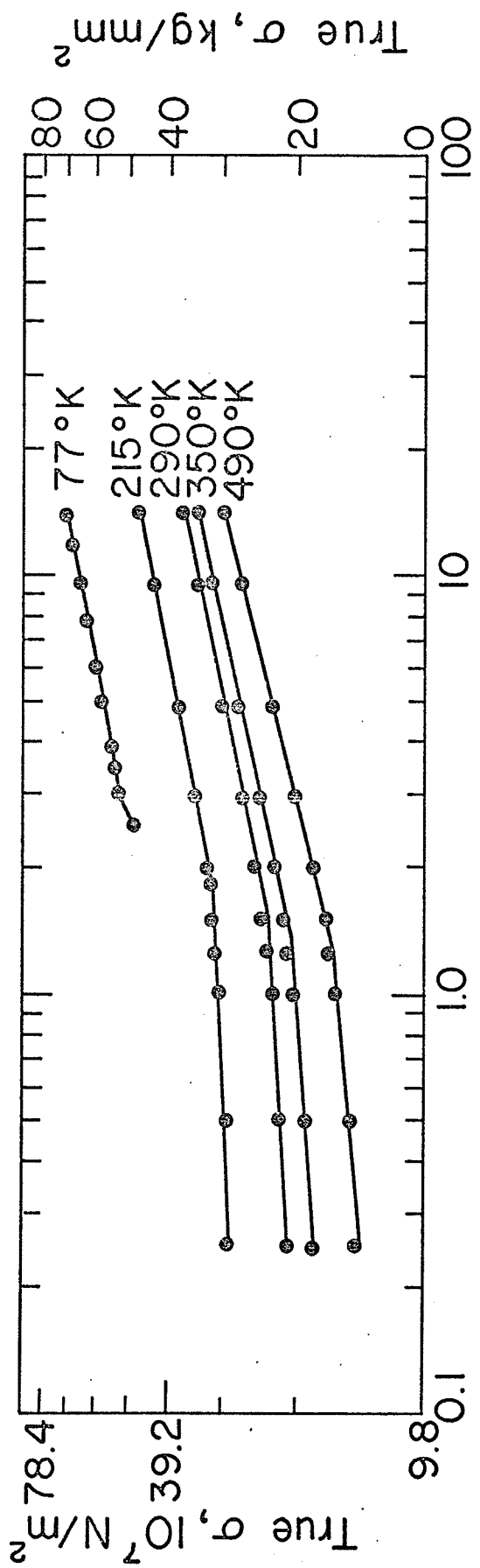

Figure 37: Log (stress) - log (strain) plot for Nb - 3.0 at%Zr at various temperatures.

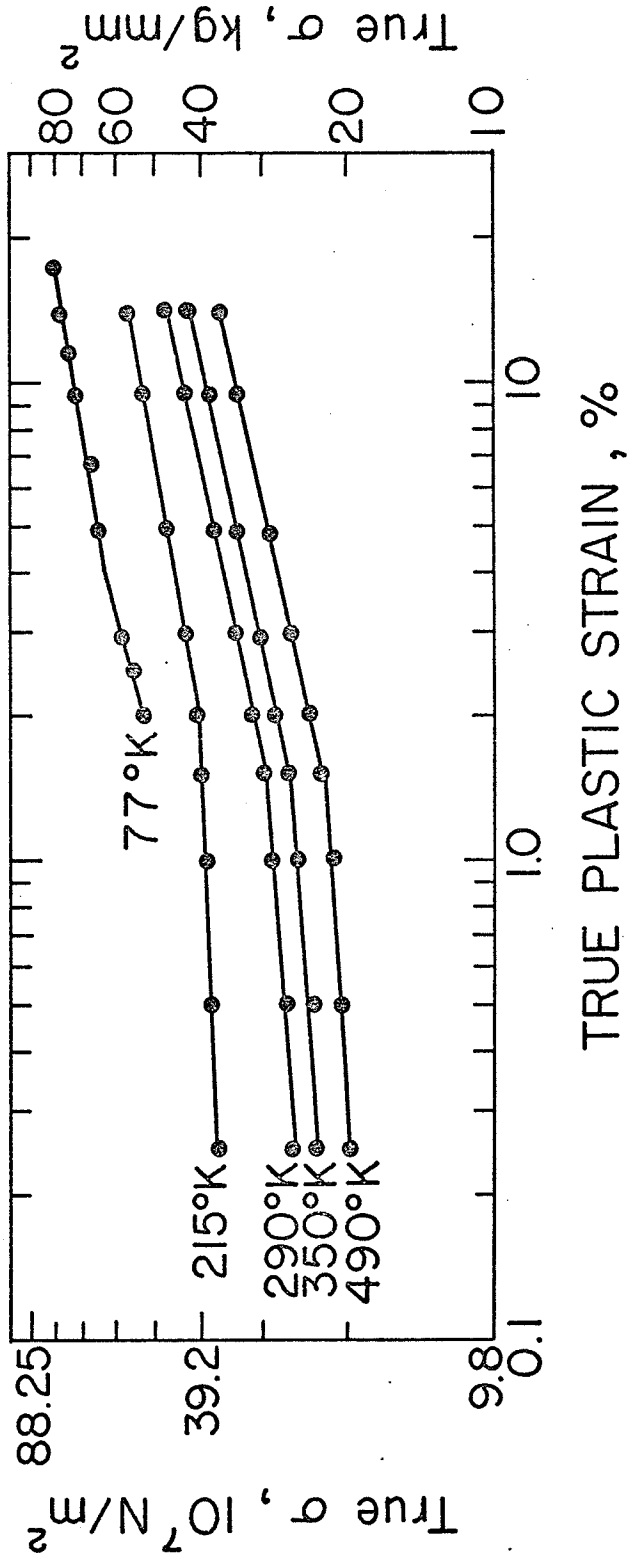

Figure 38: Log (stress) - log (strain) plot for Nb - 4.7 at%Zr at various temperatures.

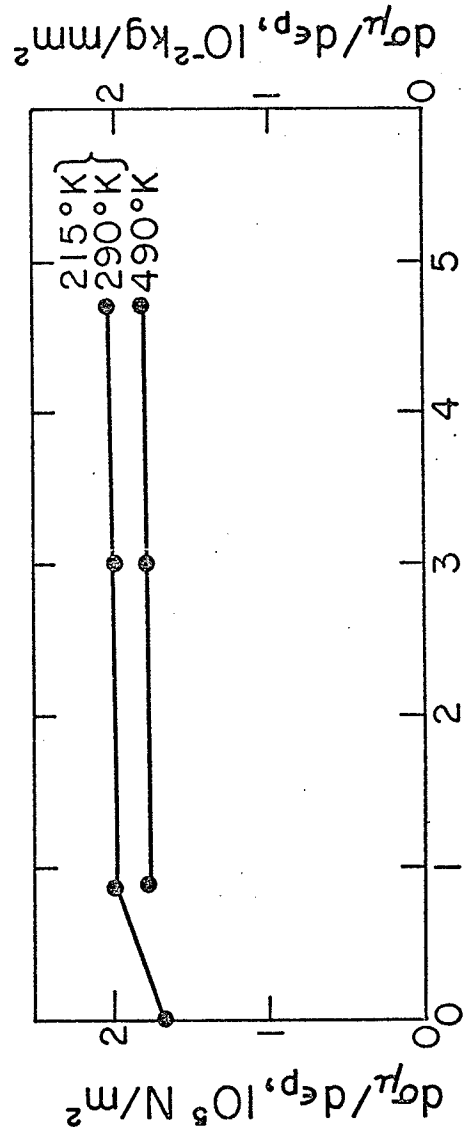

Figure 39: $\frac{d\sigma\mu}{d\varepsilon_p}$ at 2.5% plastic strain Vs concentration at various temperatures.

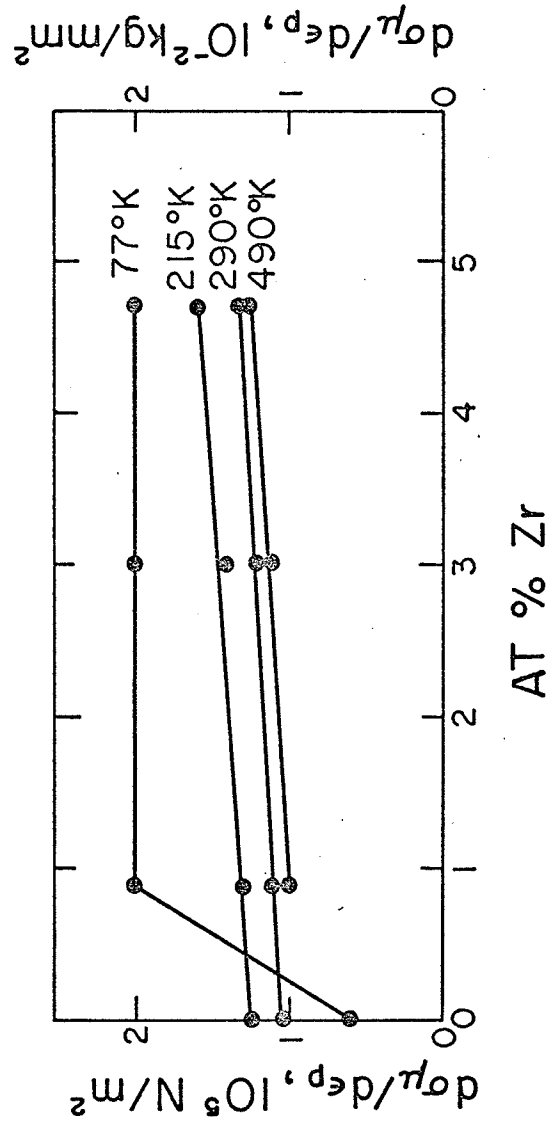

Figure 40: $\frac{d\sigma\mu}{d\epsilon_p}$ at 5.0% plastic strain Vs concentration at various temperatures.

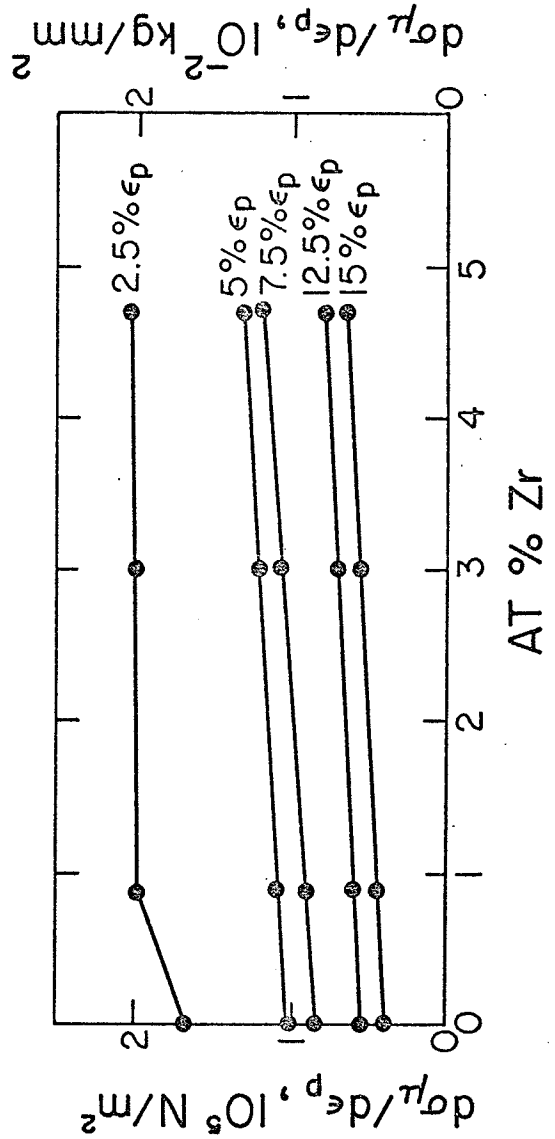

Figure 41: $\frac{d\sigma\mu}{d\varepsilon_p}$ Vs concentration at 290^{o}K for various strain levels.

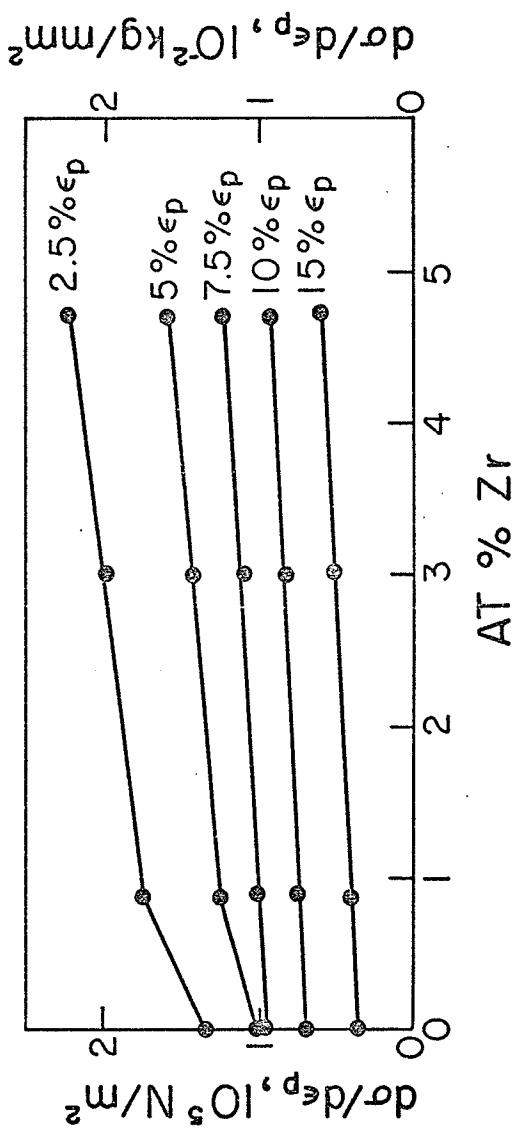

Figure 42: $\frac{d\sigma}{d\varepsilon_p}$ Vs concentration at 290°K for various strain levels.

3.0 Activation Parameters of Deformation

The activation parameters of deformation were found by using the conventional methods i.e. strain rate cycling, and determining the flow stress at several temperatures. The various formulae employed for these calculations are given in Section 1.2.

3.1 Concentration, Strain and Temperature Dependence of V^*

The activation volume V^* for Nb and Nb-Zr alloys are shown in figs. 43-46, as a function of strain and temperature. It remains essentially constant with strain at any temperature, however it is an increasing function of strain with increase in temperature for Nb and Nb-0.87 at% Zr beyond 290^{o}K but was not so in the case of Nb-3 and 4.7 at% Zr alloys. In general, V^* at any strain decreased with either increase in the solute content or decrease in temperature. Where alloy softening was present, at any strain it increased with initial alloy additions and then reversed the trend on further alloying. The concentration, where this change occured was dependent upon the temperature, and it can be seen in fig. 47 where $\Delta\sigma$ for $\Delta\dot{\varepsilon}$ at 5% plastic strain has been plotted as a function of temperature. Such plots are important in getting further insight into the deformation mechanism by studying the change in the overall shape of the curves for any metal and its alloys. In niobium, it has been shown[25] that the thermally activated process also had an activation energy of the type

$$H = A - B \ln (\sigma^*/\sigma_p)$$

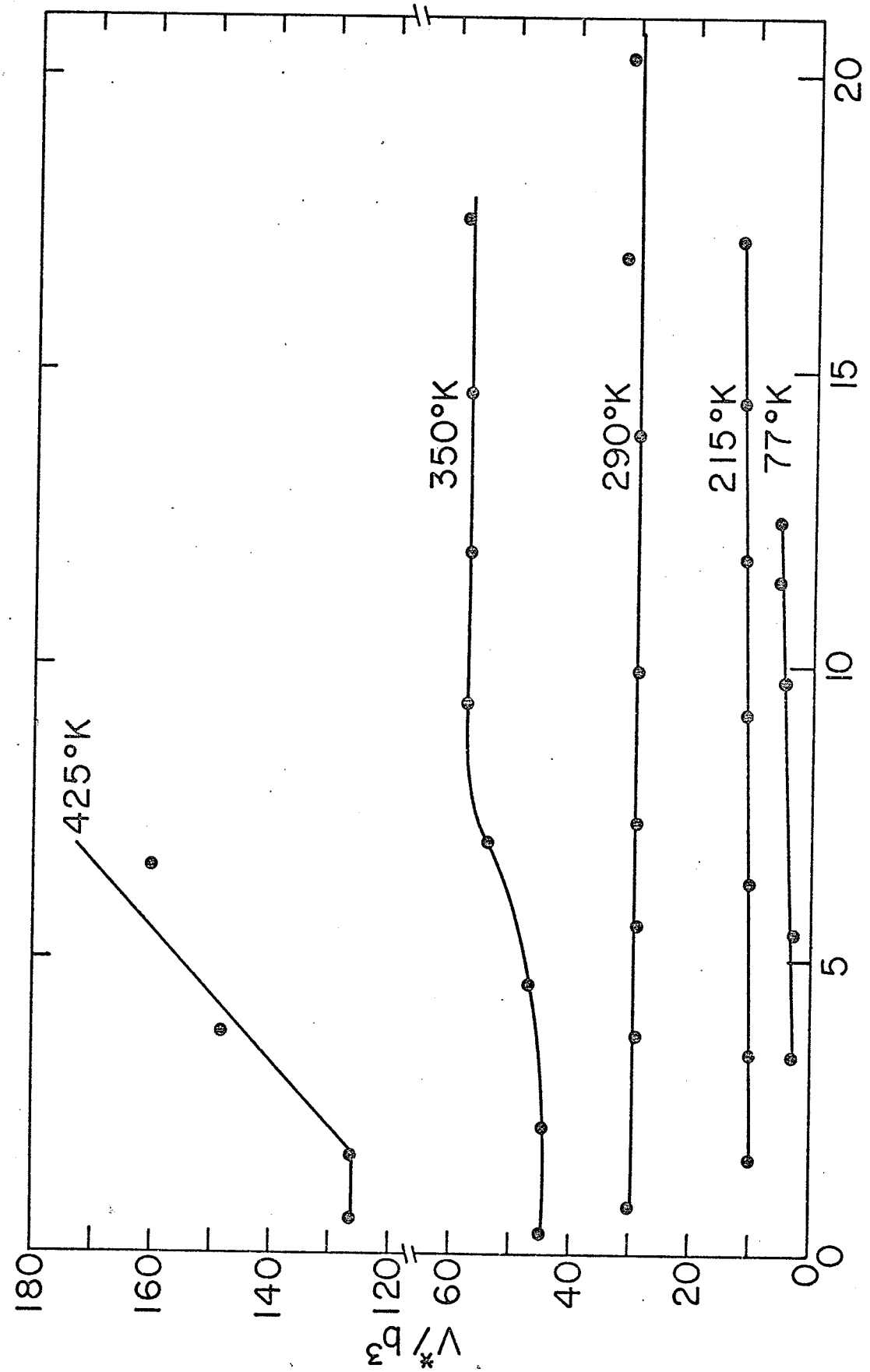

Figure 43: Activation volume V^*/b^3 Vs plastic strain for Nb at various temperatures.

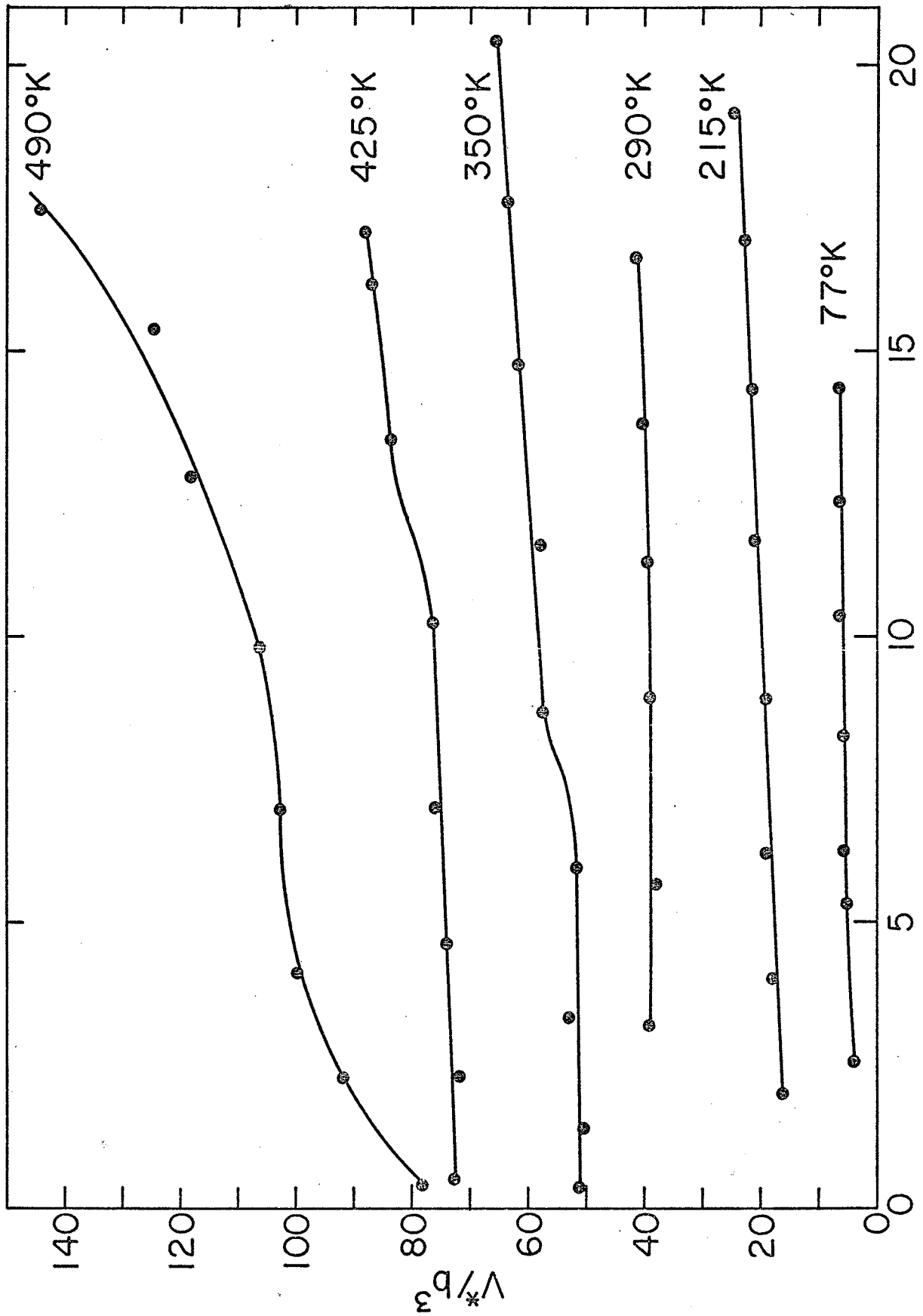

Figure 44: Activation volume V^*/b^3 Vs plastic strain for Nb - 0.87 at%Zr at various temperatures.

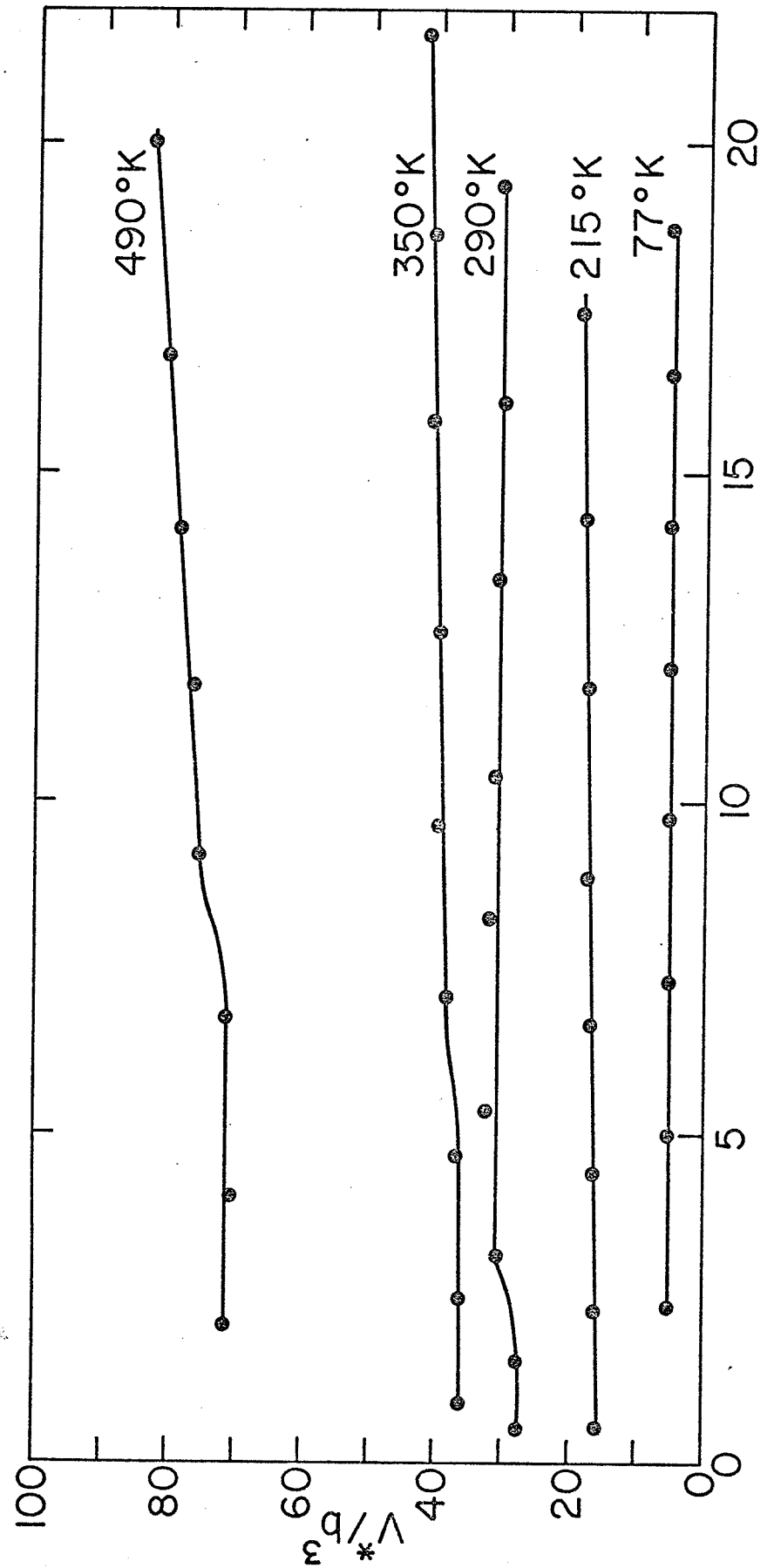

Figure 45: Activation volume V^*/b^3 Vs plastic strain for Nb - 3.0 at%Zr at various temperatures.

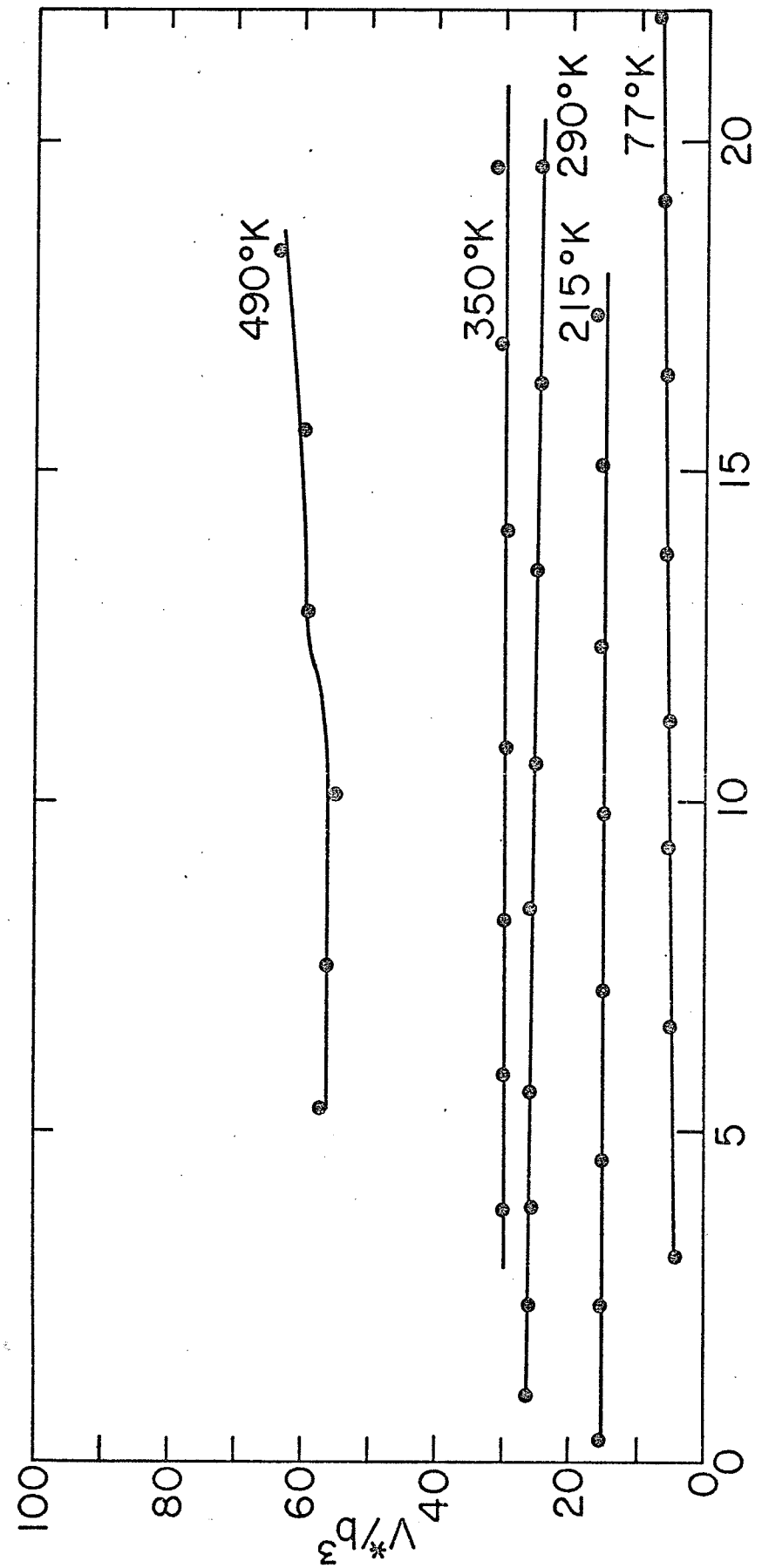

Figure 46: Activation volume V^*/b^3 Vs plastic strain for Nb - 4.7 at%Zr at various temperatures.

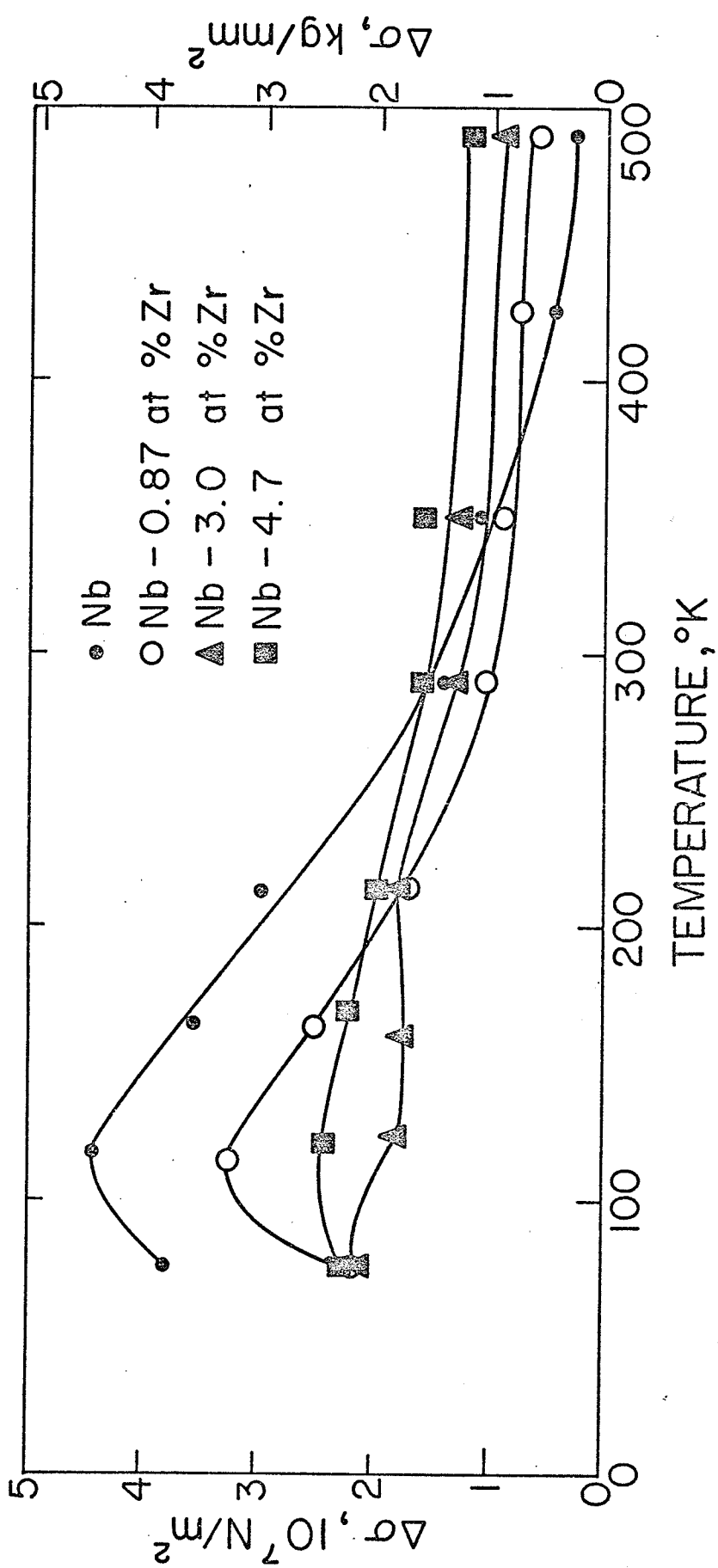

Figure 47: Increase in stress $\Delta\sigma$ due to strain rate change at 5% plastic strain plotted against temperature for Nb and Nb - Zr alloys.

and hence the curve will pass through a maximum at a certain temperature Tm in the $\Delta\sigma$ vs ^{o}K plot. The values of Tm were calculated using σ^* and $\Delta\sigma$ at different temperatures and reasonable agreement between the calculated Tm values was found in the case of only Nb and Nb-0.87 at% Zr. The predicted Tm for higher compositions were not observed, however, as drawn fig. 47 shows peaks. In the absence of still lower temperature data and also some intermediate values, it was not possible to draw a complete curve.

3.2 Stress Dependence of V^*

The stress dependence of V^* is shown in fig. 48, and it can be seen that beyond a certain σ^*, the activation volume was smaller for the alloys than that for Nb. This range of stress was in the alloy softening region where Nb had the largest σ^*. In the lower stress or higher temperature region, V^* for the alloys was larger for the Nb-Zr alloys than that for Nb. The general shape, however, of the $V^* - \sigma^*$ curve was similar in all the cases i.e. V^* having smaller values at higher stresses and then increasing very rapidly at lower σ^*. In a $\log(V^*/b^3) - \log(\sigma^*)$ plot, fig. 49, inflexions in the curves for Nb-3 and 4.7 at% Zr, occurred much earlier than in the curves for Nb and Nb-0.87 at% Zr.

3.3 The Activation Energy

The activation energy versus effective stress plot in fig. 50 shows that at higher stress levels i.e. lower temperatures,

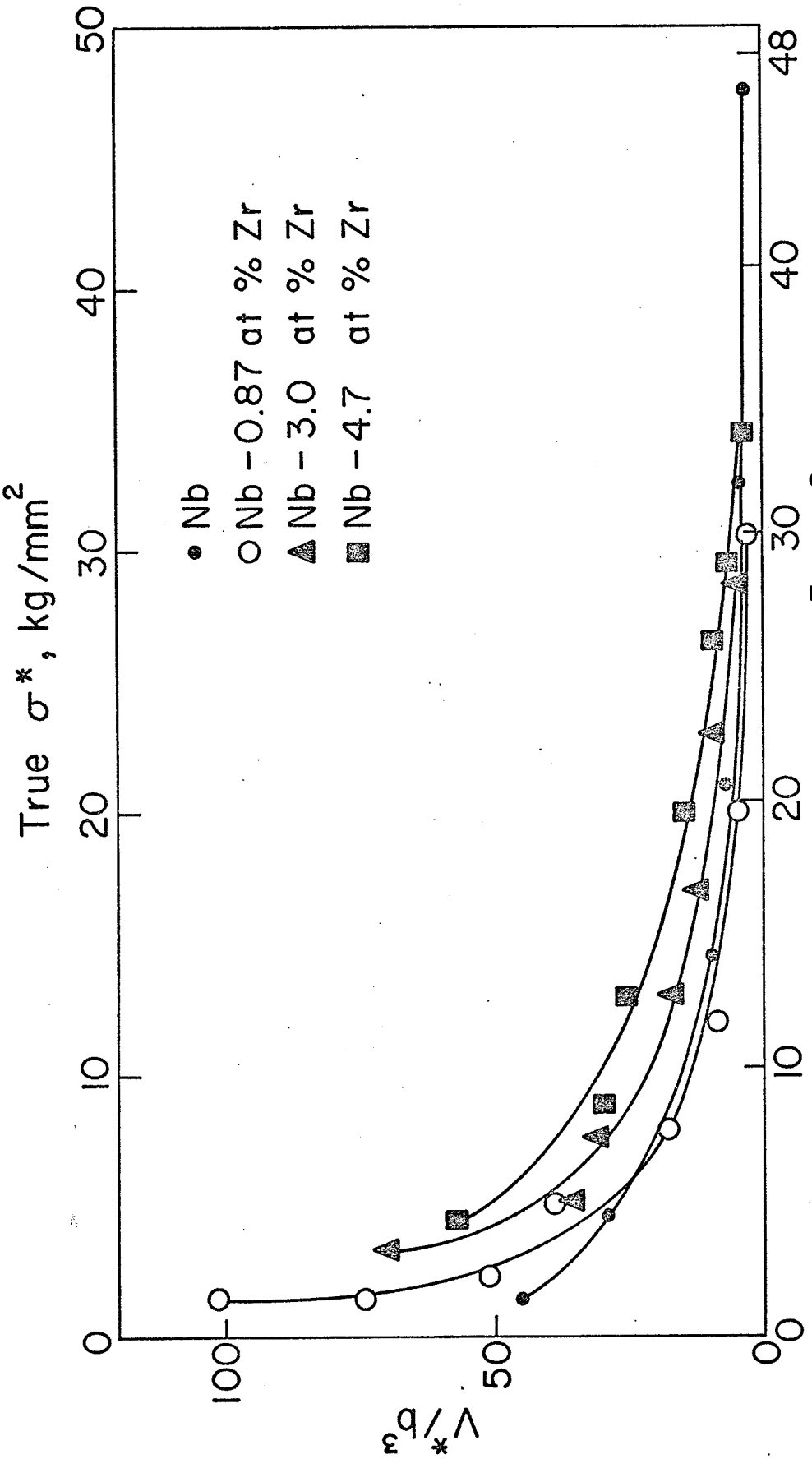

Figure 48: Activation volume V^*/b^3 Vs thermal stress σ^* for Nb and Nb - Zr alloys.

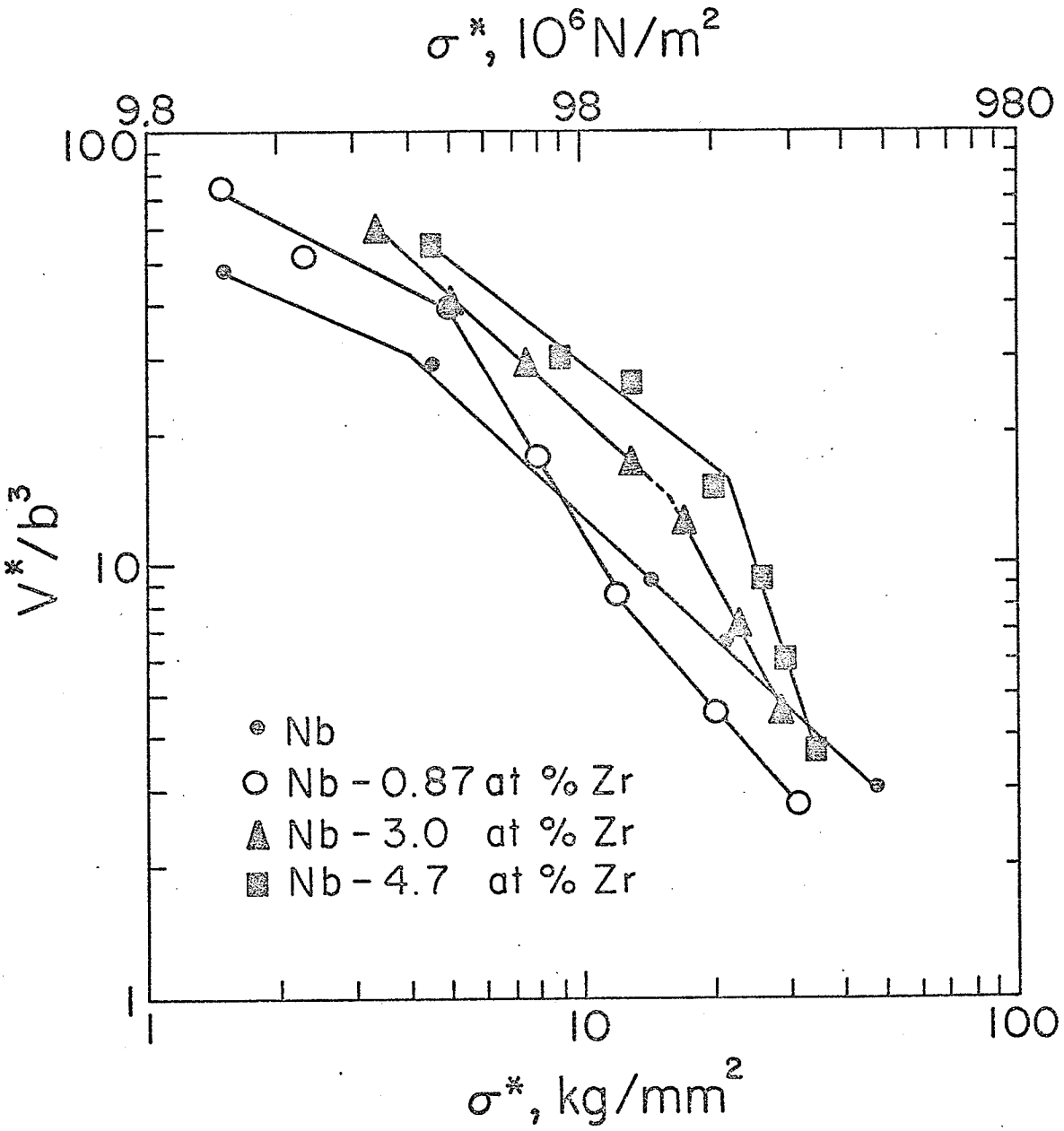

Figure 49: Log (V^*/b^3) - log (σ^*) plot for Nb and Nb - Zr alloys.

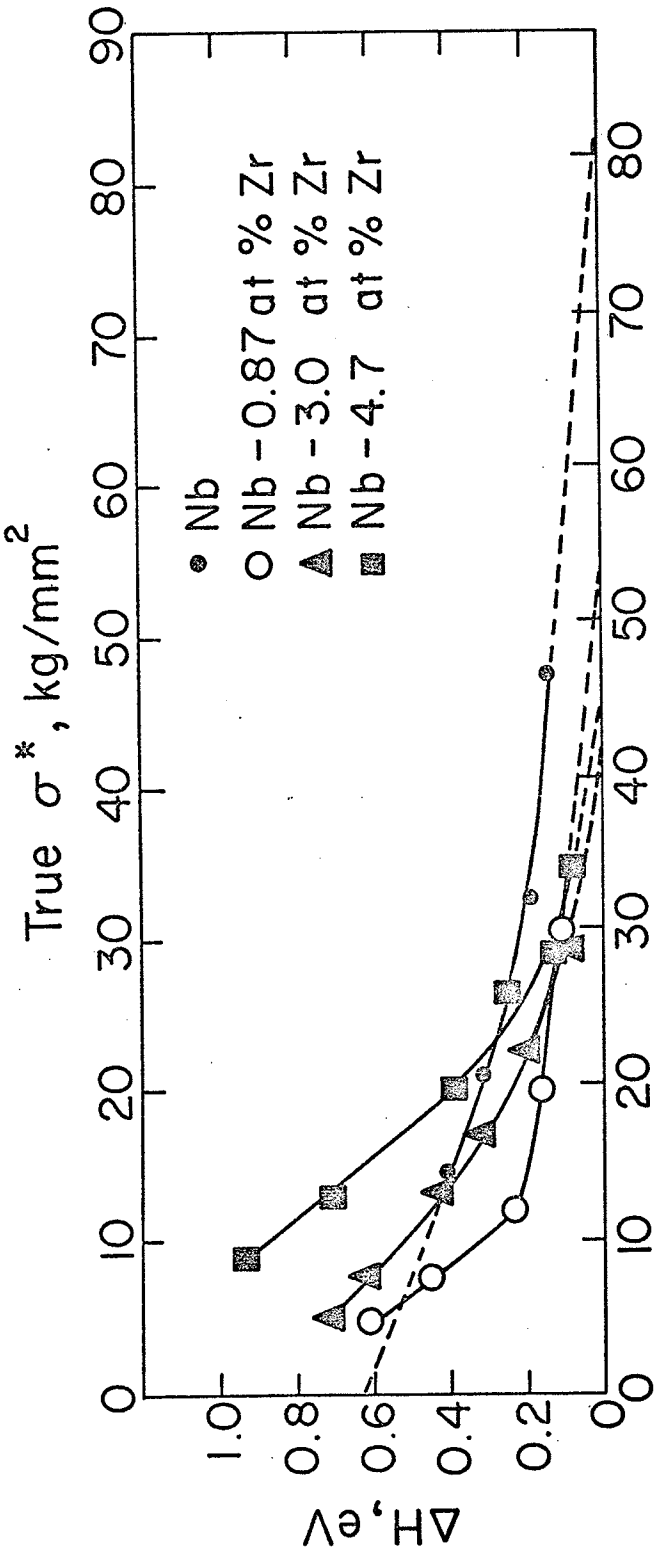

Figure 50: Activation energy ΔH plotted against true thermal stress σ* for Nb and Nb - Zr alloys.

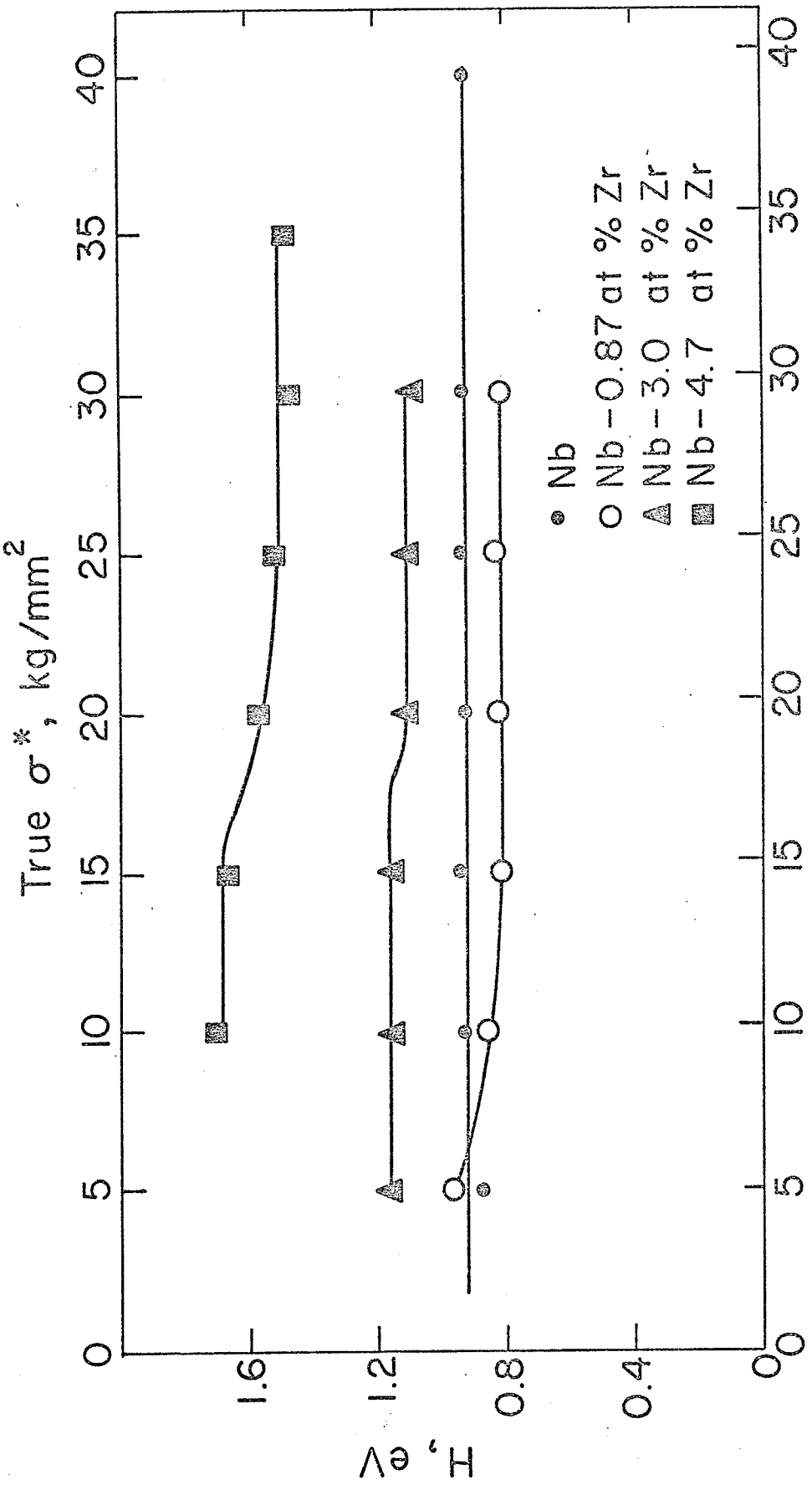

Figure 51: Total energy H plotted against true thermal stress σ* for Nb and Nb - Zr alloys.

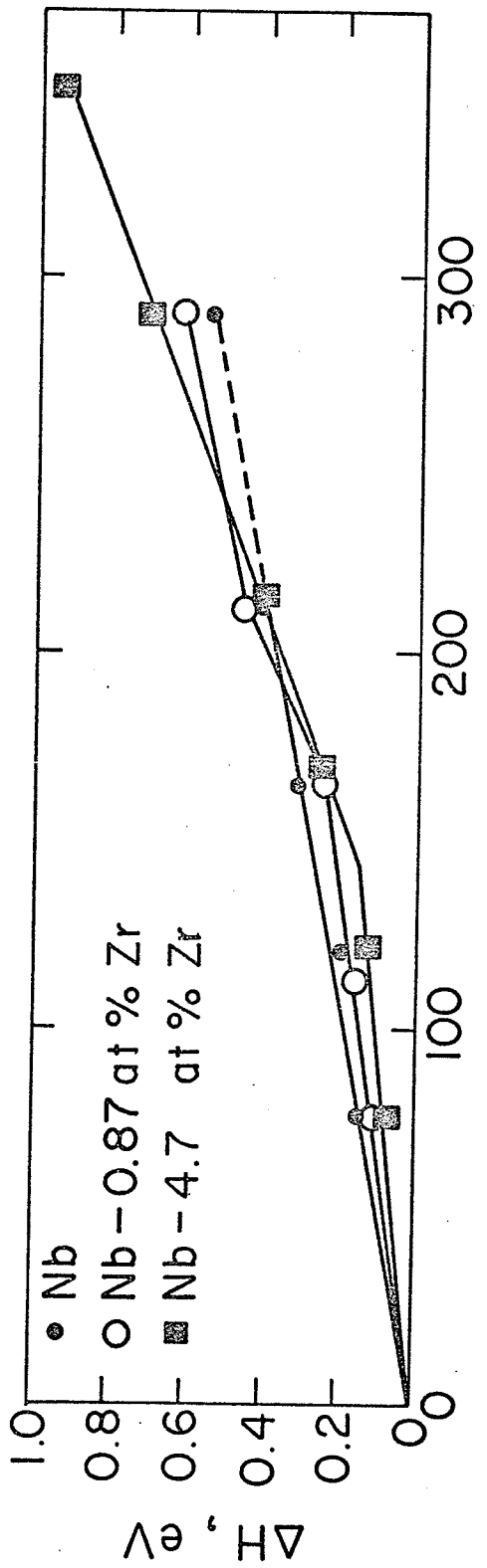

Figure 52: Activation energy ΔH plotted against temperature for Nb and Nb - Zr alloys.

the activation energy ΔH for the alloys was smaller than that for Nb, however below a certain stress level (i.e. beyond a certain high temperature), which decreased with decrease in solute content, ΔH for the alloys increased rapidly with decrease in σ^* and became larger than that for the parent metal. On extrapolating the curves, ΔH_o for Nb, Nb-0.87 at% Zr, Nb-3 at% Zr and Nb-4.7 at% Zr was 0.63 ev, 0.8 ev, 1.0 ev and 1.4 ev respectively. H values found as a sum of thermal and mechanical energies are shown as a function of σ^* in fig. 51. In each case H is $\sim$0.2 ev larger than the corresponding ΔH_o in fig. 50.

While ΔH for Nb increased linearly with temperature upto about 215^{o}K, fig. 52, there were inflexions in the case of alloys, viz. at 165^{o}K for Nb-0.87 at% Zr and at 145^{o}K for Nb-4.7 at% Zr. The initial slopes of the curves in fig. 52 are not similar and hence give different values of the pre-exponential factor for different alloys in the rate equation.

4.0 Dislocation Dynamics in Nb-Zr Solid Solutions

The stress relaxation and strain rate cycling techniques were used to evaluate m^* as a function of strain, concentration and temperature. In general, agreements between the values of m^* obtained via the two methods were satisfactory (the maximum difference being $\sim$ 3) and it put confidence in the values used in this study.

4.1 Strain Dependence of m^*

m^* for Nb-4.7 at% Zr has been shown as a function of plastic strain at various temperatures in fig. 53. It is seen that m^* was essentially independent of strain at all temperatures. However, it seemed to decrease initially by a small amount and then attained a plateau. The initial region coincided with the yield strain and thus the decrease could be due to the initial inhomogeneous nature of the deformation. There was a similar decrease at strains approaching necking in the specimen. These variations in m^* from a mean value were only about $\pm$ 1.5 which was about the expected experimental variation in m^* and did not seem to have any significance. Similar behaviour was observed in all the alloys.

4.2 Concentration Dependence of m^*

The effect of solute content on m^* at various temperatures can be seen in fig. 54. It shows that m^* increased continuously

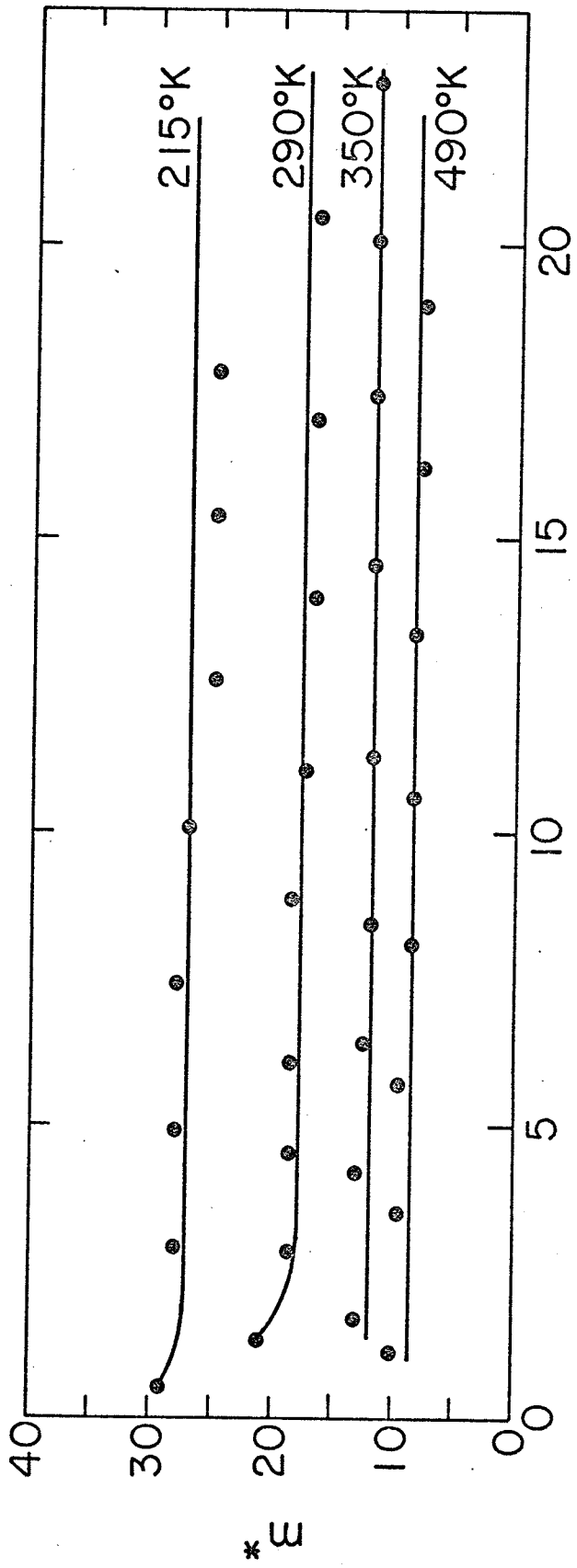

Figure 53: Dislocation velocity stress exponent m* Vs plastic strain for Nb - 4.7 at%Zr at various temperatures.

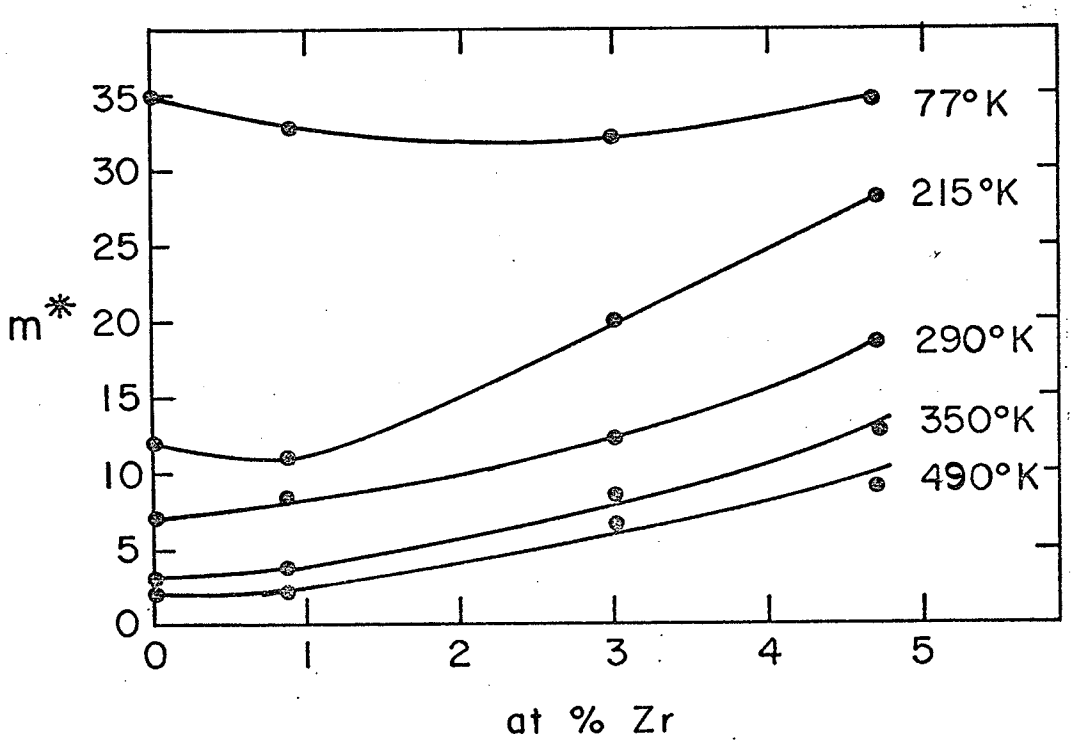

Figure 54: Effect of concentration on dislocation velocity stress exponent m* at various temperatures.

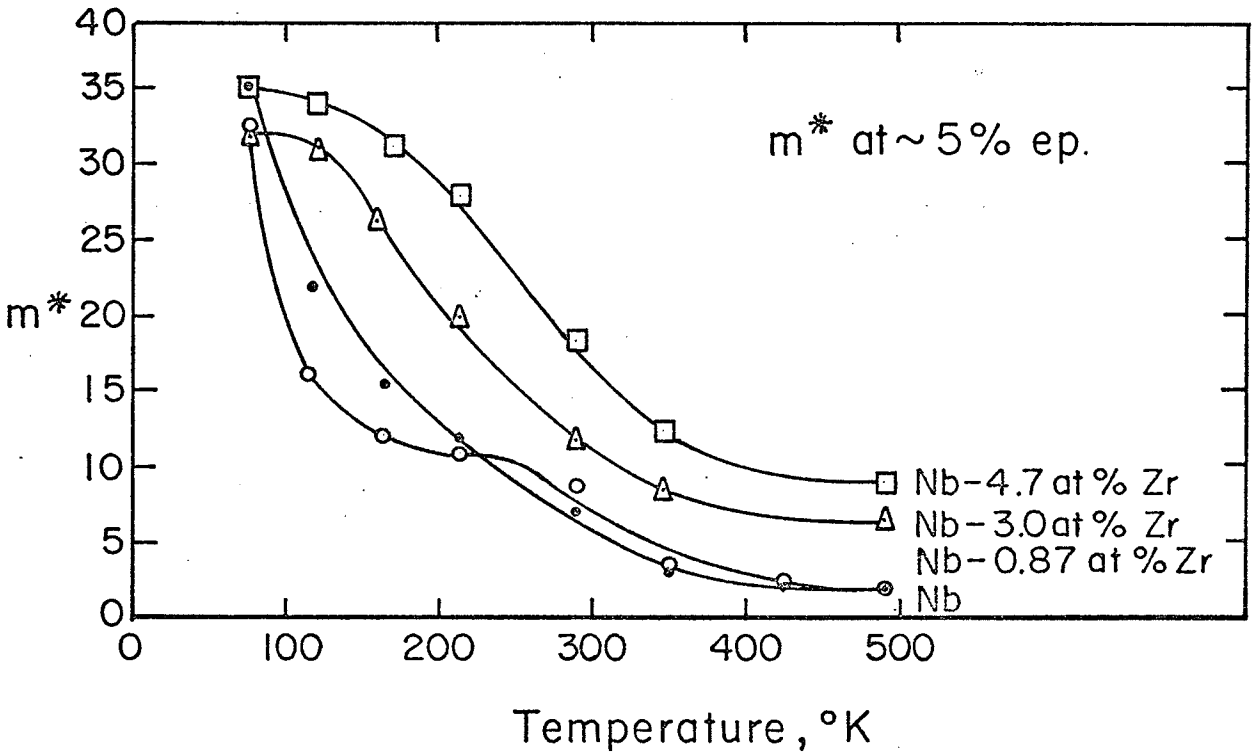

Figure 55: Effect of temperature on dislocation velocity stress exponent m* for Nb and Nb - Zr alloys.

but non-linearly with solute at ambient and higher temperatures, but behaved differently at subambient temperatures. This low temperature behaviour of m^* is similar to that of σ^*, viz. fig. 60 . The rate of increase in m^* with Zr seemed to be similar at 290°K and above whereas below 290°K the values of m^* were altered by solution softening.

4.3 Temperature Dependence of m^*

m^* has been plotted against temperature in fig. 55 and it roughly resembled the σ^* vs °K plot in fig. 61 , however the softening temperatures T_s were different than those in fig. 61 .

5.0 DISCUSSION

5.1 Stress Strain Curves

The stress versus strain curves showed, in general, that the addition of zirconium raised the whole curve above that for niobium when tested at ambient and higher temperatures. However, this normally expected behaviour of alloying was not observed at subambient temperatures. At 215^{o}K the stress-strain curve for Nb-0.87 at% Zr which was originally below the Nb curve, rose above it after about 2.5% plastic strain, fig. 14. At 77^{o}K the curves for all the alloys were below the Nb curve but the curve for Nb-4.7 at% Zr only rose above it after $\sim$ 12% plastic strain, fig. 13. This clearly indicates the higher work hardening extent in the alloys compared to the pure Nb. This was also reflected in the slightly increasing slope of the stress-strain curves for the alloys as the solute content was increased, figs. 13-16.

A decrease in the test temperature had a somewhat similar effect on the stress-strain curves. Figs. 17-20 show that as the test temperature decreases, the level of the whole curve rises. The typical behaviour of pure Nb at higher strains at 490^{o}K will be discussed later in the work hardening section. The rise in level of the stress-strain curves with an increase in the solute content or more effectively, with a decrease in the test temperature is a general characteristic of the b.c.c. metals and their alloys.

In the present study the occurrence of an initial yield point and its magnitude was found to be dependent on concentration

TABLE VI

Alloys	Legend	77°K	215°K	290°K	350°K	425°K	490°K
Nb	(1)	no yield point	23.2kg/mm^2	14.75kg/mm^2	no yield point	no yield point	no yield point
	(2)		22.85kg/mm^2	14.5			
	(3)		0.35kg/mm^2	0.25			
	(4)		15.0kg/mm^2	5.5kg/mm^2			
	(5)		3.0kg/mm^2	1.4kg/mm^2			
Nb-0.87 at% Zr	(1)	no yield point	22.3kg/mm^2	no yield point	no yield point	no yield point	no yield point
	(2)		22.1kg/mm^2				
	(3)		0.2kg/mm^2				
	(4)		9.0kg/mm^2				
	(5)		2.3kg/mm^2				
Nb-3.0 at% Zr	(1)	no yield point	28.3kg/mm^2	21.3kg/mm^2	18.3kg/mm^2	-	13.9kg/mm^2
	(2)		28.3kg/mm^2	21.0kg/mm^2	18.0kg/mm^2		13.85kg/mm^2
	(3)		very small*	0.3kg/mm^2	0.3kg/mm^2		0.05kg/mm^2
	(4)		14.5kg/mm^2	8.5kg/mm^2	5.0kg/mm^2		3.5kg/mm^2
	(5)		2.0kg/mm^2	1.5kg/mm^2	1.4kg/mm^2		0.95kg/mm^2
Nb-4.7 at% Zr	(1)	no yield point	36.4kg/mm^2	28.3kg/mm^2	25.1kg/mm^2	-	19.55kg/mm^2
	(2)		36.2kg/mm^2	27.85kg/mm^2	24.7kg/mm^2		19.25kg/mm^2
	(3)		0.2kg/mm^2	0.45kg/mm^2	0.4kg/mm^2		0.3kg/mm^2
	(4)		22.0kg/mm^2	13.0kg/mm^2	9.0kg/mm^2		5.0kg/mm^2
	(5)		1.9kg/mm^2	1.6kg/mm^2	1.6kg/mm^2		1.4kg/mm^2

Legend:
1) The upper yield stress, kg/mm^2
2) The lower yield stress, kg/mm^2
3) The yield drop, kg/mm^2
4) The thermal stress, σ^*
5) The increase in stress $\Delta\sigma$ on increasing the strain rate by ten times.

B. - 1. the strain associated with the inhomogeneous deformation was 1-1.5%.
2. the strain to the upper yield point was 0.15%.

and temperature, table VI, and it was also found that no yield point occurred on subsequent loading and relaxation tests. However, at 490°K the deformation in pure niobium was not uniform and regular. There were frequent load drops. On reloading the specimen after unloading it, a very small yield point was observed every time. The irregular deformation and the repeated yield points were not found in the case of Nb-Zr alloys. The interaction is much stronger and the dislocations are more strongly pinned in the case of interstitial solutes than in the case of substitutional solutes. The yield drop is larger the stronger the pinning. In the case of impure Nb the yield drop observed was 2.73 Kg/mm^2 at room temperature whereas in the zone refined pure Nb it was only 0.25 Kg/mm^2. In general, to produce a yield point, it is necessary that the mobile dislocation density increases sufficiently rapidly with strain and the rate of work hardening is small. Fig. 56 is a

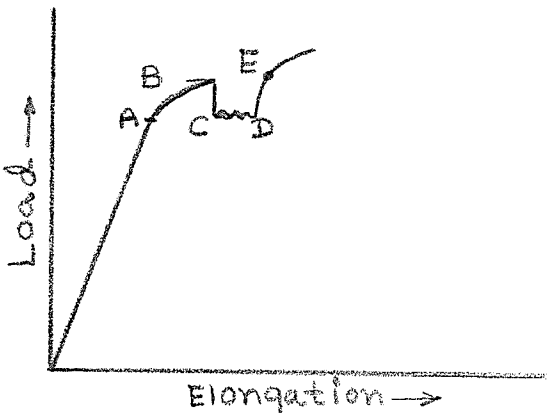

Figure 56: Schematic representation of the load-elongation relationship in Nb and Nb - Zr alloys.

schematic representation of the load-elongation relationship in Nb and Nb-Zr alloys. OA is the elastic region, AB is the plastic strain prior to the yield drop, B is the upper yield point, BC is the yield drop, CD is the yield elongation and DE is the rise in load again. It was found by transmission electron microscopy that the dislocation density in Nb and Nb-Zr alloys increased manifold after $\sim$ 1% plastic strain. The pre-yield microstrain region is probably associated with the heterogeneous nucleation and multiplication of mobile dislocations and the upper yield stress B seems to be the stress at which the slip propagates from grain to grain in the specimen. The total plastic strain associated with the inhomogeneous deformation of the specimens was 1-1.5% in all cases, AE in fig. 56 and during this strain the rate of work hardening was almost negligible, figs. 35.

The yield drop in pure Nb and Nb-Zr alloys was, in general, very small. All specimens were predeformed at room temperature for the 77^{o}K test to avoid twinning. However, an impure Nb specimen was tested at 77^{o}K in an annealed condition and no yield drop was observed. Christian and Masters[25] and Harris[9] have also reported that no yield drops were seen in Nb and Nb alloys at 77^{o}K which could be due to a very high rate of work hardening in these materials at this temperature.

5.2 Solid Solution Hardening

As mentioned earlier, the main purpose of this investigation was to find out the effects of solute and strain on the thermal and athermal components of the flow stress at different temperatures and not a study of solid solution hardening, per se, in niobium. In order to find out the mechanism of hardening operative in any system, it would be necessary to study a variety of solutes before any general conclusions can be drawn. In several such studies made earlier on binary niobium alloys, it was the general conclusion that the size mismatch and not the modulus mismatch was a dominant factor in solution hardening and the yield/flow stress was linearly proportional to composition. In the present study although only four compositions were employed, a linear relationship between stress and zirconium concentration was also found - see fig. 21. However, it is evident from table VII, that this is by no means the situation in all the binary niobium solid solutions investigated to date. This could be due to one or more of the several factors discussed below.

1. The amount of interstials present in these alloys and their overall purity varied widely from one study to another and because of the fact that interstitials are very effective hardeners (the athermal stress is more profoundly affected than the thermal stress in b.c.c. transition metals),it is possible that the real hardening effect of the substitutional atoms was masked, giving erroneous results. It is thus probable that due to very high interstitial content in the alloys, Begeley & Bechtold[8] could not observe any concentration dependence of hardening.

TABLE VII

	Alloying Element	Crystal	Total intersti. ppm	Concentration dependence of hardening σ	σ_μ	Mechanism	Reference & Year
1.	Cr	Poly	720	None	None	None	Begley etal[8] (1961)
2.	Hf	"	"	"	"	"	"
3.	Mo	"	"	"	"	"	"
	Mo	single	80	C	C		Peters & Hendrickson[18] (1970)
	Mo	"	60		C		Jax[12] (1971)
	Mo	"	100		C		Kam[13] (1971)
4.	Pd	"	100		$C^{2/3}$ or C		Jax[12] (1971)
5.	Ta	Poly	250	C	C	size mismatch	Harris[9] (1966)
	Ta	single	1500 at ppm		C		Kostorz[10] (1968)
	Ta	"	80	C	C		Peters & Hendrickson[18] (1970)
6.	Ti	Poly	720	None	None		Begley[8] (1961)
7.	V	"	"	"	"		"
	V	"	250	C	C		Harris[9] (1966)
	V	single	1500 at ppm		C		Kostorz[10] (1968)
8.	W	poly	720	None	None	None	Begley[8] (1961)
	W	"	250	C	C		Harris[9] (1966)
	W	single	1500 at ppm		C		Kostorz[10] (1968)
	W	"	60		C		Jax[12] (1971)
	W	"	20	None	None	None	Koss[16] (1971)
9.	Zr	poly	720	"	"	"	Begley & Bechtold[8] (1961)
	Zr	"	250	C	C		Harris[9] (1966)
	Zr	"	500		C		Palmer & Flewitt[14] (1970)

2. In order to observe the predicted hardening value based on any solution hardening model, it is necessary to use the correct size mismatch and modulus mismatch values, and also their temperature dependence should be taken into account.

3. In a study of single crystals it is essential to maintain the orientation constant and this does not seem to be the case in any of the previous investigations on Nb alloys where single crystals of random orientations have been used. It has been shown by Bowen et al[29] and Foxall et al[41] in niobium that the orientation had a profound effect on the activation of slip planes and the Schmid's law was no longer applicable as is also the case in other b.c.c. metals. It would therefore seem that spurious results will be obtained if the orientation dependence is neglected.

4. Finally, it should be noted that the current solution hardening theories do not take into account the variation of stress with temperature in the temperature dependent region and the stress could be influenced by core interactions of shorter range that can be calculated by using the theory of elasticity. Hence it can not be assumed that the effects due to size misfit or modulus mismatch or short range ordering etc. remain constant over an entire range of temperature. It would, therefore, seem more appropriate that the comparison between experimental observations and theoretical predictions are made in the temperature independent region of stress i.e. the athermal component of stress rather than

with the flow stress itself. While Kostorz[10], Palmer and Flewitt[14], Jax[12], Koss[16] and Kan[13] considered the athermal stress, Harris[9] and Peters & Hendricson[18] compared the total stress in niobium alloys.

In view of the observations made above it is not surprising that different studies find different correlations between the solute content and solution hardening in niobium, and also that there is no agreement amongst various authors[21,40] with regard to the relative importance of the size and modulus mismatches in b.c.c. metals. In the present investigation, however, a linear correlation was observed between the total stress and solute Zr atoms in niobium at any level of strain, fig. 21. The stress values for intermediate Zr concentrations have been determined by Harris[9] at comparable strain rate and interstitial impurity level and they are in agreement with the present results - see (0.2% e_p) fig. 21. Palmer and Flewitt[14] found the yield stress of Nb-25 wt% Zr solid solution (30 μ grain size) containing 50 ppm interstitial impurities and tested at 3.7×10^{-3} $\dot{\varepsilon}$ to be 75 kg/mm^2 at room temperature which is in reasonable agreement with the extrapolated value of 71 kg/mm^2 in the present investigation. The Mott-Nabarro theory predicts an increase of 3.47 kg/mm^2 in stress per at% of Zr in Nb which is of the same order of magnitude but larger than the observed increase of 2.2 kg/mm^2 in the present study. At higher level of strains the scatter in the data points was a little more which could be due to the different work hardening effects in the different alloys.

While this linear relationship was maintained at ambient and higher temperatures, it was not the case at lower temperatures, fig. 22. At 215°K strengthening in niobium was realized only beyond 0.87 at% Zr whereas at 77°K, no strengthening occurred; on the other hand softening of the parent metal (Nb) took place. This behaviour of alloy softening will be discussed in detail later.

In order to get an insight into the strengthening and softening behaviour and to obtain a correlation with concentration, strain and temperature, we will now consider separately the thermal and the athermal components of stress in niobium and its alloys. The values of $\Delta\sigma_\mu$ deduced from earlier studies on various niobium base alloys have been plotted against the solute concentration in fig. 57. Increases in stress $\Delta\sigma$ in Nb-Mo and Nb-W alloys have been also shown in fig. 58. It is now apparent that the data of Peters and Hendricson[18] on Nb-Mo single crystals, and Koss's data[16] on Nb-W single crystals beyond 1 at% W, followed the linear dependence upon concentration for both σ and σ_μ. According to the linear equation

$$\sigma = \sigma^* + \sigma_\mu$$

it would, then, mean that σ^* was also linearly dependent upon solute content in these alloys. However Harris' results[9] on Nb-Zr showed that only σ obeyed the linear dependence. σ_μ increased rapidly upto 0.5 at% Zr and then the rate of increase was slower and linear similar to Koss's observations on Nb-W alloys. According to the Mott-Nabarro theory[15] the solution strengthening rate for various solutes in Nb are as shown in table VIII. It is seen that the observed solution

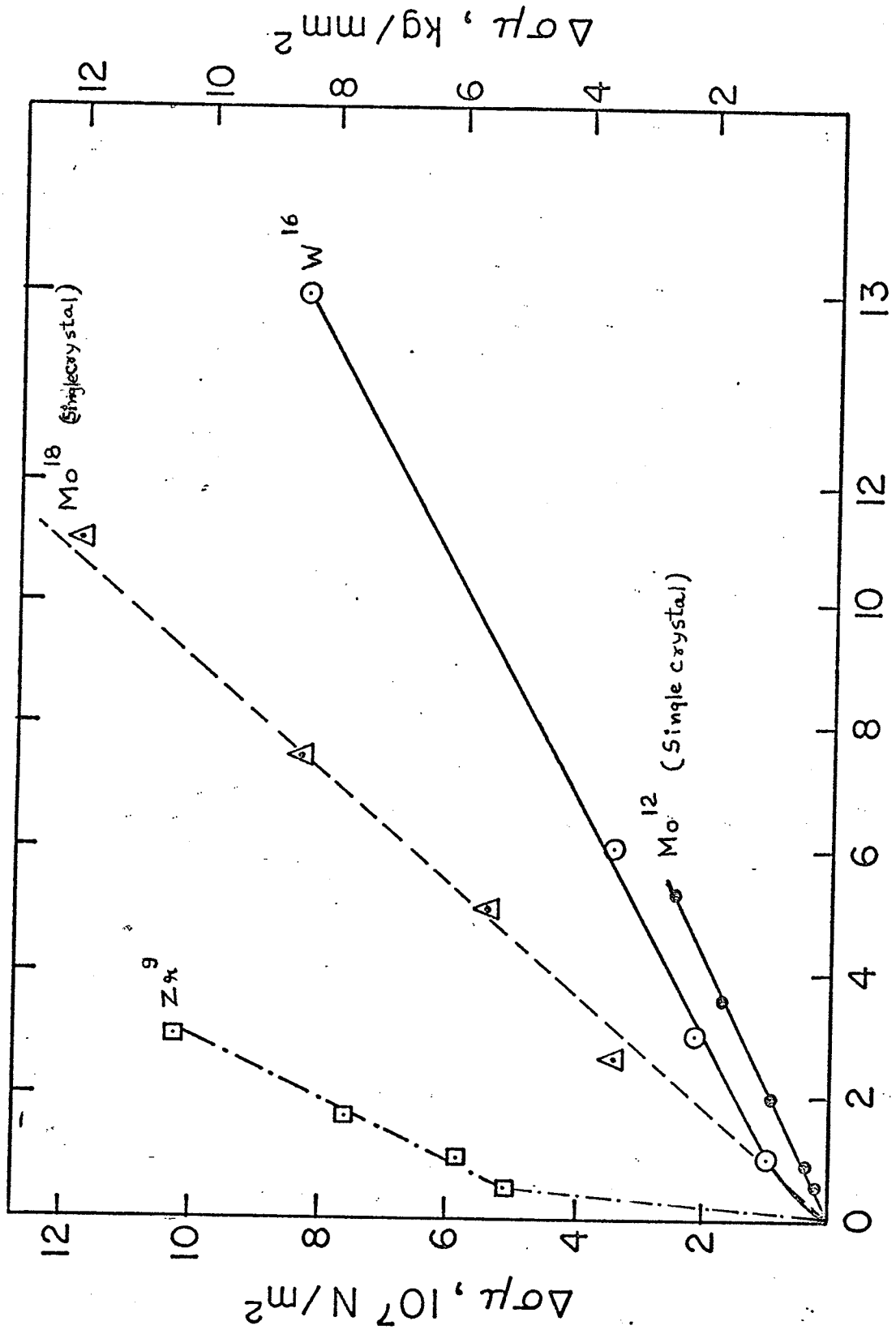

Figure 57: Solution hardening of the athermal stress $\Delta\sigma\mu$ as a function of concentration for various solutes.

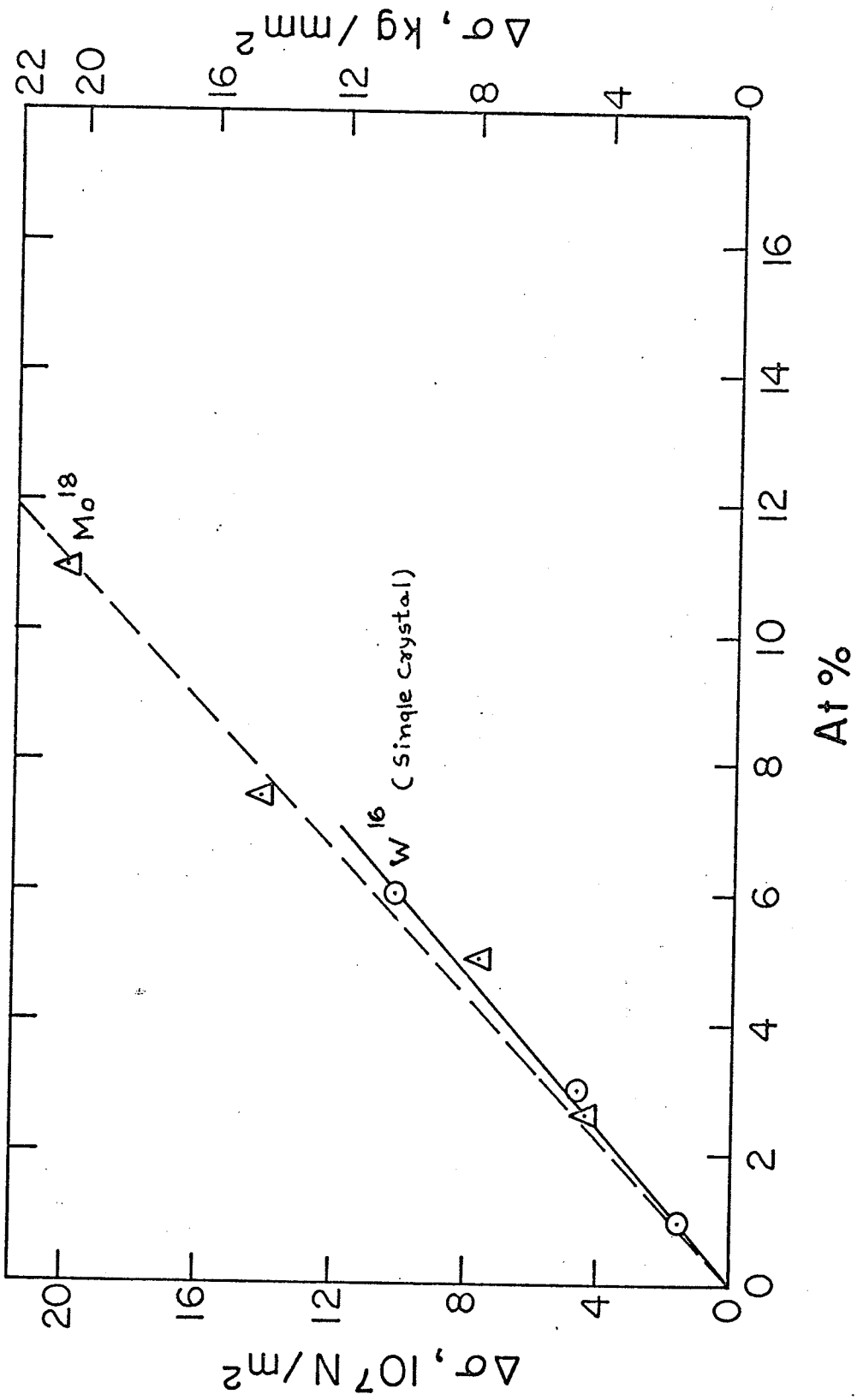

Figure 58: Solution hardening $\Delta\sigma$ as a function of concentration for various solutes.

TABLE VIII

Solute	$\varepsilon_a = \frac{1}{a}\cdot\frac{da}{dc}$	$G\varepsilon_a^{2}$	$\varepsilon_a^{4/3}$	$2.5G\varepsilon_a^{4/3}$	Observed $\Delta\sigma$ per unit solute	Remarks
Ta	0	0	0	0		G for Nb 3.73×10^3 kg/mm^2
Mo	4.7×10^{-2}	8.2 kg/mm^2	1.72×10^{-2}	160kg/mm^2	217kg/mm^2	
W	6.1×10^{-2}	13.8 kg/mm^2	2.44×10^{-2}	227kg/mm^2	173kg/mm^2 (for single crystals)	
Zr	8.44×10^{-2}	26.6 kg/mm^2	3.72×10^{-2}	347kg/mm^2	220kg/mm^2	

strengthening rates are either too low or too high, depending upon the formula used. However, the linear concentration dependence of strengthening is obeyed in the cases of all the solutes. Another noticeable feature is the presence of a considerable amount of solution hardening in the Nb-Ta alloys inspite of the fact that the size misfit is zero in this system. This is indicative of some important factor in solution hardening other than the size mismatch.

In the present investigation $\Delta\sigma_{2.5\%e_p}$ and $\Delta\sigma_{\mu_{2.5\%e_p}}$ at room temperature showed c and $\sqrt{c}$ dependences respectively. $\Delta\sigma_\mu$ at 0.2% e_p for 25 wt% Zr at 290^{o}K is also shown in fig. 59 but this value is too small by $\sim$ 5 kg/mm^2 than the extrapolated value. If $\sigma = \sigma^* + \sigma_\mu$ relationship is true, then it would mean that σ^* had a complex dependence on concentration. Moreover, this kind of correlation for σ^* is not very meaningful since this relationship would be varying due to changes in σ^* and σ_μ with change in temperature,

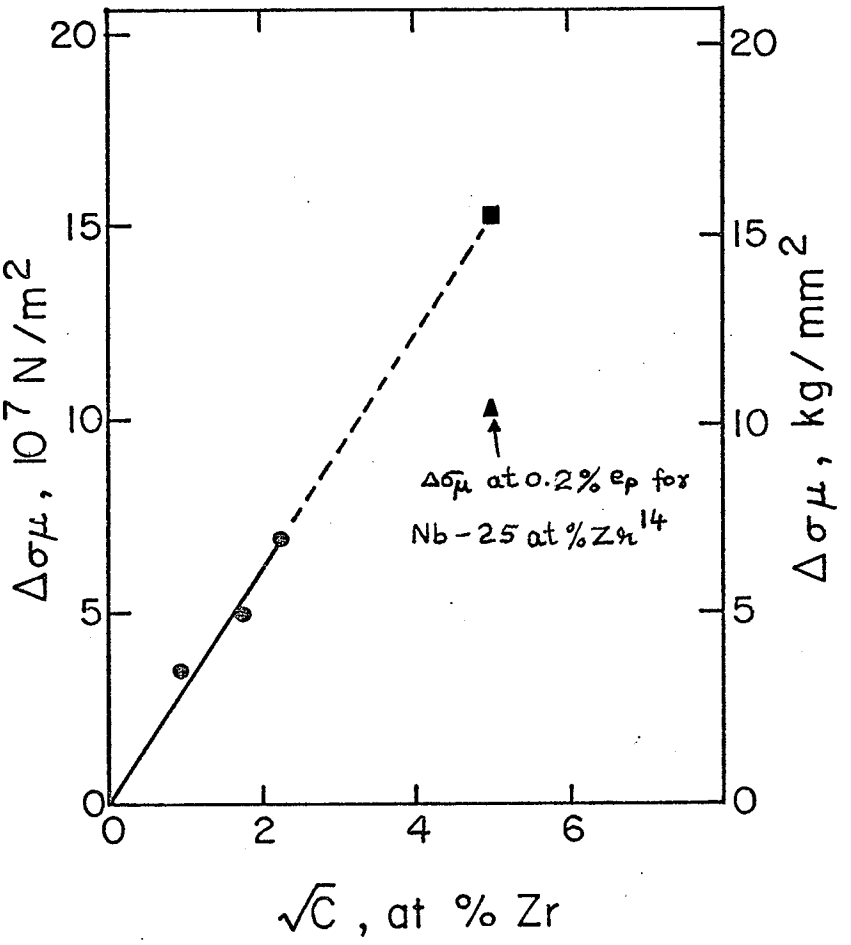

Figure 59: Increase in the athermal stress $\Delta\sigma\mu$ plotted against (concentration)$^{1/2}$ of Zr.

fig. 60. The complication is further aggravated by the occurrence of solution softening. Kostorz[10] studied the solid solution hardening in niobium alloy single crystals at 570°K and found a linear relationship in a semi-log plot, the slope $\frac{d\tau u}{d\sqrt{c}}$ and the misfit parameter ε from the Fleischer's theory[11] of solution hardening. According to this theory the increase in strength due to the solution hardening of metals is given by

$$\Delta\tau = \frac{G}{760} \varepsilon^{3/2} C^{1/2}$$

$$= \frac{G}{760} \left| \alpha\varepsilon_a - \varepsilon_G' \right| C^{1/2}$$

where G = shear modulus

ε_a = size mismatch = $\frac{1}{a} \cdot \frac{da}{dc}$

a = lattice parameter of the solvent

c = atomic concentration of solute

$\varepsilon_a' = \varepsilon_G/(1 + |\varepsilon_a|/2)$

$\varepsilon_G = \frac{1}{G} \cdot \frac{dG}{dc}$

α = 3 for screws and $\pm$16 for edges

In the case of Nb-Zr solid solutions ε_a is 8.44×10^{-2}, ε_G' is 1.43 and G for Nb is 3.73×10^3 kg/mm^2. The different values of α in the above equation yield different ε values as seen below.

When $\alpha = 3$, $\varepsilon = |3 \times 0.084 - 1.43|$ $\varepsilon^{3/2} = 1.3$

$\alpha = 16$, $\varepsilon = |16 \times 0.084 - 1.43|$ $\varepsilon^{3/2} = 0.058$

or $\alpha = -16$, $\varepsilon = |-16 \times 0.084 - 1.43|$ $\varepsilon^{3/2} = 4.46$.

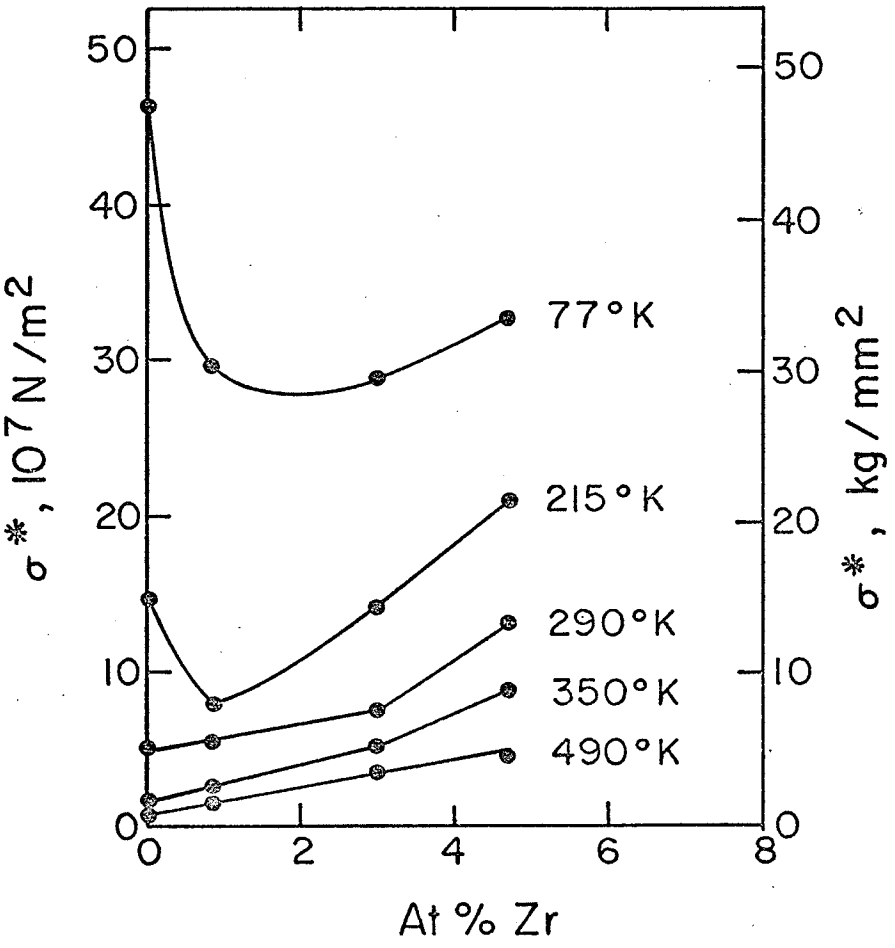

Figure 60: Effect of Zr concentration on the thermal stress σ* at various temperatures.

And

$$\Delta\tau = \frac{G\varepsilon^{3/2}c^{1/2}}{760} = \frac{3.73 \times 10^3 \times 1.3 \times 1}{760 \times 10}$$

$$= 0.637 \text{ kg/mm}^2 \text{ when } \alpha = 3 \text{ and } c = 1\%$$

$$\Delta\tau = \frac{G\varepsilon^{3/2}c^{1/2}}{760} = \frac{3.73 \times 10^3 \times 0.058 \times 1}{760 \times 10}$$

$$= 0.028 \text{ kg/mm}^2 \text{ when } \alpha = 16 \text{ and } c = 1\%$$

or $$\Delta\tau = \frac{G\varepsilon^{3/2}c^{1/2}}{760} = \frac{3.73 \times 10^3 \times 4.46 \times 1}{760 \times 10}$$

$$= 2.19 \text{ kg/mm}^2 \text{ when } \alpha = -16 \text{ and } c = 1\%.$$

Kostorz[10] found that the results were in close agreement with the theory when $\alpha = \pm 16$ and 680 instead of 760 were used in the formula. In the present case the increase in athermal stress $\Delta\sigma_\mu$ was 3.0 kg/mm^2 per at% Zr, fig. 59, which is slightly higher than the predicted value of 2.19 kg/mm^2. If we use $\alpha = -16$ and 680, the predicted value will be 2.45 kg/mm^2 which is still lower than the observed result. In conclusion it may be said that most likely the linear concentration dependence of $\Delta\sigma$, $\sqrt{c}$ dependence of $\Delta\sigma_\mu$ and a complex concentration dependence of $\Delta\sigma^*$ are true in Nb-Zr solid solutions.

The $\sqrt{c}$ dependence of $\Delta\sigma_\mu$ was almost independent of strain and temperature but the linear concentration dependence of $\Delta\sigma$ is not observed due to solution softening at subambient temperatures. C dependence of $\Delta\sigma$ is independent of strain.

5.3 Alloy Softening

It was found that the hardening behaviour of solute Zr atoms changed completely at subambient temperatures and instead of hardening, softening was observed in the alloys. It was most predominant at the lowest temperature studied i.e. 77°K, Figure 22. A comparison of the thermal and athermal components of flow stress in Nb - Zr alloys showed that it was the thermal component that decreased on initial alloying and thus, the stress level in the alloys at lower temperatures was below that of the parent metal. Unlike in the fcc lattice, the phenomenon of alloy softening has been observed in several bcc metals.[18-21] Recently, Leslie[42] has cited 21 alloy systems of iron which exhibit softening and suggested the following:

1. Alloy softening could occur regardless of whether:
   a. the solute atoms are substitutional or interstitial,
   b. the elastic constants are increased, decreased or unchanged with solute addition,
   c. the solute reacts strongly with interstitial solutes (C, N & O).
2. Softening was not the result of scavenging processes in solid solutions.
3. The earlier suggestion[43,44] that substitutional atoms larger than those of the solvent would produce little softening, was found to be incorrect.
4. Only those elements which were effective strengthners

produced alloy softening.

5. There is a 'critical' concentration of substitutional solutes required to produce the maximum softening and this concentration is inversely proportional to the effectiveness of the solute as a strengthening agent. Beyond this concentration softening is replaced by strengthening throughout the entire temperature range.
6. Solid solution softening occurred because of the promotion of double kink nucleation on screw dislocations as a result of the presence of solute atoms having appreciable size misfits.
7. In the temperature and strain rate ranges in which softening occurred, solutes reduced the thermal component of stress to less than that of the parent metal.

In the wake of foregoing conclusions we can now discuss the solution softening in Nb - Zr in terms of the present results and those of Harris,[9] also on Nb alloys.

(1) At $77^{o}K$ the thermal stress σ^* (and therefore σ) decreased with the initial additions of up to 3.0 at%Zr, and then it took an upward trend but the stress level at 4.7 at%Zr still remained lower than that of the pure Nb, Figure 22.

(2) From the curve for $77^{o}K$ in Figure 22 it is seen that the maximum softening i.e. a 12.5 kg/mm^2 decrease in σ occurs at about 2.4 at%Zr.

(3) Despite the fact that the Zr atom is much larger than the

Nb atom this substantial softening (12.5 kg/mm^2) is produced, and this is in variance with the earlier suggestion[43,44] that only those solute atoms that are smaller than the solvent atoms, will produce softening.

4. With an increase in the concentration of Zr, the temperature dependence of σ^* decreased and the range of temperature in which softening was present, narrowed markedly.
5. The flow stress-concentration curves of Harris[9] at 173°K had minima at 0.9 at%V, 1.0 at% Zr and 0.5 at% W but no minima were observed in the Nb - Ta alloys. At room temperature and these particular concentrations, while Zr and W increased the elastic constants of the alloys, V and Ta decreased them, thus showing that the softening was independent of changes in the elastic constants.
6. Of Ta, V, W and Zr solutes, the Ta atom is similar in size, V and W are smaller and the Zr atom is larger than the Nb atom. Softening was absent in the Nb - Ta alloys which indicated the importance of size misfit and thus of the effectiveness of the solute as a strengthening agent, in observing softening in the Nb alloys. Ta was the least effective hardener in niobium.
7. Solution softening by interstitial solute has been shown by Ravi and Gibala[47] in niobium-oxygen alloys. They also found a critical concentration of oxygen atoms beyond which

the softening was replaced by hardening.

The general explanations given for solution softening in bcc metals are:-

(I) The promotion of cross slip[50,51] and increase in the mobile dislocation density[48,49] due to the presence of solute atoms. Harris[9] studied the surface slip characteristics of Nb - V alloys at ambient and low temperatures where solution softening was observed and found that additions of V considerably reduced the incidence of long wavy slip lines which are caused by cross slipping and are so characteristic of pure bcc metals. Thus, the case of cross slip does not seem to be important in determining the solution softening in Nb.

In the present investigation ΔH was a linear function of temperature for Nb and Nb - Zr alloys in the temperature range where solution softening was observed but the slope of the curves decreased slightly with increase in the content of Zr, Figure 52. From the rate equation

$$\dot{\varepsilon} = \dot{\varepsilon}_o \exp(-\Delta H/KT)$$

we can see that $\ln(\dot{\varepsilon}_o/\dot{\varepsilon}) = \Delta H/KT$

i.e. the pre-exponential factor $\dot{\varepsilon}_o$ which contains the mobile dislocation density factor, decreases when the slope of the curve in ΔH-temperature plot decreases. This shows that the mobile dislocation density in the Nb - Zr alloys did not increase in the solution softening region and

thus the increase in mobile dislocation density also was not important in determining the solution softening in Nb.

(II) The scavenging of residual interstials by the solute has been proposed by Ravi and Gibala[47] as the reason for solution softening. However, there are two problems with the scavenging mechanism namely (a) the softening was not present at higher temperatures and the temperature range in which it was present narrowed with increase in the Zr content, Figure 61, which one may expect to remain nearly constant for all the compositions. Thus it is necessary to postulate a temperature-dependence of the relevant interaction in the scavenging mechanism to explain the observance of solution softening in only a small low-temperature range, and (b) it is not clear why the association of interstial and/or solute atoms will cause softening; clustering is generally assumed to strengthen a solid solution because the reduction in the number of obstacles is more than offset by the increased strength of each obstacle. The base material had $\sim$ 1500 at. p.p.m. interstitial impurities and it is not known why 47000 Zr atoms/10^6 will be required to scavenge them. It is, thus, apparent that scavenging was not the complete explanation for the softening of the Nb - Zr solid solutions but it is possible that it might have had some effect.

(III) Alternatively, a reduction in the lattice frictional stress

on adding solute atoms has been suggested to explain substitutional softening. It was originally suggested by Weertman[53] that facilitation of kink nucleation on screw dislocation by the strain field of the solute atom caused softening. The reduction in the thermal component of the flowstress and the magnitude of the activation parameters for deformation observed experimentally indicates that a reduction in the lattice frictional stress was responsible for the observed softening in Nb - Zr alloys. The variation in the activation parameters during softening will be discussed in detail in the next section on deformation mechanism.

5.4 Deformation of Nb and Nb - Zr Alloys

The early studies[25,29] on the deformation behaviour of Nb have indicated that the rate controlling mechanism was the overcoming of the Peierls-Nabarro hills by the thermally activated nucleation of kinks. The present results have been considered in terms of this mechanism and the activation parameters evaluated as a function of solute concentration in the Nb - Zr alloys. We will first discuss the deformation of pure Nb and then consider the Nb - Zr alloys.

Deformation of Nb

The σ^* - temperature plot for Nb in Figure 61 shows that the curve is almost horizontal beyond $\sim 350^{\circ}K$ and for this reason the critical temperature T_c was found by taking the intersection point of the transient & horizontal portions of the curve. (However, it is realized that this procedure is followed in σ - temperature plot and not σ^* - temperature. The critical temperature $330^{\circ}K$ should not be in too much error as the magnitude of σ^* is only ~ 1 kg/mm^2 at this temperature). On extrapolating the curve to $0^{\circ}K$ we find that σ^* is 87 kg/mm^2. Knowing the critical temperature T_c and σ_o^* i.e. σ^* at $0^{\circ}K$, we can compare the results of this investigation with the predictions of the Dorn-Rajnak[54] theory. Figure 62 shows that good agreement exists between the results and theory when $\alpha = -1$. Christian and Masters[25] have also shown that the Dorn-

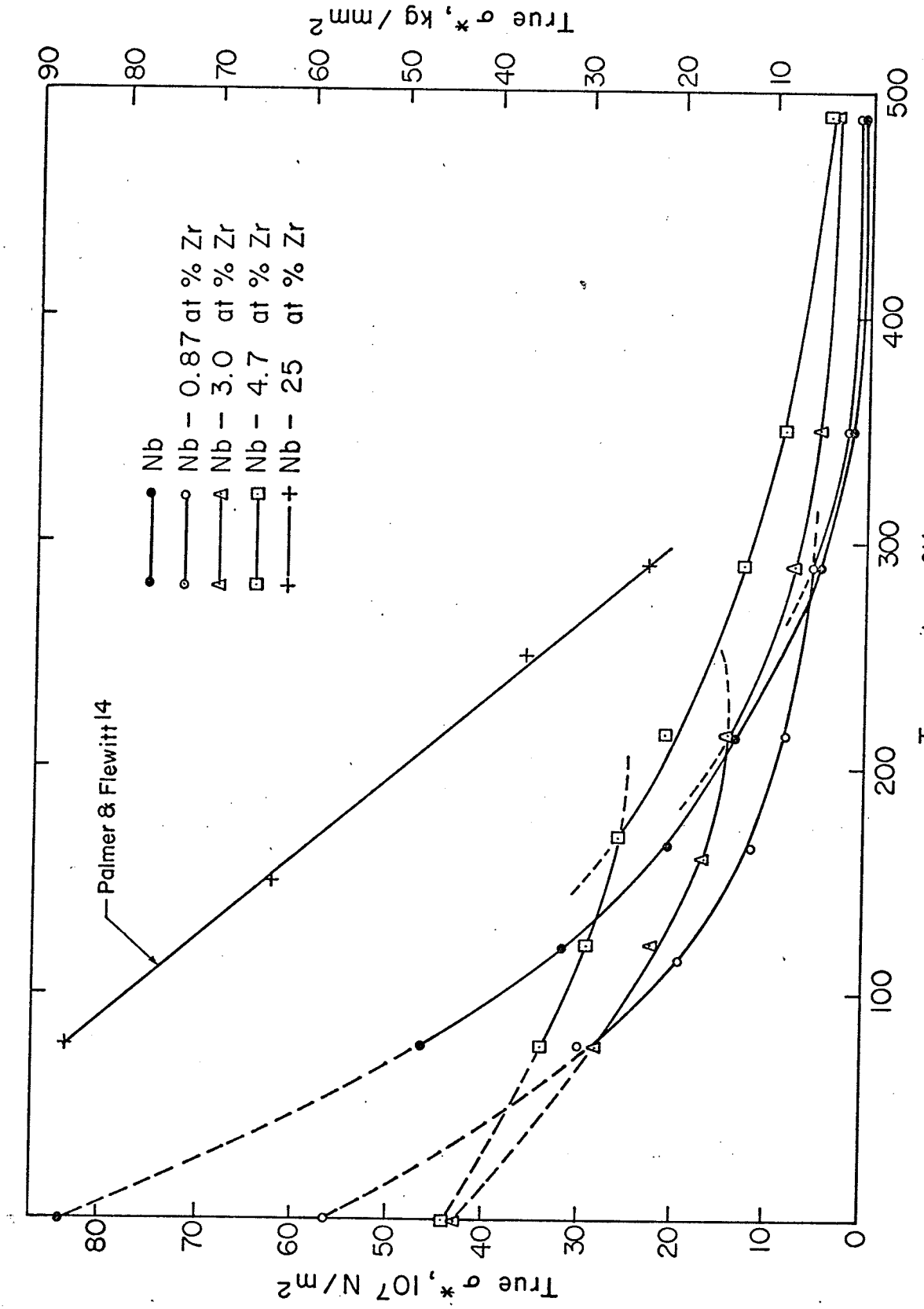

Figure 61: True thermal stress σ* as a function of temperature for Nb and Nb - Zr alloys.

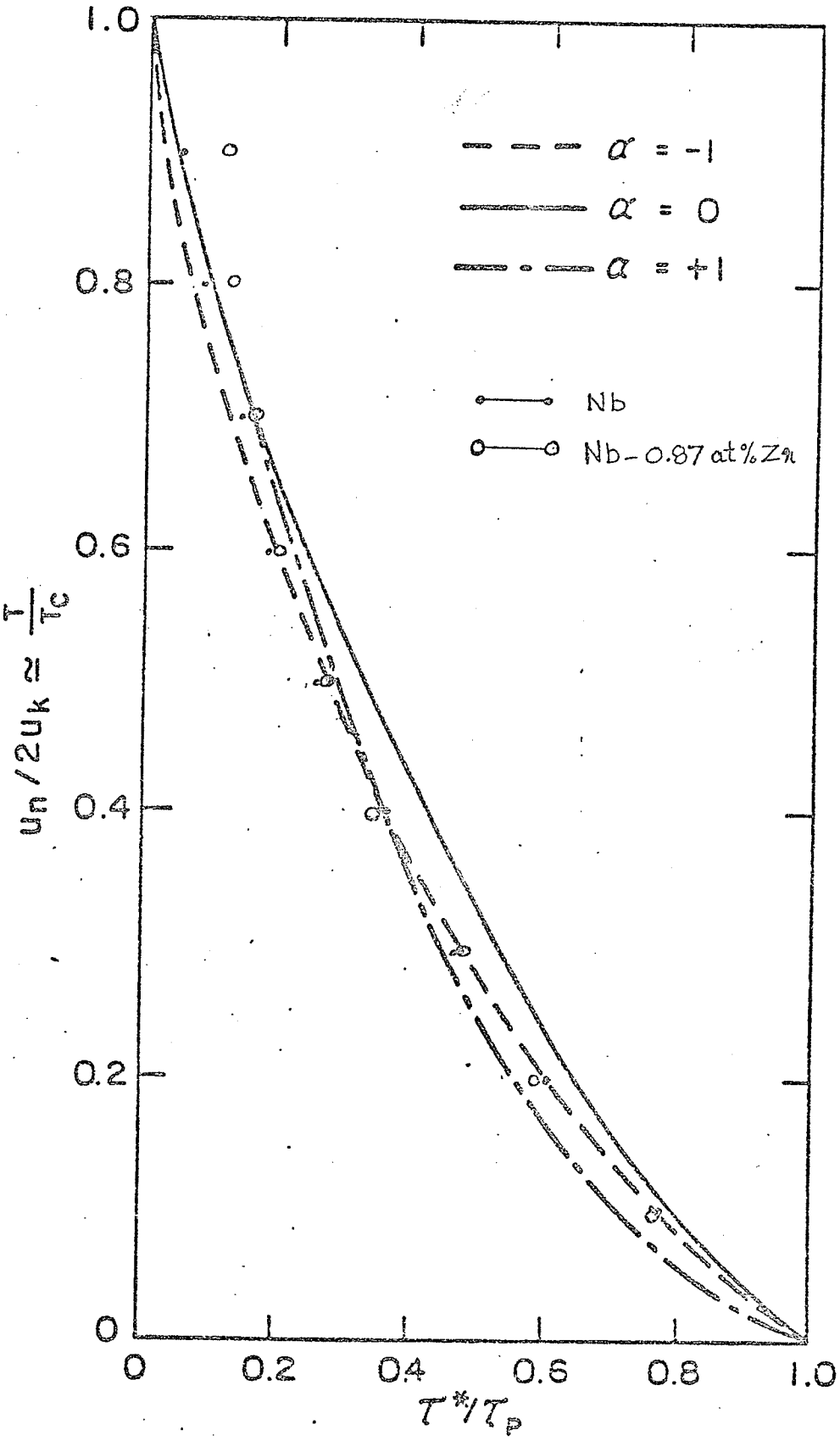

Figure 62: Dorn-Rajnak plot of temperature (activation energy) against thermal stress for Nb and Nb - 0.87 at%Zr.

Rajnak theory is obeyed in pure Nb and the overcoming of the Peierls hills by the double kink nucleation is the deformation rate controlling mechanism.

An important observation of this study was the occurrence of alloy softening in a limited range of temperature and then the takeover of softening by hardening above this range. The temperature range of alloy softening narrowed with increase in the Zr content and it seemed that the softening effect may be removed completely in higher Zr content alloys, Figure 61. Palmer and Flewitt[14] have shown that in Nb - 25 at%Zr softening was absent in the entire range of temperature. The solution softening in Nb - Zr alloys decreased the temperature dependence of σ^*. However, in Nb - 25 at%Zr[14] the temperature sensitivity was increased considerably, Figure 61. This shows that it is the thermal stress σ^* that is decreased and is smaller in the alloys than the solvent metal in the softening range of temperature.

Nb - 0.87 at%Zr -

In Figure 61 the Nb - 0.87 at%Zr curve is above the Nb curve only beyond $\sim 290^{\circ}K$ and the extrapolated value σ_o^* of σ^* at $0^{\circ}K$ is 58 kg/mm^2. If we take $290^{\circ}K$ as the critical temperature T_c and $\sigma_o^* = 58\ kg/mm^2$, good agreement is found between the results and the Dorn-Rajnak theory upto $T/T_c \simeq 0.7$ in Figure 62 but beyond this, considerable deviation occurs. This indicates that in the low temperature region where alloy softening is more pronounced, the double kink nucleation is the rate controlling mechanism as in

pure Nb.

The alloy softening in Nb - 0.87 at%Zr was accompanied by smaller values of the activation parameters V*, ΔH and H. However, these parameters had larger values than those of pure Nb beyond the range of solution softening, Figures 48, 50 and 51. The decrease in total energy H indicates a barrier softening (i.e. decrease in the Peierls Stress) in this alloy in the low temperature region. It was first suggested by Weertman[53] that the solute atoms can decrease the Peierls Stress (thermal stress) of the solvent metal and facilitate the nucleation of a kink provided the attractive force between the dislocation and the solute atom is not too strong. The Peierls Stress σ_o^* is given by

$$\sigma_o^* = c\,\mu \exp(-2\pi\omega)$$

where c = constant

μ = shear modulus

and ω = width of the dislocation

Since it has been shown by Harris[28] that Zr increases the shear modulus of Nb by a small amount, σ_o^* can be decreased only when ω is increased. Being an exponential term, this could lead to a large decrease in the Peierls Stress. In a regular lattice the presence of a solute atom causes a local distortion; such a distortion near a dislocation will produce a more diffused core i.e. the dislocation width will increase, the Peierls Stress will decrease and thus in the vicinity of solute atoms a kink will nucleate more easily with the help of thermal activation.

Nb - 3 at%Zr and Nb - 4.7 at%Zr -

Figure 61 shows that the thermal stress σ^* at 77^oK decreases upto 3 at%Zr and then the trend reverses. A similar trend in σ VS at%Zr is seen in Figure 22 where a minima in stress at 77^oK occurs at $\sim$2.4 at%Zr. It is, thus, seen that beyond a certain concentration at any temperature, hardening starts taking over from softening. This behaviour has also been seen in Nb - Mo[18], Nb - O[17] and V - Ti[52] and it may be explained as follows.

The plastic deformation takes place by the nucleation and propagation of the kinks through the lattice and the addition of the solute atoms may have two opposing effects: a) the decrease in the Peierls Stress as discussed earlier and b) the usual solid solution hardening. These two effects are not necessarily equal and may have different concentration and temperature dependences. Assuming the effects are linearly additive, the thermal stress σ^*_{alloy} of 3 at% and 4.7 at%Zr alloys can be written as:

$$\sigma^*_{alloy} = \sigma^*_{Nb} + \sigma^*_{Zr}\,(\text{softening}) + \sigma^*_{Zr}\,(\text{hardening})$$

where σ^*_{Nb} = thermal stress of Nb

σ^*_{Zr}(softening) = decrease in the Peierls Stress (barrier softening) on the addition of Zr (this is a negative contribution).

and σ^*_{Zr}(hardening) = increase in σ^*_{Nb} through solid solution hardening on the addition of Zr (this is a positive contribution).

The presence of solute atoms will decrease the Peierls Stress and thus assist in the nucleation of double kinks but the propagation

of kinks may become more difficult because of solution hardening. It seems that the initial Zr additions decrease the Peierls Stress and make the kink nucleation easier while at the same time making kink propagation harder. However, kink nucleation is still much more difficult than the kink propagation and therefore it is the rate controlling process. With the later addition of Zr, the 'stress-decreasing' effect starts minimising due to the 'stress-increasing' effect becoming significant. As mentioned earlier, this may happen if the two effects have different concentration dependence. The present results showed that $\sim$2.4 at%Zr is the concentration beyond which the 'stress-increasing' effect becomes noticeable at $77^{o}K$.

In 3 at% and 4.7 at%Zr alloy the decrease in σ^* in the alloy softening region is accompanied by an increase in V^* and H unlike in 0.87 at%Zr alloy, however the activation energy ΔH decreased, Figures 48, 50 and 51. The increase in H indicates an increase in barrier strength. It was checked if the sudden rise in ΔH, Figure 50 was due to dynamic strain-aging (d.s.a.). The d.s.a. was observed in only 4.7 at%Zr at $350^{o}K$. The temperature where the sudden rise in ΔH occurred was $\sim 150^{o}K$ which is much lower than the d.s.a. temperature. Figure 51 shows an upward inflexion in the H - σ^* plot suggesting a modification in the rate controlling mechanism for 3 at% and 4.7 at%Zr below a certain σ^*. The inflexions coincide closely with σ^* where the 3 and 4.7 at%Zr curves go above the Nb curve in Figure 61 (i.e. alloy softening is replaced by alloy

hardening). Thus the lower H value is for the low temperature (softening) region and the higher H value is for the high temperature (hardening) region. Under ideal condition i.e. when the pre-exponential factor $\dot{\varepsilon}_o$ in the rate equation remains constant with temperature the σ^* - $\bar{V}^*$ plot is also a force-distance curve. $\dot{\varepsilon}_o$ which is the slope of the curve in ΔH - ^oK plot, changed in the present case, Figure 52, yet, the σ^* - V^*/b^3 plot in Figure 48 gives some idea about the force-distance curve for various compositions. It is seen that the areas under the 3 and 4.7 at%Zr curves have become more than that under the Nb curve and the slope of the curves has also decreased in the case of these alloys.

The foregoing results on the deformation of Nb and Nb - Zr alloys may be represented schematically as shown in Figure 63

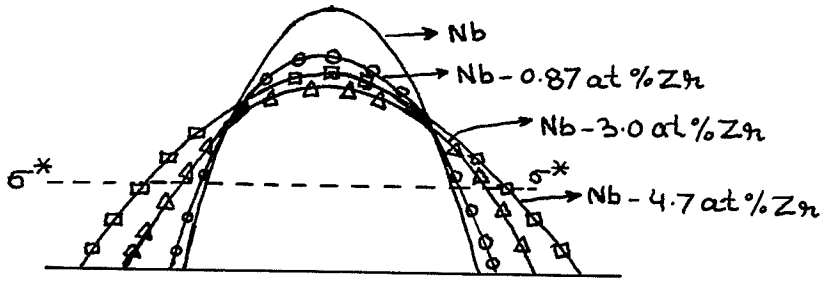

Alloy Softening Region

Figure 63: Schematic stress-activation area plot for Nb and Nb - Zr alloys.

Although the addition of Zr decreases the activation energy ΔH, it modifies the stress-activation area plot in such a way that the total area under the curve i.e. the total energy H is smaller for 0.87 at% and increasingly larger for 3 at% and 4.7 at%Zr in the alloy softening region, Figure 51. If we consider the deformation of 3 at% and 4.7 at%Zr alloy in terms of kink nucleation and kink propagation, the decrease in σ^* on alloying suggests that the kink nucleation is still the rate controlling mechanism in these alloys, however the barrier strength has increased considerably as a result of a new force-distance curve modified by the solutes in some complex manner.

In the higher temperature (alloy hardening) region of 3 at% and 4.7 at%Zr alloy, Figure 61, there is an increase in H, Figure 51, suggesting a modification in the rate controlling mechanism. It would seem reasonable to think that at these temperatures the kink nucleation has become much easier and is no longer the rate controlling process. On the other hand kink propagation or the overcoming of solute atoms is important, which is controlled by the solute size-misfit and dislocation-solute atom interaction, each solute atom acting as a thermally activatable barrier. The $c^{1/2}$ dependence of σ_μ and c dependence of σ show that the Zr atoms are randomly distributed. The fact that σ^* and ΔH are being affected with the addition of Zr shows that the deformation by either overcoming the solute barrier or kink propagation is a thermally assisted process in this temperature range.

If the solute atom acts as a strong pinning point for the dislocations, the situation will be equivalent to the one considered by Ono and Sommer[55]. However, according to their calculations the interparticle distance in the 3 at% and 4.7 at%Zr alloy will be too small for the thermally activated nucleation of kinks to be possible. In such a situation it would seem that the solute barriers will be overcome by the screw dislocations with the help of thermal activation.

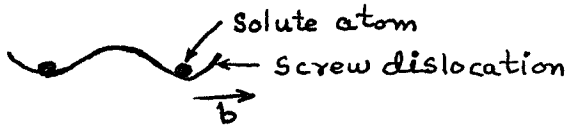

Alternatively, the solutes may be weak pinning points and the kink nucleation will not be on a finite dislocation length. In this case it will be the dislocation kinks which will be in edge orientation, overcoming the strain field of the solute with the help of thermal activation. It is not clear which of the above two mechanisms is operative in the hardening region.

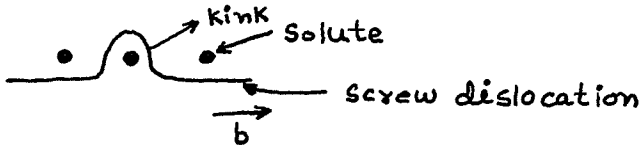

5.5 Dislocation Dynamics

In agreement with earlier investigations on the dislocation dynamics of Nb,[13,37] the present study showed that m* for Nb and Nb - Zr decreased initially with plastic strain upto ∿5% and then was essentially independent of strain at all temperatures investigated - see Figure 53. Gupta and Li[37] observed that m* for commercial purity Nb and one zone pass Nb dropped from an initial value of 14 to 7 after ∿7% plastic strain at room temperature. However, m* was independent of strain and had a value of 7 in 3 zone pass Nb. They thought that it was due to the plastic deformation which has some kind of strain-induced purifying effect in the impure niobium matrix. However, the fact that such initial decreases were observed in highly purified Nb and Nb - Mo crystals by Kan[13] and three zone passed Nb and Nb - Zr polycrystals in this investigation, does not seem to support the sweeping mechanism. Most probably, it was due to rapid multiplication of dislocations and hence a non-steady state process of deformation during yielding and initial macroscopic flow. Since yielding and initial plastic flow behaviour depend greatly on the purity and orientation of the niobium crystals, these two factors must be considered while comparing the results of the different or even the same investigations.

Guberman[35] used etch pit and relaxation techniques to determine $m^* = \frac{\Delta \ln \dot{\varepsilon}}{\Delta \ln \tau}$ for niobium crystals and found it to be increasing with plastic strain. The strain dependence of m* was due

to the fact that τ instead of τ^* was used in the calculation and whereas $\Delta \ln \tau^* = \ln\left(\frac{\tau^* + \Delta\tau}{\tau^*}\right)$ remains constant in Nb, $\Delta \ln \tau = \ln\left(\frac{\tau + \Delta\tau}{\tau}\right) = \ln\left(\frac{\tau\mu + \tau^* + \Delta\tau}{\tau\mu + \tau^*}\right)$ decreases because $\Delta\tau$ remains constant. A change in $\Delta \ln \tau$ in the denominator of the expression for m* will lead to a variable m*.

The strain independence of σ^* and V* in Nb and Nb - Zr would also dictate via the relation $m^* = \frac{V^*\sigma^*}{KT}$ (1) that m* be independent of strain because V* and σ^* are essentially independent of strain at a constant temperature and strain rate. This in turn showed that the rate controlling obstacle did not change during plastic deformation and the mobile dislocation density remained essentially independent of strain and the imposed strain rate.

An increase or decrease of m* on addition of solute Zr depended upon whether solution hardening or softening was taking place at any particular temperature, Figure 54. At room temperature solution hardening was observed for all the compositions and m* increased continuously. The calculated value of m* for Nb - 25 at%Zr was found to be 52 at $77^{o}K$, compared to 35.5 for pure Nb. Kan[13] showed that m* for Nb - Mo crystals increased rapidly in the beginning with Mo content but later on the rate was slower. m* for Nb - 5.3 at%Mo crystals was $\sim$20 as compared to $\sim$5 for Nb at room temperature. However, no systematic variation was found in Nb - Zr at temperatures where solution softening was present.

The m*-temperature curve, Figure 55 is essentially in concert

with σ^*-temperature plot, Figure 61, indicating that the dislocation dynamics approach and the thermally activated rate approach are essentially equivalent. m^* evaluated at 5% strain for Nb and Nb - Zr increased rapidly below $300^{\circ}K$ and was affected by solution softening in alloys at subambient temperatures.

If the thermally activated deformation approach is equivalent to the dislocation dynamics approach in a system, then the relationship (1) should be valid assuming that the entropy effect is not significant. In the present study m^* was determined by both the stress relaxation and the strain rate change techniques and close agreement was found between the two values. Further, from equation (1) we see that m^*T should be independent of temperature. However, at higher temperatures entropy effects may become important and it was shown by Li[38] via the use of the third law of thermodynamics that since $\Delta S \rightarrow 0$ as $T \rightarrow 0^{\circ}K$, for a single activated process, m^*T approaches a limiting value. Thus, in the limit $T \rightarrow 0^{\circ}K$, m^*T can be evaluated with the minimum entropy effect. The m^*T - T curves for Nb and its alloys in Figure 64 show that m^*T is essentially constant for Nb upto $\sim 250^{\circ}K$, followed by a sudden drop and then it remains constant again. In the alloys however, m^*T is influenced by solution softening and its value is brought down at lower temperatures. Beyond the hump, the curves for alloys are at higher levels and have a similar shape as that for Nb. Had there been no solution softening, it seems that the curves probably would have followed the dashed lines in Figure 64. The (m^*T) in the lower

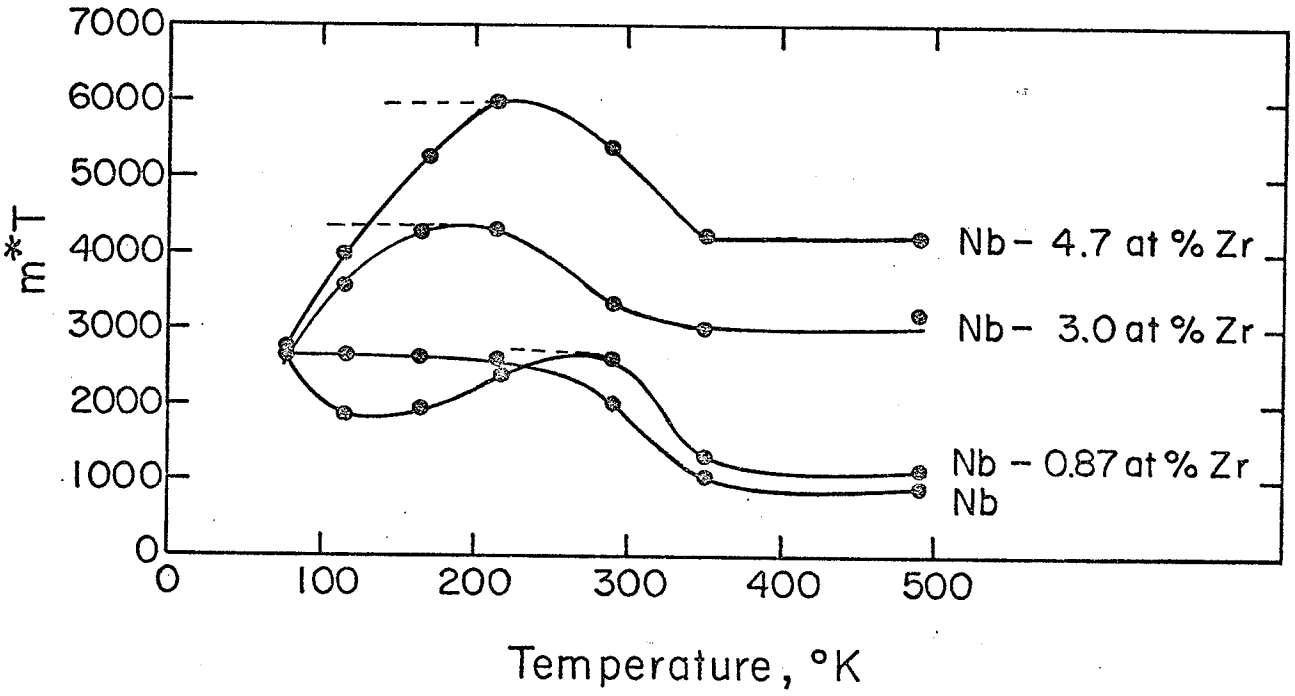

Figure 64: m*T - T plot for Nb and Nb - Zr alloys.

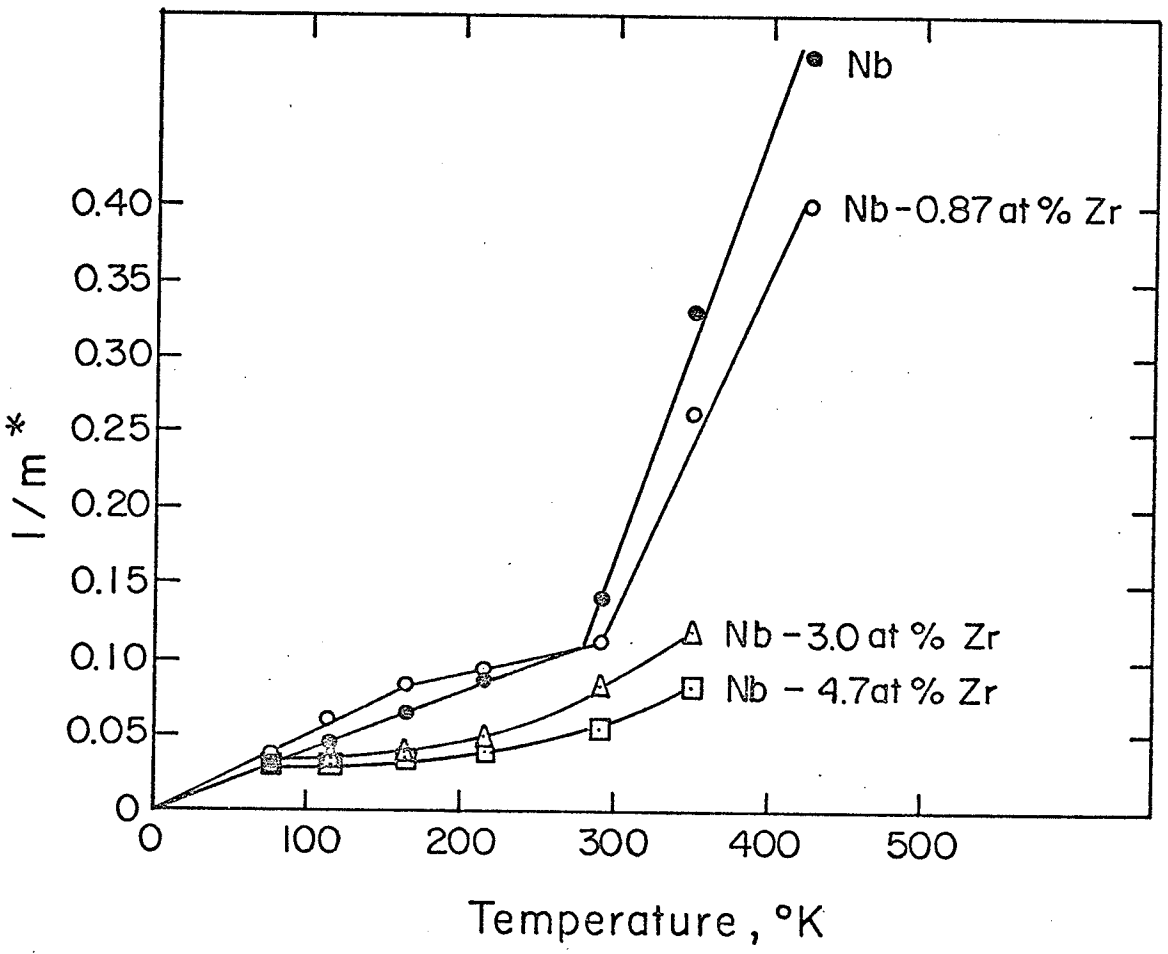

Figure 65: (1/m*) - temperature plot for Nb and Nb - Zr alloys.

temperature region can also be found by taking the limiting slope in the $\frac{1}{m^*}$ - T plot, Figure 65. If we draw tangents from $0^{o}K$ to the three alloy curves then the tangential points are at $290^{o}K$, $215^{o}K$ and $250^{o}K$ for 0.87 at%Zr, 3 at%Zr and 4.7 at%Zr alloys respectively. (In 0.87 at%Zr alloy $\sim 290^{o}K$ was the temperature where solution softening was replaced by solution hardening in this alloy). The calculated (m*T). from Figure 65 are 2650, 4300 and 5550 for 0.87, 3 and 4.7 at%Zr alloys and are in reasonable agreement with the extrapolated values (i.e. the peak values in this case) 2900, 4400 and 6000 from Figure 64.

Thus, we see that the presence of a hump in the m*T - T curves in Figure 64 is due to the occurrence of solution softening (decrease in σ^*) in the alloys. The consistency of the dislocation dynamics approach with the thermally activated deformation in Nb and Nb - Zr alloys can be shown further if we consider the m^* - $\frac{1}{T}$ plot, Figure 66 and V^* - σ^* data, Figure 49 in conjunction with the σ^* - T plot, Figure 61. As indicated above, the relationship $m^* = \frac{V^*\sigma^*}{KT}$ is valid if the two approaches to deformation are equivalent. Therefore the linear relationship between m^* - $\frac{1}{T}$ should fit with the V^* - σ^* data. In other words the inflection in the m^* - $\frac{1}{T}$ plot should correspond with the inflection in the V^* - σ^* plot. From the m^* - $\frac{1}{T}$ plot, Figure 66 we see that the temperature of inflections are $290^{o}K$, $185^{o}K$ and $215^{o}K$ for 0.87, 3.0 and 4.7 at%Zr alloys. The corresponding σ^* at the temperatures of inflection are 5.5 kg/mm^2, $\sim$15 kg/mm^2 and 21.5 kg/mm^2 from Figure 61. It is seen that the inflections in V^* - σ^* plot, Figure 49 are at 5.0 kg/mm^2,

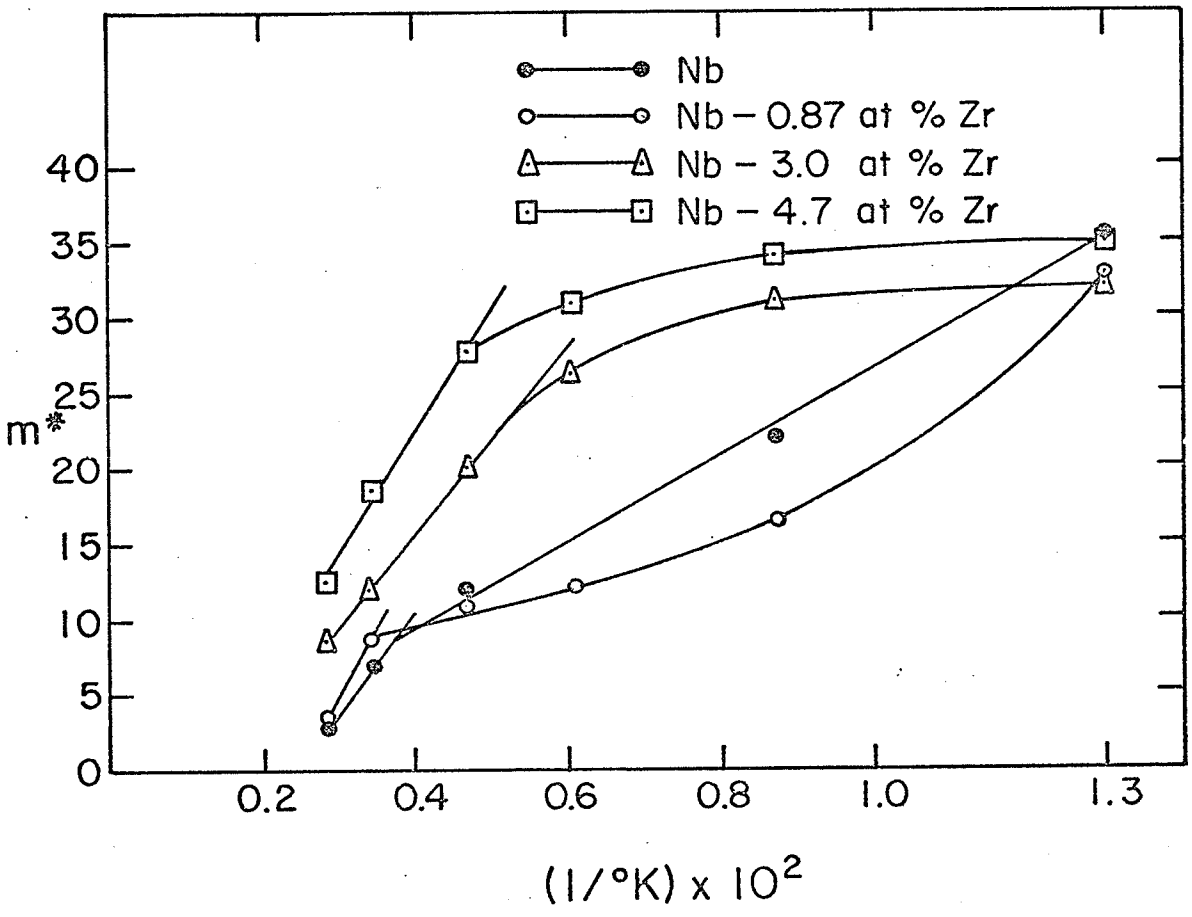

Figure 66: m* - (1/^{o}K) plot for Nb and Nb - Zr alloys.

16 kg/mm^2 and 22 kg/mm^2 for 0.87, 3.0 and 4.7 at%Zr respectively which are in close agreement with the σ^* values from Figure 61. Thus we find that the two approaches to deformation are essentially equivalent in Nb and Nb - Zr alloys and within the experimental limits the Peierls mechanism and the "Power law" seem to agree in the present case.

5.6 Work Hardening

In iron, the change to smaller slope (η) in $\log \sigma$ - $\log \varepsilon$ plot was attributed by Morrison[58] to the formation of a well-defined cellular structure due to cross slip and recovery beyond a particular strain. The tensile-test data and transmission electron microscopy were employed to check this suggestion and study the work hardening behaviour in Nb and Nb - Zr alloys. The results of electron microscopy will be discussed in the next section, however the work hardening behaviour during the tensile tests will be discussed here. The results of work hardening analysis are depicted in Figures 34 - 42 and it is apparent that, in general, solute Zr atoms had only a minor influence on the rate of work hardening $\frac{d\sigma}{d\varepsilon}$ of pure niobium at any strain level and temperature. Because of the relative strain independence of σ^* $\frac{d\sigma}{d\varepsilon}$ should be equal to $\frac{d\sigma\mu}{d\varepsilon}$ and thus the increase in athermal stress $\sigma\mu$ was the major source of strain hardening in niobium and its alloys as found in other bcc metals. While an increase in strain and temperature decreased the rate of work hardening, Figures 34, 39 and 40, solute Zr atoms increased it linearly, though not very substantially, Figures 39 - 42. The temperature dependence of $\frac{d\sigma\mu}{d\varepsilon}$ was decreased slightly by alloying, Figure 40, suggesting that Zr stabilized the dislocation structure. The amount of

work hardening realized in any system is equivalent to the difference in total work hardening and recovery taking place during deformation. While at a constant concentration the difference in $\sigma\mu$ values at the maximum and minimum temperatures investigated increased with strain, at constant strain this gap narrowed down with increase in Zr concentration, Figures 30 - 33. It would, therefore, seem that the presence of solute atoms retarded the recovery process in deformed structure and thereby raised the level of hardening observed experimentally. It should also be noted that at a particular temperature the thermal stress σ^* was different in different compositions and as the dislocation arrangement depends upon σ^*, it is possible that due to the difference in dislocation arrangements in different alloys the $\sigma\mu$ was different. The results of transmission electron microscopy of deformed structure will be discussed later.

The flow stress at a particular strain is a sum of two components namely the initial strength of the system and the contribution from work hardening. The stress strain curves and the work hardening analysis showed that although both the components were equally important in pure Nb, it was the initial strength that was increased comparatively much more than the rate of work hardening $\frac{d\sigma}{d\varepsilon}$ with increase in the solute content.

The analysis based on power law of work hardening $\sigma = K\varepsilon^{n}$, Figures 35 - 38, showed that beyond 1 - 2% plastic strain the

strain hardening exponent η acquired a new and about 3 - 4 times higher value in the log σ - log ε plot. The initial 1 - 2% plastic strain was the region of pre-macro yield strain, yield drop and yield elongation and during this 1 - 2% plastic strain the deformation is inhomogeneous (as only a few discrete grains are deforming) and the rate of work hardening low. The manifold change in η beyond 1 - 2% strain was also observed by Gregory et. al.[26] in polycrystalline Nb. The initial 1 - 2% plastic strain in the present case can probably be identified with the stage I hardening i.e. the easy glide region in single crystals. The easy glide region increases as the friction stress increases i.e. as the solute content increases. Table IX shows that the strain ε_c where η rises sharply, increases very slightly with increase in Zr content in the solution hardening region. e.g. 290 - 450^{o}K but if softening occurs, then ε_c decreases viz. No-0.87 at%Zr at 215^{o}K.

ε_c% \ ^{o}K	77	215	290	350	490
Nb		2	1.5	-	-
Nb 0.87at%Zr		1.75	1.5	1.0	1.0
Nb 3at%Zr		1.85	1.7	1.35	1.25
Nb - 4.7at%Zr		2	1.7	1.5	1.3

TABLE IX

The addition of solute seemed to have very little effect, if any, on η and it was essentially temperature independent. The only atypical example was that of Nb at 490^{o}K where η has the maximum value for Nb. The deformation of Nb at 490^{o}K was very irregular and strain ageing was observed. It is thought that

due to this the level of the stress-strain curve was raised and η increased. However the strength constant K - the flow stress at strain equals one, increased systematically with increase in Zr content or decrease in temperature Figures 35 - 38, in a way similar to σ in the solution hardening region. After the sudden rise in η value beyond the initial 1 - 2% strain no downward inflexion was observed which is different to the behaviour of iron observed by Morrison[58]. No further inflection was seen even though the Nb specimens in the present study were strained very close to the necking strain. However, at $77^{o}K$ the value of η acquired a lower value in all the compositions at $\sim$4% strain. The specimens for $77^{o}K$ tests were predeformed to $\sim$2%ε at room temperature and possibly due to the presence of room temperature dislocation structure the initial work hardening rate was too high and after $\sim$2%ε at $77^{o}K$, the system acquired its real η value.

Since $\eta = \varepsilon$ at the necking strain, any change in η with change in temperature and solute content will correspond to variation in the amount of uniform elongation of pure Nb. In the present case however, solute and temperature had almost no effect on η and the strain upto necking would be expected to remain constant. The average value of η was 0.23 which was in close agreement with the value 22 - 24% uniform elongation observed in niobium and its alloys.

The results, thus, show that on addition of solute Zr to Nb, the frictional stress was affected strongly. As a result of this, it was found that the dislocation arrangement was affected.

5.7 Electron Microscopy of the Deformed Substructure

In a specimen the flow stress is a function of dislocation density at a given strain. If we consider an arrangement of a given number of total dislocations N, then the total elastic energy is comprised of a) the self energies of these dislocations which is constant for a fixed N and b) the interaction energies of the various dislocations. Thus if the system was to move towards a lower energy state by rearrangement (e.g. clustering) the driving force is provided by the stored energy of the material. In other words the driving force for rearrangement of dislocations is the athermal component $\sigma\mu$ of the flow stress ($\sigma = \sigma^* + \sigma\mu$). Furthermore, as the dislocations have to move under the influence of this driving force provided by $\sigma\mu$ to achieve a low energy configuration, it is apparent that the kinetics of this process of rearrangement would depend upon the frictional stress σ^*.

In the present study a range of σ^* was obtained by testing a series of Nb - Zr alloys at a fixed test temperature. The frictional stress can also be manipulated by testing an alloy of a fixed composition at several temperatures. However, manipulation of σ^* by alloying is preferred because of minimizing the complications arising from the change in the test temperature.

Micrographs 1 - 2, 3 - 4 and 5 - 6 show the dislocation arrangement in alloys as a function of σ^* at a fixed strain and temperature. The general observation from the above micrographs is that at any temperature the dislocation tangling decreases and the

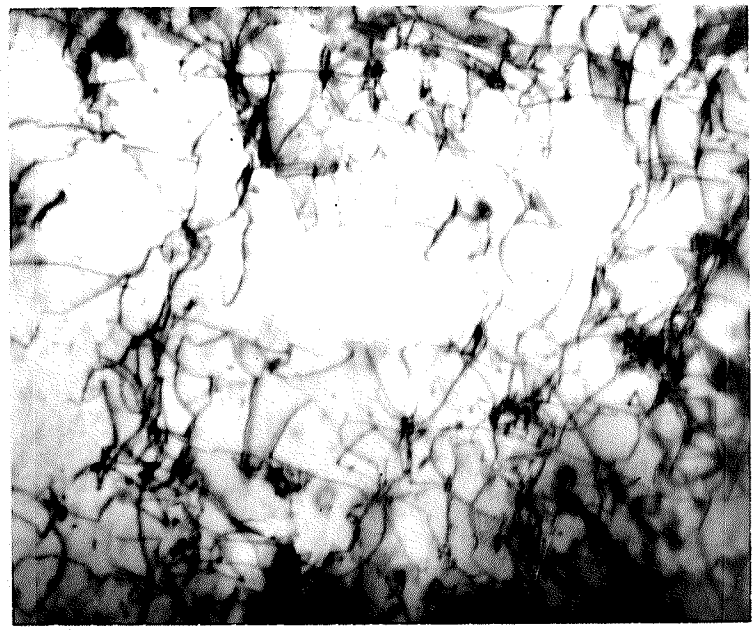

Micrograph 1: Nb - 0.87 at%Zr, 3% e_p at 290^{o}K

X 48240

σ^* 5 kg/mm^2

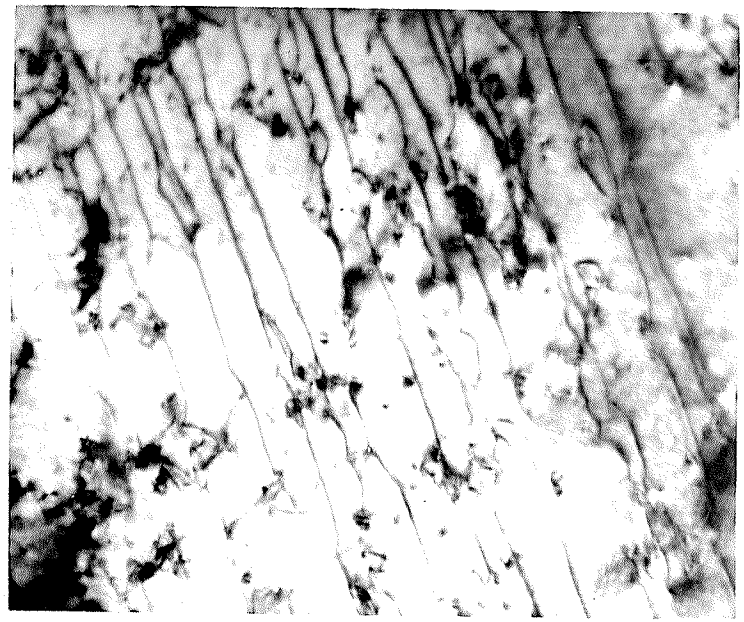

Micrograph 2: Nb - 4.7 at%Zr, 3% e_p at 290°K

X 48240

σ^* 13 kg/mm^2

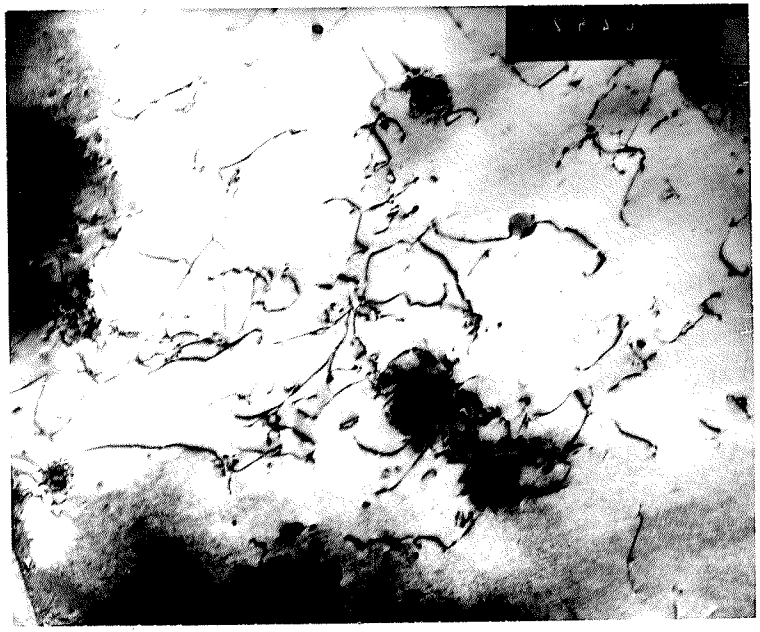

Micrograph 3: Nb - 0.87 at%Zr, 3% e_p at 215°K

X 59400

σ^* 8 kg/mm^2

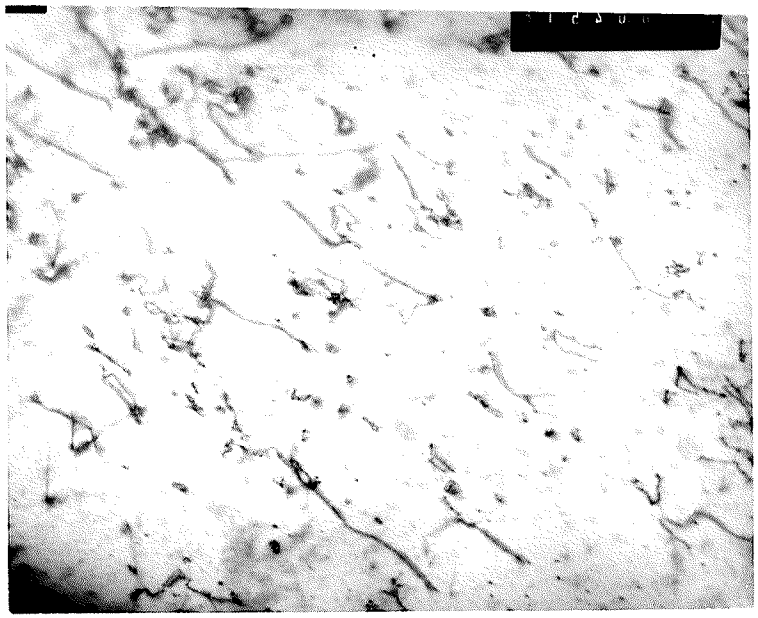

Micrograph 4: Nb - 4.7 at%Zr, 3% e_p at 215^{o}K,

Foil plane (111), dislocations along [$\bar{1}01$] & [$0\bar{1}1$]

X 59400

σ^* 21 kg/mm^2

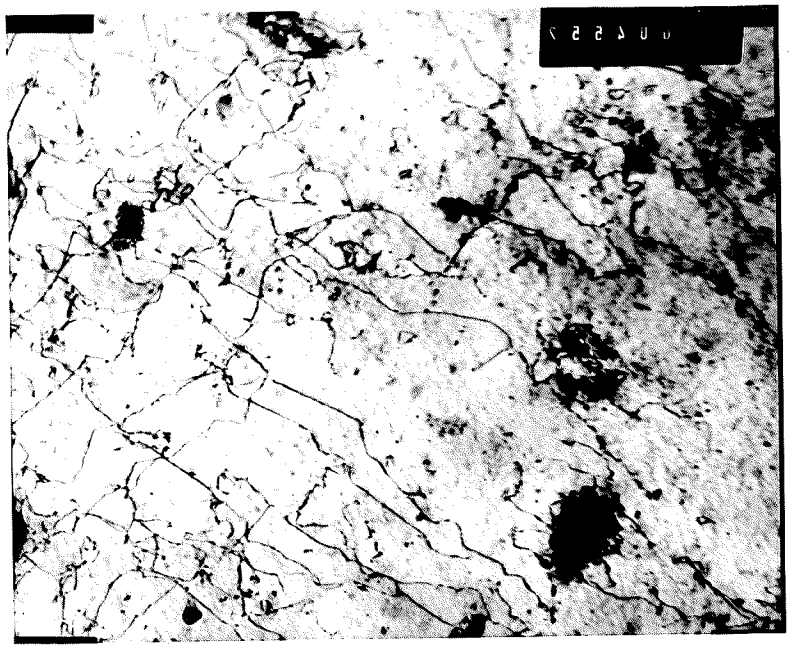

Micrograph 5: Nb - 0.87 at%Zr, 3% e_p at 77^{o}K,

Foil plane (110), dislocations along [$\bar{1}11$] & [$1\bar{1}1$]

X 73440

σ^* 31.5 kg/mm^2

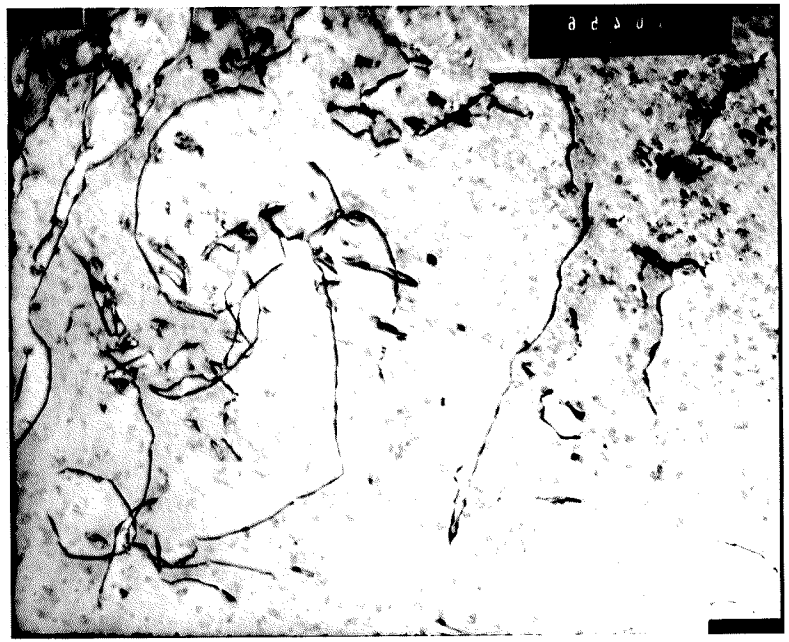

Micrograph 6: Nb, 3% e_p at 77°K,

X 59400

σ^* 47.5 kg/mm^2

distribution becomes more uniform as σ^* increases. Where the dislocations were long and straight it was possible to find their orientation unambiguously. In such cases it was found that they were in screw orientation and that their Burgers vector was <111> - see micrograph 5. Loops and trails indicate that the majority of dislocations are in screw orientation. The microstructures from regions with lower dislocation density showed that for an essentially similar dislocation density, tangling becomes less evident as σ^* increases i.e. the total dislocation density at which tangling is evident increases with increase in σ^*. Also, the density of screw dislocations increases and they accumulate more and more jogs creating small and uniformly distributed loop debris as σ^* increases. These results are similar to those found by Foxall and Statham[17] who studied the dislocation arrangement in Nb - Mo crystals as a function of shear stress. Originally, the effect of stress on dislocation distribution in Nb crystals was studied by Taylor and Christian[31]. These authors considered the cross slip of two opposite screw dislocations in planes 'd' apart under the combined influence of the applied stress and the attractive force between the screws. Now as 'd' decreases the attractive force between the two opposite screws increases. Therefore, for a given applied stress, the higher the frictional stress for screws, the higher must be the attractive force or in other words, the smaller the separation 'd'. Smaller 'd' in turn means a higher density of dislocations because the opposite screw dislocations will be cross slipping and annihilating in only

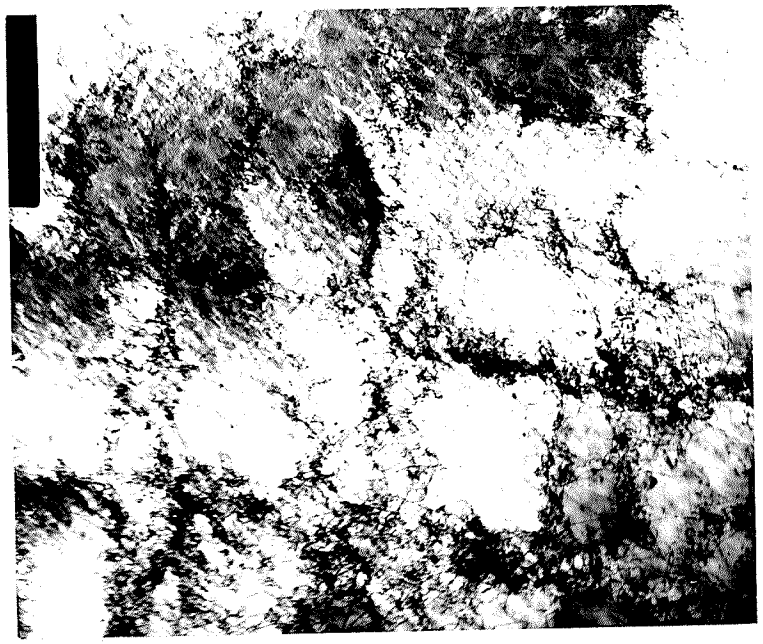

Micrograph 7: Nb, 14% e_p at 295^{o}K,

X 21960

σ^* 5 kg/mm^2

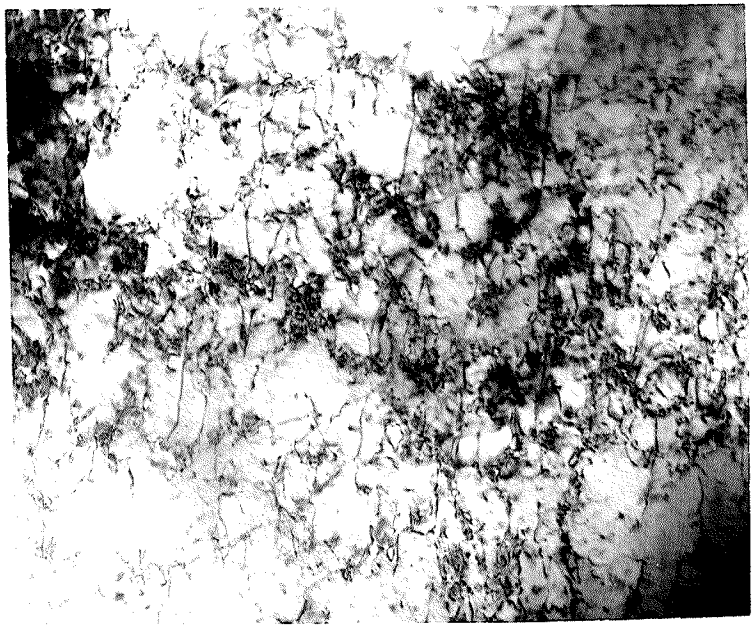

Micrograph 8: Nb - 4.7 at%Zr, 14% e_p at 295°K,

X 48240

Foil plane (110), cell walls along [$\bar{1}11$]

σ^* 13 kg/mm^2

a small region.

Thus, it may be suggested that as σ^* increases (i) the critical screw density at which cross slip and annihilation become important, will increase, and (ii) cross slip will be difficult and hence the probability of dipole producing jogs created by cross slip (Gilman - Johnston probability) will decrease, (iii) the interaction between a single dislocation and a dipole becomes smaller and thus the probability of cluster formation decreases.

Since clustering and tangling occured at higher dislocation densities with increasing σ^*, cell formation also followed this trend. The result was a decrease in the resultant cell size with increasing σ^*, Micrographs 7 and 8.

The specimens in the micrographs 7 and 8 were strained to $\sim$14% and even though well defined cells have formed, no downward inflexion in the corresponding log σ - log ε plot was observed - see Figures 35 to 38. The downward inflexion in the slope of log σ - log ε plot for polycrystalline iron was observed by Morrison[56] and he suggested that this may be due to the formation of well defined cells. However, the present observations are not in agreement with this approach.

6.0 Summary and Conclusions

1. In the Nb - Zr alloys the increase $\Delta\sigma$ in the flow stress σ was linearly proportional to concentration at ambient and higher temperatures and the atom-size-misfit seemed to be the predominant factor in solution hardening.
2. The increase $\Delta\sigma\mu$ in the athermal stress $\sigma\mu$ showed the (concentration)$^{1/2}$ dependence whereas a complex concentration dependence was observed for the thermal stress σ^*. The $c^{1/2}$ dependence of $\Delta\sigma\mu$ was almost independent of strain and temperature.
3. At subatmospheric temperatures alloy softening was observed in the Nb - Zr alloys which was most predominant at the lowest temperature studied i.e. $77^{o}K$. At $77^{o}K$, $\sim$2.4 at%Zr in Nb seemed to have the maximum solution softening effect but beyond 2.4 at%Zr no further softening was observed.
4. The temperature range where solution softening was present decreased with increase in Zr content.
5. During alloy softening it was the thermal component of the flow stress that decreased on adding zirconium.
6. It is suggested that the decrease in the lattice frictional stress was responsible for the observed softening however scavenging might have had some effect.
7. The deformation of Nb and Nb - 0.87 at%Zr was controlled by the double kink nucleation on screw dislocations and the Dorn-Rajnak theory was obeyed however, in the 3 at% and 4.7 at%Zr the kink propagation seemed to be important and the solute hardening

controlled deformation in the higher temperature (beyond alloy softening) region.

8. The analysis of activation parameters showed that both the σ^* and the barrier strength decreased in Nb - 0.87 at%Zr but in the 3 at% and 4.7 at%Zr alloys only σ^* decreased; the barrier strength increased.

9. m^* was essentially independent of strain at all the temperatures studied.

10. The effects of concentration and temperature on m^* were analogous to those on σ^*. The present results on dislocation dynamics showed that the thermally activated deformation approach and the power-low approach to deformation are essentially equivalent in Nb and Nb - Zr alloys.

11. The work hardening rate of Nb was only modestly increased by zirconium. The work hardening was completely due to increase in $\sigma\mu$ with strain; σ^* was essentially independent of strain.

12. In the log (σ) - log (ε) plots the slope of the curve increased to a new slope ($\sim$3 times higher) beyond 1 - 2% plastic strain and then remained constant.

13. The slope of the curve in the log (σ) - log (ε) plot was almost independent of temperature and concentration. No downward inflexion in the slope was observed even though the corresponding structure consisted of well-formed dislocation cells.

14. The transmission electron microscopy of the deformed specimens showed that the dislocation arrangement was dependent on σ^*.

As σ^* increased the screw dislocation density increased and dislocation tangling decreased. At higher strains the cell diameter decreased with increase in σ^*.

REFERENCES

1. Knapton A. G., J. Less-Comm. Met., 2, 113 (1960)
2. Taylor A. & Doyle N. J., J. Less-Comm. Met., 13, 338, 413, 511, (1967)
3. Pearson W. B., Lattice spacings & Structures of metals & alloys, Pergamon, London (1967)
4. Tarasov N. D., Ul'yanov & Ya. D. Mikhaylov, Phys. Met. & Metallo., 18, 740 (1964)
5. Nedykha I. M. & Chernyy V. G., Phys. Met. & Metallo., 18, 599 (1964)
6. Nedykha I. M. & Chernyy V. G., Phys. Met. & Metallo., 20, 787 (1965); 22, 114 (1966)
7. Harris B., J. Less-Comm. Met., 12, 247 (1967)
8. Begley R. T. & Bechtold J. H., J. Less-Comm. Met., 3, 1 (1961)
9. Harris B., Phys. Stat. Sol., 18, 715 (1966)
10. Kostorz G., Ph. D. Thesis, Gottingen (1968)
11. Fleischer, R. L., Strengthening of Metals, ed. Peckner D., Reinhold Pub., New York (1964)
12. Jax P., Z. für Metallkunde, 62, 279 (1971)
13. Kan, T., Scripta Met., 5, 607 (1971)
14. Palmer, D. E. B. & Flewitt P. E. J., J. Less-Comm. Met., 21, 459 (1970)
15. Mott N. F. and Nabarro F. R. N., Report on conf. on strength of solids, Phys. Soc. London, p. 1 (1948)
16. Koss, D. A., Met. Trans., 2, 245 (1971)
17. Foxall R. A. & Statham C. D., Acta. Met., 18, 1147 (1970)

18. Peters B. C. & Hendricson A. A., Met. Trans., 1, 2271 (1970)

19. Hoone G. T., Roy R. B. and Paxton H. W., J. I. S. I., 201 161 (1963)

20. Kranzlein H. H., Burton M. S. & Smith G. V., Trans. TMS-AIME, 233, 64 (1965)

21. Mitchell, T. E. & Raffo, P. L., Can. J. Phys., 45, 1047 (1967)

22. Georgiyeva, I. Ya & Gulyaev A. P., Phys. Met. & Metallo., 20, 592 (1965)

23. Lundin C. E. & Cox R. H., J. Less-Comm. Met., 13, 501 (1967)

24. Mitchell, T. E., Foxall R. A. & Hirsch P. B., Phil. Mag. 8, 1895 (1963)

25. Christian J. W. and Masters B. C., Proc. Roy. Soc., Ser. A 281, 223, 240 (1964)

26. Gregory D. P., Stroh A. N. & Rowe G. H., Trans. TMS-AIME., 227, 678 (1963)

27. Wronski A. & Fordeaux A., J. Less-Comm. Met., 7, 205 (1964)

28. Harris B., J. Less-Comm. Met., 7, 185 (1964)

29. Bowen, D. K., Christian J. W. and Taylor G., Can. J. Phys., 45, 907 (1967)

30. Hirsch P. B., Relation between Struct. & Properties of Metals, H. M. S. O., London, p. 39 (1963)

31. Taylor G. and Christian J. W., Phil. Mag., 15, 893 (1967)

32. Bowen D. K., D. Phil. Thesis, Oxford (1966)

33. Statham C. D., Vesely D. and Christian J. W., Acta. Met. 18, 1243 (1970)

34. Fordeaux A. and Wronski A., J. Less-Comm. Met., 6, 11 (1964)

35. Guberman H. D., Acta Met., 16, 713 (1968)

36. Evans K. R. and Schwenk E. B., Acta Met., 18, 1 (1970)

37. Gupta I. and Li J. C. M., Met. Trans., 1, 2323 (1970)

38. Li, J. C. M., Can. J. Phys., 45, 493 (1967)

39. Ravi K. V. and Gibala R., Met. Trans., 3, 3081 (1972)

40. Mordike B. L., Rogausch K. D. and Braithwaite A. A., Met. Sc. Journal, 4, 37 (1970)

41. Foxall R. A., Duesbery M. S. and Hirsch P. B., Can. J. Phy., 45, 607 (1967)

42. Leslie W. C., Met. Trans., 3, 5 (1972)

43. Arsenault R. J., Microplasticity, Interscience, N. Y., 91 (1968)

44. Statham C. D. and Christian J. W., Scripta Met., 5, 399 (1971)

45. Villagrana R. E. & Thomas G., Phys. Stat. Sol., 9, 499 (1965)

46. Seraphim D. P., Stemple N. R. & Nanick D. J., J. Appl. Phys., 33, 136 (1962)

47. Ravi K. V. and Gibala R., Acta Met., 18, 623 (1970)

48. Nakada Y. and Keh A. S., Acta Met. 16, 903 (1968)

49. Christ B. W., Gamble R. P. and Smith G. V., Scripta Met., 3, 521 (1969)

50. Gamble R. P., M. S. Thesis, Cornell University (1969)

51. Jolley W., Trans. AIME-Met. Soc., 242, 307 (1968)

52. Pink E. and Arsenault R. J., Metal Sc. J., 6, 1 (1972)

53. Weertman H., J. Appl. Phys., 29, 1685 (1958)

54. Dorn J. E. and Rajnak S., Trans. Met. Soc.-AIME, 230, 1052 (1964)

55. Ono K., and Sommer A. W., Met. Trans., 1, 877 (1970)

56. Morrison W. B., Trans. ASM, 59, 824 (1966)